UCLA
· Department of Physics

D D C

JAN 25 1978

RECEIVED
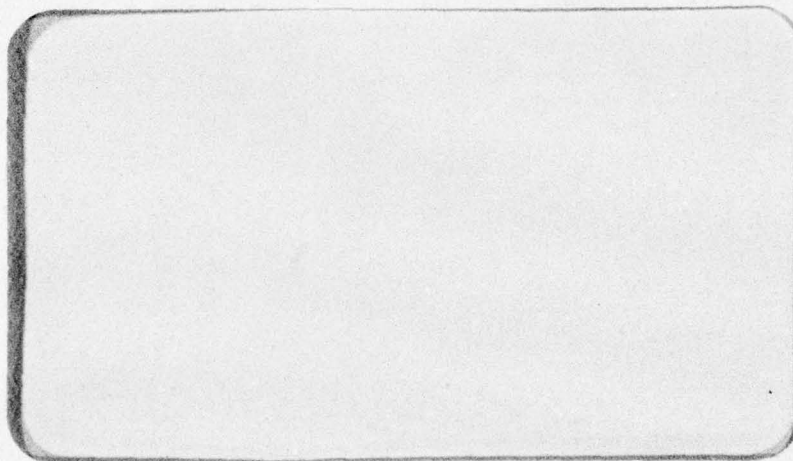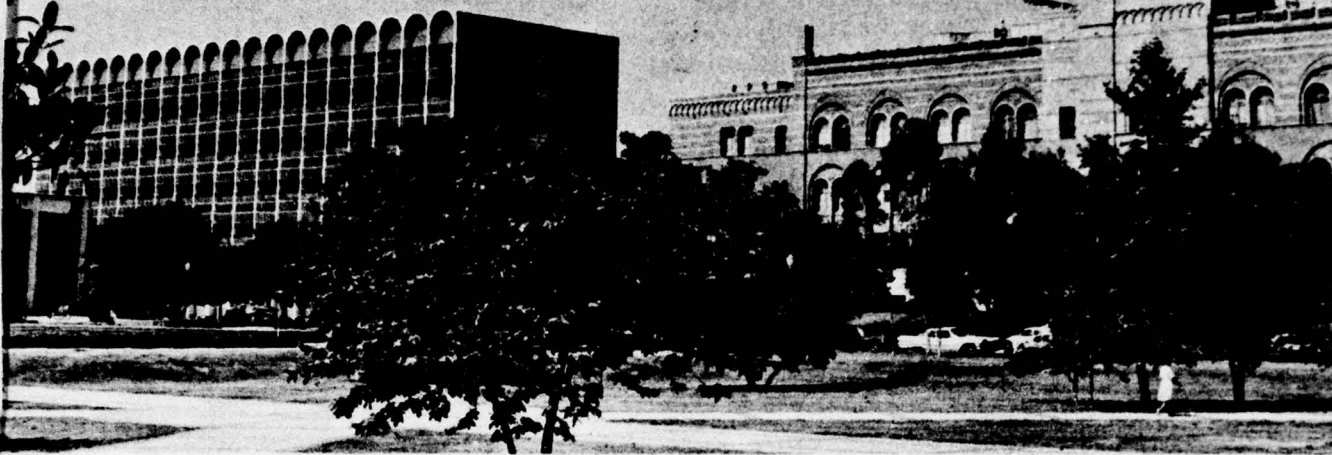
F

LOS ANGELES 90024

CALIFORNIA

TECHNICAL REPORT No.39

December 1977

Submitted by

I. Rudnick, Project Director

Non-Linear Parametric Generation of

Sound by Resonant Mode Conversion

by

Steven Lurie Garrett

SECURITY CLASSIFICATION OF THIS PAGE *(When Data Entered)*

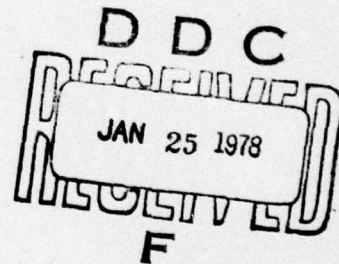| REPORT DOCUMENTATION PAGE		READ INSTRUCTIONS BEFORE COMPLETING FORM
1. REPORT NUMBER (14) πR - 39	2. GOVT ACCESSION NO.	3. RECIPIENT'S CATALOG NUMBER
4. TITLE *(and Subtitle)* (6) Non-Linear Parametric Generation of Sound by Resonant Mode Conversion.		5. TYPE OF REPORT & PERIOD COVERED (9) Interim
		6. PERFORMING ORG. REPORT NUMBER Technical Report, No. 39
7. AUTHOR(s) (10) Steven Lurie Garrett		8. CONTRACT OR GRANT NUMBER(s) (15) N00014-75-C-0246
9. PERFORMING ORGANIZATION NAME AND ADDRESS University of California, Los Angeles Physics Department Los Angeles, California 90024		10. PROGRAM ELEMENT, PROJECT, TASK AREA & WORK UNIT NUMBERS NR. No. 384-302
11. CONTROLLING OFFICE NAME AND ADDRESS Office of Naval Research, Physics Program Office Arlington, Virginia 22217	(11)	12. REPORT DATE December 1977
		13. NUMBER OF PAGES 181
14. MONITORING AGENCY NAME & ADDRESS *(if different from Controlling Office)* (12) 187p.		18. SECURITY CLASS. *(of this report)* UNCLASSIFIED
		15a. DECLASSIFICATION/DOWNGRADING SCHEDULE

16. DISTRIBUTION STATEMENT *(of this Report)*

Approved for Public Release, Distribution Unlimited

17. DISTRIBUTION STATEMENT *(of the abstract entered in Block 20, if different from Report)*

18. SUPPLEMENTARY NOTES

19. KEY WORDS *(Continue on reverse side if necessary and identify by block number)*

Non-linear acoustics	Scattering of Sound by Sound	First Sound
Superfluid helium-4	Parametric amplification	Second Sound
Mode conversion	Phonon-phonon interactions	Waveguides
Sound absorbtion	Reciprocity calibration	Cryogenics

20. ABSTRACT *(Continue on reverse side if necessary and identify by block number)*

See over

072 267
LP

When non-linear terms are included in the two fluid hydrodynamic description of superfluid helium-4, first sound and second sound are coupled. The interaction of two second sound waves to produce a propagating first sound wave is shown to occur at a specific angle which makes the point of intersection of the second sound waves travel at the speed of first sound.

An experiment to observe this mode conversion process in a waveguide of rectangular cross-section is described. Measurements show that the resonant conversion occurs at the theoretically predicted frequency. The amplitude of the mode converted first sound is found to exhibit a quadratic dependence on the amplitude of the primary wave which is characteristic of a second order effect. A new application of the reciprocity calibration technique allowed an absolute calibration of the pressure microphones in situ. Absolute measurements of the coupling of first sound to second sound agree with theory. This agreement is a direct confirmation of the importance of the additional, intrinsically non-linear, Galilean invariant variable, $(\vec{v}_n - \vec{v}_s)^2$, in the thermohydrodynamics of superfluid helium.

The theoretical formalism is applied to the parametric amplification of second sound by high intensity first sound and the results are in disagreement with a previous calculation by Khokhlov and Pushkina.

ACCESS

NTIS
DDC
UNAN
JUST

BY
DISTRIBUTION/AVAILABILITY CODES

Dist.   SPECIAL

A

S/N 0102-LF-014-6601

TABLE OF CONTENTS

LIST OF FIGURES AND TABLES

ACKNOWLEDGEMENTS

It is my great pleasure to acknowledge the immeasurable contribution made by my thesis advisor, Professor Isadore Rudnick, to this work and all aspects of my education. His physical insight, incomparable abilities as an experimentalist, and his readiness to share his gifts with me at any time, have been the focus of my scientific evolution of the last four years. The warmth and strength of his personality have created an environment in which my studies were made as pleasant as they were enlightening.

I would also like to acknowledge the contributions of Professor Seth Putterman who has shared his insights into phenomenological theory with me and taught me how to travel the "royal road" to its applications. His creativity and flamboyance as a theoretician, lecturer, critic, and friend have been an inexaustible source of stimulation.

I would like to thank the other member of my doctoral committee, Professor Richard Stern, who gave me valuable instruction in engineering acoustics. I am also grateful to Professor Marvin Chester who gave me my first opportunity to do experimental work in low temperature physics as a undergraduate member of his research group.

A special thanks goes to Professor Kenneth Telschow and Dr. Joseph Heiserman who started me in this research group when they were the post doctoral fellow and senior graduate student respectively. I hope I will be able to repay, in part, the patient help they gave me when I started, by helping the new students who are now beginning

Isaac Gabaeff for their continuing interest in this work and their
efforts to help me keep everything in its proper perspective.

Sadgurunath Maharaj Kai Jay!

ABSTRACT OF THE DISSERTATION

Non-Linear, Parametric Generation of

Sound by Resonant Mode Conversion

by

Steven Lurie Garrett

Doctor of Philosophy in Physics

University of California, Los Angeles, 1977

Professor Isadore Rudnick, Chairman

When non-linear terms are included in the two fluid hydrodynamic
description of superfluid helium-4, first sound (pressure-density waves)
and second sound (temperature-entropy waves) are coupled. The inter-
action of two second sound waves to produce a propagating first sound
wave is shown to occur at a specific angle which makes the point of
intersection of the second sound waves travel at the speed of first
sound. The growth of the mode converted first sound wave is calculated
with and without attenuation of the primary (second sound) waves from
$1.2°K$ to $2.15°K$ and from saturated vapor pressure to twenty atmospheres.

An experiment to observe this mode conversion process in a wave-
guide of rectangular cross-section is described. In the waveguide the
intersection angle of the second sound waves is controlled by the ratio
of the frequency of the higher order propagating mode of second sound to
the cut-off frequency for that mode. Experimental measurements show

that the resonant conversion of second sound to first sound in the waveguide occurs at the theoretically predicted frequency to within experimental error (0.1% to 0.2%) between 1.14°K and 2.04°K at saturated vapor pressure. The amplitude of the mode converted first sound is found to exhibit a quadratic dependence on the amplitude of the primary wave which is characteristic of a second order effect over the same range of temperatures. The quadratic dependence was observed over as much as 1.3 decades in primary wave power at a given temperature. A new application of the reciprocity calibration technique to a plane wave resonator geometry allowed an absolute calibration of the pressure microphones in situ. Absolute measurements of the coupling of the first sound generated by the resonant mode conversion process to the second sound agreed with theory to within 16% between 1.26°K and 1.41°K. The agreement between measured and theoretical values is a direct confirmation of the importance of the additional, intrinsically non-linear, Galilean invariant variable, $(\vec{v}_n - \vec{v}_s)^2$, in the thermohydrodynamics of superfluid helium. These results confirm the validity of the two fluid hydrodynamic description of He II up to terms of second order through the observation of a new non-linear acoustical interaction in fluids.

The theoretical formalism developed for the study of the mode conversion process is applied to the parametric amplification of second sound by high intensity first sound and the results are in disagreement with a previous calculation by Khokhlov and Pushkina. Using existing thermodynamic data, it is shown that the amplification

process will give less than unity gain for first sound (pump)

intensities which are below the cavitation threshold at saturated

vapor pressure.

CHAPTER I.

INTRODUCTION

Chitireva chetana padadavarurha chetyasankochini chittam.
(Chiti herself, descending from the plane of pure consciousness, becomes the mind by contracting in accordance with the object perceived.)
Pratyabhijnahridayan[1]

The generation of a propagating sound wave through the non-linear interaction of two other sound waves in classical fluids and isotropic solids has been the subject of many theoretical and experimental investigations over the past two decades. The application of this non-linear process, commonly called the "scattering of sound by sound,[2,3] to the production of long distance highly directional transmission of sonar signals has engendered a great deal of interest. Although the principles underlying non-linear generation of a sound wave which propagates out of the region of interaction of two primary waves are identical in fluids and solids, the scientific literature on the subject has evolved independently with regard to the two media for many reasons.

The reason most significant to this work is that a classical fluid can support only longitudinal sound modes, and in the absence of dispersion, the non-linear production of a propagating wave can only take place if the primary waves are co-linear.[4] The general thrust of investigations concerning this effect in fluids has been along the direction set by Westervelt.[5] His analysis of the transmission of

a "difference frequency" signal considers it to be radiated from an array of sources, driven by the non-linear terms in the hydrodynamics and equation of state, distributed continuously throughout the volume of interaction of the two primary waves. This virtual source array is analogous to an end-fire array antenna and for this reason is frequently called a parametric end-fire array. Solids, on the other hand, can support both longitudinal and transverse waves. In addition to the non-linear process which creates a third longitudinal wave from two co-linear longitudinal waves,[6] it was shown theoretically by Jones and Kobett[7] that, for instance, two transverse waves interacting at the proper angle can generate the faster longitudinal mode at a frequency equal to the sum of the frequencies of the two transverse waves. Such a "resonant mode conversion" has been observed experimentally.[8] Most studies of the scattering of sound by sound in solids go under the heading of three-phonon or phonon-phonon interactions. In the study of the non-linear acoustical properties of superfluid ^{4}He the artificial separation of sound scattering research into parametric arrays and three phonon processes is not sensible.

As a result of a finite fraction of the superfluid ^{4}He occupying the quantum ground state for temperatures below 2.17°K, there can appear mass flow with no entropy flow and reversible entropy flpw accompanied by zero mass flow. Classical hydrodynamics is incapable of describing such a situation and for the superfluid the appropriate macroscopic theory was first presented by Landau.[9, 10] By incorporating the possibility of reversible entropy flows, this theory predicted that the temperature disturbances would propagate as waves

2

(second sound) rather than by diffusion. This mode appears in addition to the ordinary sound mode (first sound) by which pressure disturbances propagate.

In the linear approximation any disturbance can be separated into components which travel with the first or second sound velocities. In the second order of approximation these modes are no longer uncoupled and not only is such a separation no longer possible, but there appears the possibility of mode conversion wherein, for instance, two second sound waves incident at the required angle can generate a first sound wave which propagates out of the region of interaction of the second sound waves. This process is, in some sense, similar to the already mentioned case of two transverse waves generating a longitudinal wave in a solid except both first and second sound are longitudinal modes and in the temperature range of the experiments to be described, their velocities differ by a factor of twelve.

It is the purpose of this thesis to demonstrate that, under the proper conditions, the generation of a first sound wave through the non-linear interaction of two second sound waves is contained in the macroscopic theory of superfluidity known as Two Fluid Hydrodynamics, and also to describe an experiment which has produced quantitative verification of this process. In the interest of providing this work with some degree of self-containment and placing the experiment into the context of other work in non-linear acoustics, the remainder of this chapter will give a short historical survey of the development of the scattering of sound by sound in fluids and will introduce the general properties of superfluid ^{4}He with an emphasis on the experimental

3

motivation for the two fluid model and the role of quantum mechanics in determining the behavior of this extraordinary liquid.

A.   SCATTERING OF SOUND BY SOUND IN CLASSICAL FLUIDS

The consideration of finite amplitude or non-linear effects in acoustics requires the abandonment of two of the most useful and fundamental principles of linear acoustics: linear superposition and the stability of the monochromatic waveform. The principle of linear superposition is obviously violated when the interaction of two waves produces a third, independent wave. The distortion of a monochromatic wave can also be understood as a consequence of the scattering of sound by sound if the distortion is looked upon as a self-scattering process.

The earliest recorded observation of a sound wave which was generated by the interaction of two other sound waves was made over two hundred years ago by Sorge,[11] a German organist, and independently by Tartini,[12] an Italian violinist, both of whom claimed that the union of two loud independent tones produced a difference tone. According to Beyer,[13] Lagrange and later Young (1800) and Chaladni (1803) suggested the effect was simply the well-known linear phenomena of beating even though it was known that the tones would have to be quite intense before the difference tone was audible. When Helmholtz undertook his study of combination tones[14] he discovered the existence of the sum as well as the difference tone. The matter of whether the perceived tones were actually generated in the medium or created by the ear's own non-linearity[15] was still not settled. With the advent of modern electro-acoustical instrumentation, Thuras, Jenkins and O'Neil, basing their experimental investigations on the theoretical analysis of

4

Lamb,[16] showed that the sum and difference tones were produced by a non-linear process within the medium, in their case air, when two intense sound waves of different frequencies are propagated in a tube or exponential horn. They were able to show that "the magnitudes of the summation and difference tones are very nearly proportional to distance from the source, to the product of the magnitudes of the primary pressures and, in each case, to the frequency of the particular combination tone".[17] They found the absolute magnitude of the effect was 3 dB less than predicted by theory but in a later repetition of the experiment by Geertsen[18] the absolute amplitudes were found to be in agreement with the theory.

At the June,1960, meeting of the Acoustical Society of America, Westervelt presented a paper[19] which established theoretically that the difference frequency wave resulting from the interaction of two collimated, co-linear plane waves whose frequencies were nearly equal would be highly directional. The following paper by Bellin, Westervelt and Beyer[20] presented an experimental verification of this result. As mentioned earlier in this chapter, the possibility of exploiting this difference frequency radiation in sonar systems to achieve highly directional low frequency beams from small apertures stimulated considerable interest in the applications of non-linear acoustics.[21] If one lets an acoustical signal which is to be detected act as the primary wave which interacts with a high frequency "pump", then it has been suggested[22] that the same effect will create a highly directional parametric amplifier.

5

B.   SUPERFLUID ^{4}He - THE UNUSUAL PROPERTIES

All known substances are gases at high temperatures turning to liquids and ultimately solids as their temperatures are decreased. The one exception is the noble gas helium which, under its own vapor pressure remains liquid down to absolute zero. It will only form a solid phase when subjected to pressurization in excess of 25 atmospheres. This is due to its low mass which gives rise to a large quantum mechanical zero point motion and its high degree of symmetry which accounts for He having the weakest van der Waals interatomic attraction of any species.

Helium was first liquefied by H. K. Onnes in 1908. The common isotope, ^{4}He, condenses at 4.2°K at atmospheric pressure. Onnes used the liquid helium as a refrigerant in his experimental investigations of the low temperature behavior of electrical resistivity of metals which led him to the discovery of superconductivity in 1911.[23] Liquid helium was used as a refrigerant for thirty years before it was realized that the helium itself exhibited extraordinarily unusual properties.

Liquid helium behaves like any classical fluid obeying ordinary hydrodynamics until it is cooled to the lambda temperature which, at its vapor pressure, is $T_\lambda = 2.172$°K. Abruptly at this temperature the character of the liquid changes completely. For purposes of distinction the liquid above T_λ is referred to as He I and below T_λ it is called He II. See Fig. 1. Early indications of an abrupt change in the dynamical properties of the liquid came in 1938 when Kapitza[24] and independently Allen and Misener[25] discovered that below T_λ the liquid helium could flow through small capillaries without measurable resistance.

6

CRITICAL POINT
(T=5.20°K, 2.264 atm)

He GAS

LIQUID He I

UPPER λ POINT
(T=1.76°K, 29.8 atm.)

λ-LINE

λ POINT
(T=2.172°K, 0.0497 atm)

SOLID He

LIQUID He II

T(°K)

P(atm)

6.0   5.0   4.0   3.0   2.0   1.0   0

40   30   20   10   0
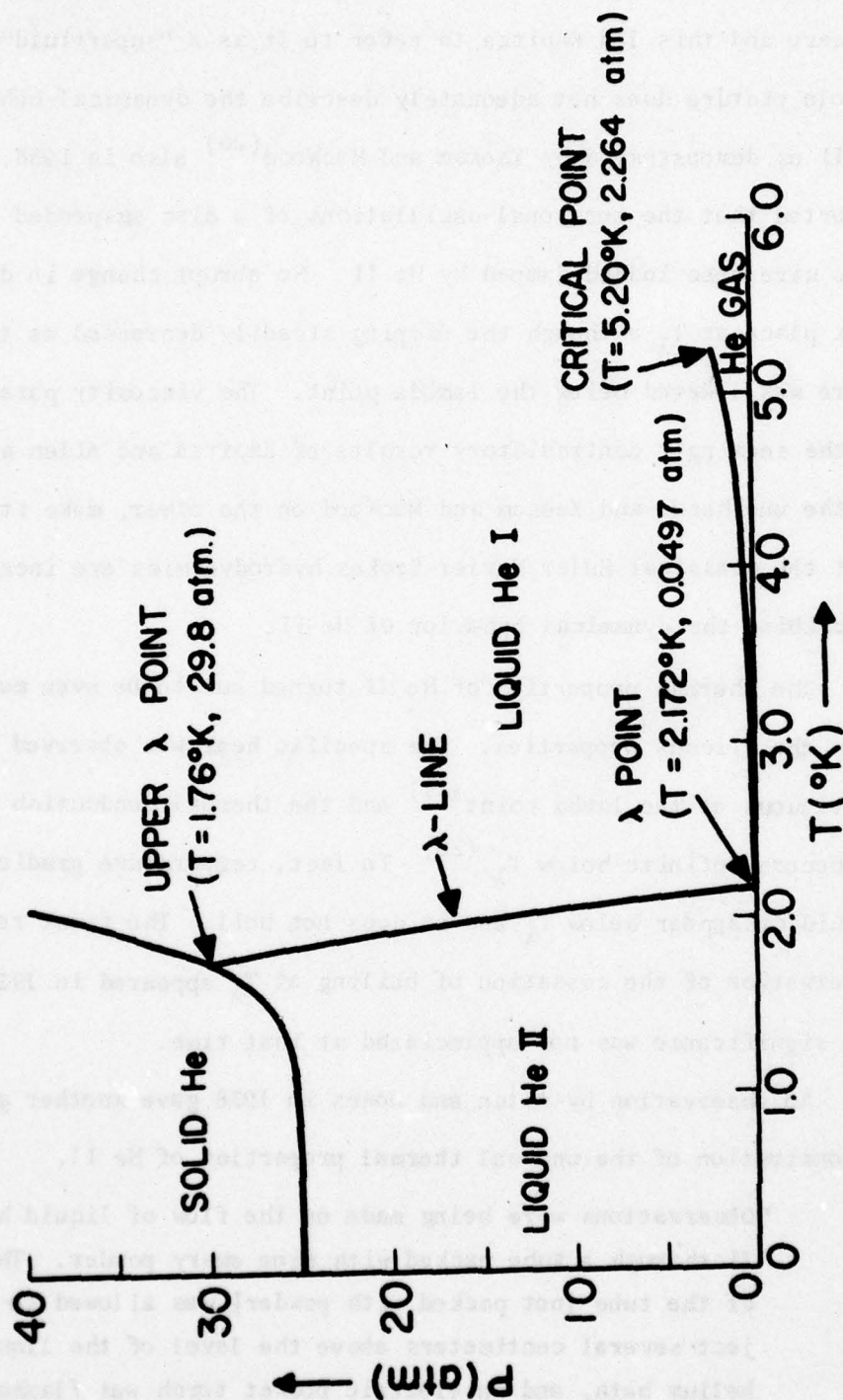
FIGURE 1.   The phase diagram of helium-4 in the P-T plane.

This discovery suggested that below T_λ the viscosity of the liquid drops to zero and this led Kapitza to refer to it as a "superfluid". This simple picture does not adequately describe the dynamical behavior of He II as demonstrated by Keesom and MacWood[26] also in 1938. They reported that the torsional oscillations of a disc suspended from a fine wire were indeed damped by He II. No abrupt change in damping took place at T_λ although the damping steadily decreased as the temperature was lowered below the lambda point. The viscosity paradox caused by the seemingly contradictory results of Kapitza and Allen and Misener on the one hand, and Keesom and MacWood on the other, make it clear that the classical Euler/Navier-Stokes hydrodynamics are incapable of describing the dynamical behavior of He II.

The thermal properties of He II turned out to be even more striking than the viscous properties. The specific heat was observed to be discontinuous at the lamba point[27] and the thermal conduction appeared to become infinite below T_λ.[28] In fact, temperature gradients in the liquid disappear below T_λ and it does not boil. The first recorded observation of the cessation of boiling at T_λ appeared in 1932[29] but its significance was not appreciated at that time.

An observation by Allen and Jones in 1938 gave another graphic demonstration of the unusual thermal properties of He II.

> "Observations were being made on the flow of liquid helium
> II through a tube packed with fine emery powder. The top
> of the tube [not packed with powder] was allowed to pro-
> ject several centimeters above the level of the liquid
> helium bath, and an electric pocket torch was flashed on
> the lower part of the tube containing the powder. A stedy
> steady stream of liquid helium was observed to flow out
> of the tube as long as the powder was irradiated."[30]

This phenomena is known as the fountain or thermomechanical effect. The inverse of this experiment was performed by Daunt and Mendelssohn[31] and showed that when He II was forced to flow by gravity out of a vessel through a porous material called a superleak, the temperature of the liquid which remained in the vessel increased.

The landmark experiment of Kapitza[32] in 1941 provided a clear and quantitative unification of the previous observations and showed that (1) the fluid which passed through the superleak had zero entropy, and (2) the fluid on either side of the superleak came to mechanical equilibrium when the chemical potentials of the liquids on both sides were equal. The Third Law of Thermodynamics states that the entropy of all substances is zero at absolute zero but Kapitza showed that the entropy of the fluid passing through the superleak was zero independent of temperature as long as it was below T_λ.

C. THE TWO FLUID MODEL

In 1924 Einstein remarked[33] that for an ideal gas of identical particles having symmetric statistics (i.e. bosons) a finite fraction of the particles dropped into the ground states at low enough temperatures. F. London,[34] in 1938, proposed that the transition to He II might be understood in terms of this "Bose-Einstein condensation" and when he put the parameters of liquid helium into the theoretical expression for the transition temperature he found T_c = 3.13°K remarkably near the observed lambda temperature! At this temperature a finite fraction of the particles condense into a state of zero momentum with a de Broglie wavelength which is determined by the size of the container. The condensed particles are distributed over the excited states

9

of non-zero momentum.

Tisza[35] used the insight of London to construct a macroscopic
description of He II called the two fluid model. In this phenomeno-
logical formation, He II is considered to consist of two interpenetrating
fluid components: the superfluid component of mass density ρ_s and a
normal fluid component of density ρ_n. The two components had independent
velocity field $\vec{v}_s$ and $\vec{v}_n$ respectively. The total mass density of the
fluid is the sum of the densities of the normal and superfluid
components

$$\rho = \rho_n + \rho_s \qquad (I-1)$$

and the total max flux is

$$\vec{J} = \rho\vec{v} = \rho_n\vec{v}_n + \rho_s\vec{v}_s \qquad (I-2)$$

where $\vec{v}$ is the velocity of the center of mass.

Tisza associated the superfluid component with the Bose-Einstein
condensate and the normal component with the uncondensed fraction of
the liquid. Since the superfluid occupies a single quantum state it
contributes no entropy to the fluid. Moreover a single discrete momen-
tum state precludes the continuous degradation of momentum which would
accompany a finite viscosity. The normal component, consisting of the
fraction of the liquid distributed over the excited states, thus carries
all of the entropy and is expected to have a viscosity comparable to
that of He I. The fraction of the fluid which is in the superfluid
state, ρ_s/ρ, is expected to increase as the temperature is decreased.

It is clear that this model contains an explanation of the viscosity
paradox. In the capillary flow experiment only the superfluid is mobile
so the liquid exhibits no viscosity. The damping of the disc in the
torsional pendulum experiment was due to the drag exerted by the normal

10

component. The observed decrease in the damping as the temperature decreased is attributed in part to the decrease in the amount of normal fluid.

D. TWO FLUID HYDRODYNAMICS

The phenomenological theory that has been most succesful in describing and predicting the dynamical behavior of He II on the reversible level (i.e neglecting dissipation) was presented first by L. D. Landau in 1941. The two fluid equations can be derived from macroscopic first principles if one assumes that eight independent variables form a complete set.[36] The application of mass and entropy conservation, Newton's Laws, the First and Second Laws of Thermodynamics and Galilean relativity force a unique set of dynamical equations which can be written in the following form.[37] The equation of mass conservation is identical to that of an Euler fluid

$$\frac{\partial \rho}{\partial t} + \nabla \cdot \rho \vec{v} = 0 \qquad (I-3)$$

where ρ and $\vec{v}$ are defined in (I-1, 2).

In contrast to the Euler fluid, the equation of entropy conservation shows explicitly that the entropy is convected solely by the motion of the normal component

$$\frac{\partial (\rho s)}{\partial t} + \nabla \cdot \rho s \vec{v}_n = 0 \qquad (I-4)$$

s is the entropy per unit mass of fluid.

The three equations for the three components of momentum are again like those for an Euler fluid

$$\frac{\partial J_i}{\partial t} + \frac{\partial P_{ij}}{\partial x_j} = 0 \qquad \begin{matrix} i = 1, 2, 3 \\ j = 1, 2, 3 \end{matrix} \qquad (I-5)$$

11

except

$$P_{ij} = p\delta_{ij} + \rho_n N_{mi} N_{mj} + \rho_s N_{si} N_{sj}$$

is the moment stress tensor. r_j are the spatial coordinates, p is the

pressure and δ_{ij} is the Kronecker delta.

The remaining three equations determine the acceleration of the super-

fluid component which is driven by gradients in the chemical potential

in accordance with the results of Kapitza presented earlier in this

chapter.

$$\frac{D_s \vec{N_s}}{Dt} = \frac{\partial \vec{N_s}}{\partial t} + (\vec{N_s} \cdot \nabla)\vec{N_s} = -\vec{\nabla}\mu \quad (I-6)$$

where

$$d\mu = -s\, dT + \frac{1}{\rho} dp - \frac{\rho_n}{2\rho} d(\vec{N_n} - \vec{N_s})^2 \quad (I-7)$$

is the differential of the Gibbs thermodynamic potential.

These eight independent equations (I-3, 4, 5, 6) for the time

development of eight independent variables, in this case ρ, s, $\vec{v}_n$ and $\vec{v}_s$,

describe the flow of He II. When supplemented with equations of state

for ρ_n, ρ and μ in terms of the eight independent variables, the equa-

tions form a close description of the flow on the reversible level.

There is an important difference between the form of the equations

of state for He II and those for an ordinary fluid that should be

pointed out at this stage since it frequently plays an essential role

in the non-linear acoustical behavior of superfluids. In a classical

fluid p = p(ρ,s) but for He II

$$p = p\left[\rho, s, (\vec{N_n} - \vec{N_s})^2\right]$$

Likewise $(\vec{v}_n - \vec{v}_s)^2$ comes into the expression for ρ_n and μ for the

choice of independent variables used thus far. The quantity $(\vec{v}_n - \vec{v}_s)^2$

12

is a scalar with respect to rotations and invariant with respect to a Galilean transformation of the co-ordinates. For these reasons it has the same general properties as the usual internal variables ρ and s and appears with them in the equations of state. The dominant terms in the coupling coefficent of the mode conversion process, which generates first sound through the interaction of two second sound waves, is proportional to a thermodynamic derivative of the density taken with respect to the square of the counter-flow velocity.[38]

E.   QUANTUM MECHANICS AND THE TWO FLUID THEORY

The role of quantum mechanics in the behavior of He II was mentioned briefly in the previous discussion of the two fluid model. In any system the characteristic length which determines the role played by quantum mechanics is the de Broglie wavelength. In classical liquids this length is always shorter than the mean free path and this accounts for the classical macroscopic description. The de Broglie wavelength of the superfluid component is determined by the size of the container so for He II the scales are exchanged and the de Broglie wavelength of a macroscopic fraction of the particles is much greater than the mean free path. Under such circumstances quantum mechanical effects would be expected to dominate the behavior of the superfluid component and this has been the case with regard to the absence of entropy and viscosity. Under such circumstances one might ask where Planck's constant enters the hydrodynamical description.

When Landau presented his two fluid equations (I-3, 4, 5) he further restricted the motion of the superfluid component by postulating, without basic justification, that the superfluid velocity field is

13

irrotational, i.e.

$$\nabla \times \vec{N_s} = 0 \qquad (I-9)$$

The justification came in a comment made by Onsager at a conference in 1948,[39] when he suggested that in order to guarantee that the super-fluid wave function be single-valued, the circulation of the superfluid component ought to be quantized in units of h/m_{He}, Planck's constant divded by the mass of a single helium atom:

$$\oint \vec{N_s} \cdot d\vec{l} = n \frac{h}{m_{He}} \, ; \quad m = 0, 1, 2.. \qquad (I-10)$$

This restriction is analogous to the Bohr-Sommerfeld quantization condition on angular momentum.

Onsager further suggested that the superfluid could exist in states of non-zero circulation by introducing quantized vortex lines into the liquid. Since the cores of the vortices would consist of normal fluid, the superfluid would be multiply connected and the non-zero values of n would still be consistent with $\nabla \times \vec{v}_s = 0$.

Several experiments were performed which detected this macroscopic quantum behavior.[40-42] By far the most striking demonstration of these quantized vortex states was provided recently by Williams and Packard[43] who photographed the quantized vortex array in a rotating bucket of He II.

14

THEORY

As far as the propositions of mathematics refer to reality, they are not certain; and as far as they are certain, they do not refer to reality.

A. Einstein[45]

A. FIRST AND SECOND SOUND - LINEAR THEORY

For the discussion of wave propagation phenomenon in He II it is convenient to re-express the two fluid equations (I-3, 4, 5, 6, 7) in terms of a different set of eight independent variables: p, T, $\vec{J}$ and $\vec{A}$ where $A = (\rho_n/\rho s)(\vec{v}_n - \vec{v}_s)$. This choice is motivated because when the isobaric expansion coefficient, β_p, is zero variations in p and $\vec{J}$, the pressure and center-of-mass momentum, are zero when second sound propagates. Likewise T and $\vec{A}$, the temperature and a variable proportional to the counter-flow velocity, vanish for first sound.

$$\frac{\partial \rho}{\partial t} + \nabla \cdot \vec{J} = 0 \qquad (\text{II-1})$$

$$\rho \frac{\partial s}{\partial t} + \vec{J} \cdot \vec{\nabla} s + \nabla \cdot \frac{\rho_n \rho s^2}{\rho_m} \vec{A} = 0 \qquad (\text{II-2})$$

$$\frac{\partial J_i}{\partial t} + \frac{\partial}{\partial n_j}\left(p \delta_{ij} + \rho N_i N_j + \frac{\rho_n \rho_s}{\rho} w_i w_j \right) \qquad (\text{II-3})$$

15

$$\frac{\partial \vec{A}}{\partial t} + \vec{\nabla}\left(T + \vec{N}_m \cdot \vec{A}\right) =$$

$$+ \vec{N}_m \times \nabla \times \vec{A} + \vec{A} \times \nabla \times \vec{N}_s \qquad (\text{II-4})$$

where

$$\vec{A} = \frac{\rho_m}{s\rho} \vec{w} \qquad (\text{II-5})$$

Again s is the entropy per unit mass; ρ is the total density, equal to

the sum of the superfluid and normal fluid component densities

$\rho = \rho_s + \rho_n$; the difference between the normal and superfluid component

velocities (i.e. counter-flow) is denoted by $\vec{w}$; $\vec{w} = \vec{v}_n - \vec{v}_s$; and the

center of mass velocity is denoted by $\vec{v}$ so that

$$\vec{J} = \rho \vec{v} = \rho_s \vec{N}_s + \rho_m \vec{N}_m$$

The pressure p and temperature T are related to the chemical potential

through the basic identity discussed in (I-D)

$$d\mu = -s dT + \frac{1}{\rho} dp - \frac{\rho_m}{2\rho} d(w^2) \quad (\text{II-6})$$

In order to elucidate the response of the fluid to small disturb-

ances, the basic variables are expanded as follows

$$P = P_0 + P_1 + P_2 \qquad T = T_0 + T_1 + T_2$$
$$\vec{J} = \vec{J}_1 + \vec{J}_2 \qquad \vec{A} = \vec{A}_1 + \vec{A}_2$$

The subscript 0 denotes the constant equilibrium value and the subscript

2 denotes the second order contribution which by definition is propor-

tional to quadratic combinations of first order terms denoted by the

subscript 1.

Assuming a negligible isobaric expansion coefficient,

$\beta_p = (-1/\rho(\partial\rho/\partial T)_p,$ [46] and retaining only first order terms, (II-1,2,3,4)

become

16

$$\left(\frac{\partial \rho}{\partial \rho}\right)_T \frac{\partial P_1}{\partial t} + \nabla \cdot \vec{J}_1 = 0 \qquad \text{(II-7)}$$

$$\rho \frac{\partial S}{\partial T} \frac{\partial T_1}{\partial t} + \frac{\beta \rho S^2}{\rho_n} \nabla \cdot \vec{A}_1 = 0 \qquad \text{(II-8)}$$

$$\frac{\partial \vec{J}_1}{\partial t} + \vec{\nabla} P_1 = 0 \qquad \text{(II-9)}$$

$$\frac{\partial \vec{A}_1}{\partial t} + \vec{\nabla} T_1 = 0 \qquad \text{(II-10)}$$

where quantities without subscripts are to be evaluated at equilibrium.

Combining these equations we get two independent, uncoupled wave equations for the linear propagation of pressure and temperature.

$$\frac{\partial^2 P_1}{\partial t^2} - U_1^2 \nabla^2 P_1 = 0 \qquad \text{(II-11)}$$

$$\frac{\partial^2 T_1}{\partial t^2} - U_2^2 \nabla^2 T_1 = 0 \qquad \text{(II-12)}$$

where the speeds of first and second sound are

$$U_1 = \left[\frac{\partial P}{\partial \rho}\right]^{1/2} \qquad \text{(II-13)}$$

$$U_2 = \left[\frac{\rho_s S^2}{\rho_n \left(\frac{\partial S}{\partial T}\right)}\right]^{1/2} \qquad \text{(II-14)}$$

17

First sound in He II was observed by Findlay et al.[47] in 1938 and second sound was observed by Peshkov[48] in 1946. The temperature dependence of first and second sound is shown in Fig. 2. Between 1.1°K and 1.9°K the speed of second sound is about one-twelfth that of first sound.

If a waveguide or cavity is packed with a fine powder or other porous material, it may be possible, depending on the temperature of the He II and the flow resistance of the porous material (See III-C-4), that the normal fluid will be completely immobilized by its finite viscosity, as in the superleaks mentioned earlier, and only the super-fluid component will be free to flow. For this case v_n is set equal to zero in the two fluid equations. This reduces the number of variables from eight to five and the system is apparently overdetermined. However the superleak is assumed to be held rigidly and the momentum conservation equation (I-5) or (II-3) no longer applies since it does not include the viscous force which locks the normal component. The five remaining equations can be linearized and solved for still another propagating mode, fourth sound. The velocity of this mode is given to a good approximation by

$$ u_4 \cong \left(\frac{\rho_s}{\rho}\right)^{1/2} u_1 $$

Fourth sound was experimentally observed by Rudnick and Shapiro[49] in 1962. Its temperature dependence is also shown in Fig. 2.

Useful facts about the sound modes of He II are summarized in Fig. 3. Also included is the propagating surface wave in thin super-fluid films (7-300Å) known as third sound. Third sound has very interesting non-linear propagation characteristics[50] but their consideration is beyond the scope of this work.

18
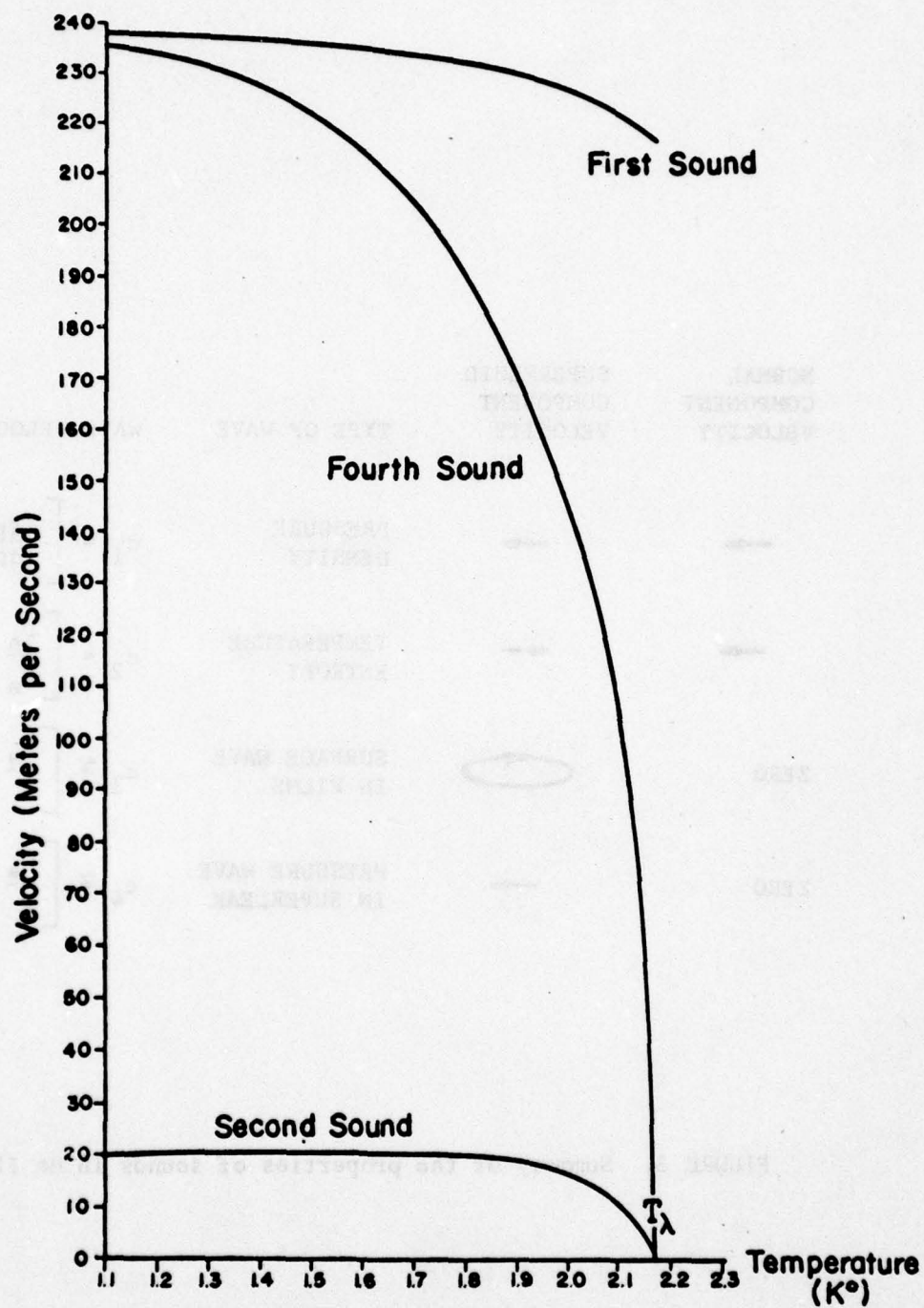
FIGURE 2. Temperature dependence of first, second and fourth sound speeds in He-II.

NORMAL COMPONENT VELOCITY	SUPERFLUID COMPONENT VELOCITY	TYPE OF WAVE	WAVE VELOCITY
→	→	PRESSURE DENSITY	$c_1 = \left[\left(\dfrac{dp}{d\rho} \right)_s \right]^{1/2}$
→	←	TEMPERATURE ENTROPY	$c_2 = \left[\dfrac{\rho_s}{\rho_n} \dfrac{Ts^2}{c_p} \right]^{1/2}$
ZERO	⟲	SURFACE WAVE IN FILMS	$c_3 \approx \left[\dfrac{\rho_s}{\rho} fd \right]^{1/2}$
ZERO	→	PRESSURE WAVE IN SUPERLEAK	$c_4 \approx \left[\dfrac{\rho_s}{\rho} c_1^2 \right]^{1/2}$

FIGURE 3. Summary of the properties of sounds in He II.

20

B. SECOND ORDER EQUATIONS FOR He II

The process begun in the previous section can be extended by collecting the terms in (II-2, 2, 3, 4) which are of second order

$$\frac{\partial \rho_2}{\partial t} + \nabla \cdot \vec{J}_2 = 0 \tag{II-15}$$

$$\rho \frac{\partial S_2}{\partial t} + \nabla \cdot \left(\frac{\rho_s \rho S^2}{\rho_n}\right)_0 \vec{A}_2 = \tag{II-16}$$
$$-\rho_1 \frac{\partial S}{\partial t} - \vec{J}_1 \cdot \vec{\nabla} S_1 - \nabla \cdot \left(\frac{\rho_s \rho S^2}{\rho_n}\right)_1 \vec{A}_1$$

$$\frac{\partial J_{2i}}{\partial t} + \frac{\partial P_2}{\partial n_i} = \tag{II-17}$$
$$-\frac{\partial}{\partial n_j}\left(\rho v_i v_j + \frac{\rho_n \rho_s}{\rho} w_i w_j\right)$$

$$\frac{\partial \vec{A}_2}{\partial t} + \vec{\nabla} T_2 = -\vec{\nabla}\left(\vec{v}_{n,1} \cdot \vec{A}_1\right) \tag{II-18}$$

As before, to obtain wave equation, we choose to eliminate ρ and s through the equations of state. To be consistent these equations must also be correct up to terms which are second order.

$$\rho_2 = \left(\frac{\partial \rho}{\partial P}\right)_T P_2 + \left(\frac{\partial \rho}{\partial T}\right)_P T_2 + \frac{1}{2}\frac{\partial^2 \rho}{\partial P^2} P_1^2$$
$$\tag{II-19}$$
$$+ \frac{1}{2}\frac{\partial^2 \rho}{\partial T^2} T_1^2 + \frac{\partial^2 \rho}{\partial P \partial T} P_1 T_1 + \frac{\partial \rho}{\partial(w^2)} w_1^2$$

21

$$S_2 = \left(\frac{\partial S}{\partial P}\right)_T P_2 + \left(\frac{\partial S}{\partial T}\right)_P T_2 + \frac{1}{2}\frac{\partial^2 S}{\partial T^2}T_1^2$$

$$+ \frac{1}{2}\frac{\partial^2 S}{\partial P^2}P_1^2 + \frac{\partial^2 S}{\partial P \partial T}P_1 T_1 + \frac{\partial S}{\partial(w^2)}w_1^2 \tag{II-20}$$

Combining (II-5, 17, 19) we get a wave equation for the second order pressure variations

$$\frac{\partial^2 P_2}{\partial t^2} - u_1^2 \nabla^2 P_2 = u_1^2\left[\frac{\partial^2}{\partial n_i \partial n_j}\left(\rho N_i N_j + \frac{P_s P_n}{\rho}w_i w_j\right)\right.$$

$$- \frac{1}{2}\frac{\partial^2 \rho}{\partial P^2}\frac{\partial^2 P_1}{\partial t^2} - \frac{1}{2}\frac{\partial^2 \rho}{\partial T^2}\frac{\partial^2 T_1^2}{\partial t^2} \tag{II-21}$$

$$\left. - \frac{\partial^2 \rho}{\partial P \partial T}\frac{\partial^2 P_1 T_1}{\partial t^2} - \frac{\partial \rho}{\partial(w^2)}\frac{\partial^2 w_1^2}{\partial t^2}\right]$$

Similarly from (II-16, 18, 19) we get a wave equation for the second order variations in temperature

$$\frac{\partial^2 T_2}{\partial t^2} - u_2^2 \nabla^2 T_2 = u_2^2 \nabla^2\left(\vec{N}_{m,1}\cdot\vec{A}_1\right) \tag{II-22}$$

$$- \left(\rho\frac{\partial S}{\partial T}\right)^{-1}\left\{\frac{1}{2}\rho\frac{\partial^2 S}{\partial P^2}\frac{\partial^2 P_1^2}{\partial t^2} + \frac{1}{2}\rho\frac{\partial^2 S}{\partial T^2}\frac{\partial^2 T_1}{\partial t^2}\right.$$

$$+ \rho\frac{\partial^2 S}{\partial P \partial T}\frac{\partial^2 P_1 T_1}{\partial t^2} + \rho\frac{\partial S}{\partial(w^2)}\frac{\partial^2 w_1^2}{\partial t^2}$$

$$\left. + \frac{\partial}{\partial t}\left[\rho_1\frac{\partial S_1}{\partial t} + \vec{J}_1\cdot\vec{\nabla}S_1 + \nabla\cdot\left(\frac{P_s \rho S^2}{\rho_n}\right)_1\vec{A}_1\right]\right\}$$

22

In (II-21, 22) all terms proportional to $(\partial\rho/\partial T)_p$ have been neglected. Unless otherwise noted, all thermodynamic derivatives are to be evaluated in the equilibrium state.

At this time it is useful to make the following remarks about how the wave equations for the second order variations of pressure and temperature (II-21, 22) differ from their first oder analogues (II-11, 12):

(i) The wave equations are no longer homogeneous, having driving terms which are proportional to quadratic combinations of the quantities characterizing the first order sound field. These quadratic terms can lead to second harmonic generation or d.c. effects and in the case of two waves of different frequencies can lead to the generation of sum and difference frequencies and wave-vectors.

(ii) The equations are no longer decoupled. Second order pressure variations, for instance, can be driven by first order pressure variations, or first order temperature variations, or a combination of first order temperature and pressure variations.

(iii) The driving terms do not necessarily lead to the generation of propagating sound modes. In fact, a propagating second order disturbance is created as a special consequence of the phase velocity of the driving terms being equal to the phase velocity of the wave operator on the right hand side of the equations.

23

These equations describe the second order pressure (temperature) swings associated with second (first) sound, the deformation of sound waves due to non-linear processes (i.e. weak shock effects)[52] and the interaction of sound waves (scattering of sound by sound), including resonant mode conversion. Although the principal interest of this work is the mode conversion process, it will be instructive to consider two other cases of experimental interest first to get a "feel" for these non-linear equations.

C. PRESSURE VARIATIONS AND DISTORTION OF SECOND SOUND

The second order pressure swings which accompany second sound can be calculated by putting $p_1 = 0$ in (II-21)

$$\frac{\partial^2 P_2}{\partial t^2} - u_1^2 \nabla^2 P_2 = u_1^2 \left[\frac{\partial^2}{\partial n_i \partial n_j} \left(\frac{\rho_s \rho_n}{\rho} w_i w_j \right) \right.$$

$$\left. \frac{1}{2} \frac{\partial^2 \rho}{\partial T^2} \frac{\partial^2 T_1^2}{\partial t^2} - \frac{\partial \rho}{\partial (w^2)} \frac{\partial^2 w_1^2}{\partial t^2} \right] \quad (\text{II-23})$$

The last two terms on the right hand side of (II-23) were omitted by Sorbello.[53] For the case of co-linear second sound they are less than 10% of the leading term but for mode conversion they are the dominant terms. Taking for example a temperature profile

$$T_1 = T' \sin(kx - \omega t)$$

$$\frac{\omega}{k} = u_2 \quad (\text{II-24})$$

and expressing w_1 in terms of T_1,[54] we obtain from (II-23)

$$\frac{\partial^2 P_2}{\partial t^2} - u_1^2 \nabla^2 P_2 = 2\alpha u_1^2 k^2 T'^2 \cos 2(kx - \omega t) (\text{II-25})$$

$$\alpha \equiv \frac{\rho_s \rho_n}{\rho} \left(\frac{\rho s^2}{\rho_n u_2}\right)^2 - \frac{u_2^2}{2} \frac{\partial^2 \rho}{\partial T^2} - u_2^2 \frac{\partial^2 \rho}{\partial(w^2)} \left(\frac{\rho s}{\rho_n u_2}\right)^2$$

The coupling coefficient, α, is plotted as a function of temperature in Fig. 4.

The particular solution to (II-25) is

$$P_2 = \frac{\frac{1}{2} \alpha T'^2 \cos 2 (kx - \omega t)}{1 - \left(\omega^2 / k^2 u_1^2\right)} \qquad \text{(II-26)}$$

If the second sound wave is propagated parallel to a free surface in the presence of a gravitational field, the second order pressure swing, p_2, will lead to a displacement of the free surface by an amount

$$\delta z = P_2 / \rho g$$

where g is the acceleration due to gravity. For temperature swings on the order of 1 m°K the level difference is about 10^{-2} cm. The displacement of the free surface will have a wavelength which is half that of the imposed second sound and will travel with the speed of second sound. Observations of the time averaged displacement of the surface due to standing waves of second sound were made by Olsen[55] and Mota et al.[56] Their observations were not quantitative so it is not possible to determine to what extent the system was adiabatic.[57]

One might expect that the coefficient α should also appear in the torque on a Rayleigh Disk placed in a second sound field. However, the presence of the disk leads to a gradient in the velocity field even in the limit of low frequency. Thus, in the experimental arrangement
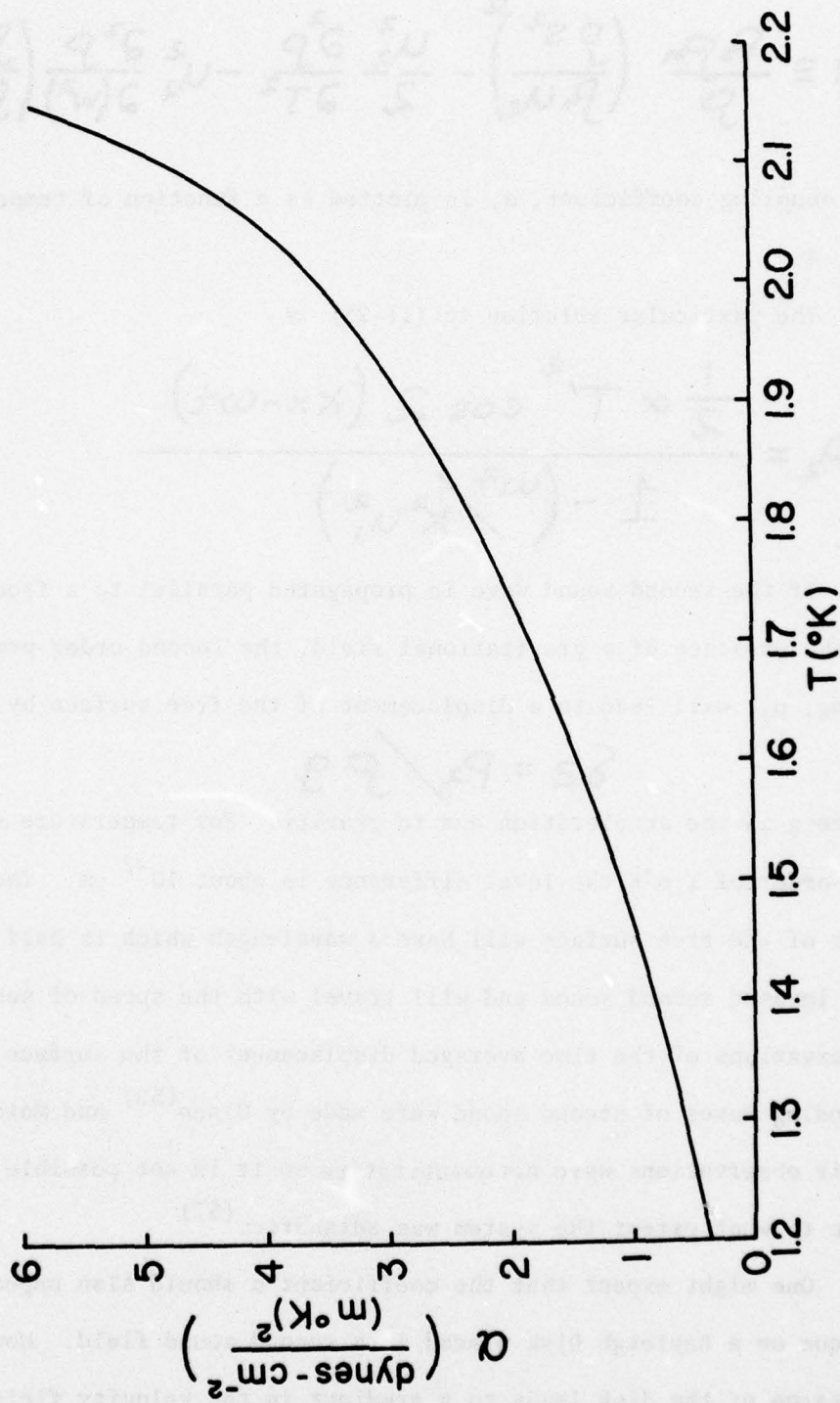
FIGURE 4. Coupling co-efficient, α, for second order pressure swings, p_2, accompanying a traveling second sound.

used,[58] the term in $w_i w_j$ can be made arbitrarily large compared to those involving time derivatives.

Equation (II-26) represents the particular solution to (II-23); it must also be supplemented by the homogeneous solutions which are arbitrary functions of $x-u_1 t$ and $x+u_1 t$ and which are determined by boundary or initial conditions. For instance, if the temperature wave is generated by heating a solid boundary at $x=0$, then $J_2(x=0)$ must vanish since there can be no mass flow normal to a solid boundary. Substitution of (II-26) into (II-17) leads to a second order mass flux given by

$$J_2(x,t) = \frac{T'^2}{2u_2} \cos(Kx - \omega t) \left\{ \frac{\alpha}{1 - \left(\omega^2 / k^2 u_1^2\right)} - \frac{\rho_s \rho_n}{\rho} \left(\frac{\rho S}{\rho_n u_2}\right)^2 \right\}$$

(II-27)

The function of $x-u_1 t$ that must be added to p_2 so that the boundary condition is satisfied is

$$P_{2h} = \frac{-u_1}{2u_2} T'^2 \cos 2\omega \left(\frac{x}{u_1} - t\right) \left\{ \frac{\alpha}{1 - \frac{\omega}{k^2 u_1^2}} - \frac{\rho_s \rho_n}{\rho} \left(\frac{\rho S}{\rho_n u_2}\right)^2 \right\}$$

(II-28)

This represents a second order first sound wave generated at the heated solid boundary.

The second order temperature swing in a second sound wave can be determined from (II-22) by letting $p_1 = 0$ and expressing v_{n1} and A_1 in terms of T_1.[54] The term in the parenthesis subscripted 1 must be evaluated with respect to first order variations of the temperature

$$\left(\frac{\rho_s \rho S^2}{\rho_n}\right)_1 = \left[\rho \left(\frac{S\rho}{\rho_n}\right)^2 \left(\frac{\partial \left(\rho_n / \rho\right)}{\partial T}\right)_P + \frac{2\rho \rho_s}{\rho_n} S \left(\frac{\partial S}{\partial T}\right)_P \right] T_1$$

27

For a place progressive wave in the x-direction (i.e.II-24) the wave equation becomes

$$\frac{\partial^2 T_2}{\partial t^2} - u_2^2 \nabla^2 T_2 = \gamma \frac{\partial^2 T_1^2}{\partial t^2}$$

$$\gamma \equiv \frac{d}{dT} \ln \left(u_2^3 \frac{\partial s}{\partial T} \right) \tag{II-29}$$

The phase velocity of the driving term on the right hand side of (II-29) is the same as the phase velocity, u_2, on the left hand side of the equation. It is clear that a solution of the type used in (II-26) "blows up" and a second particular solution must be invoked to describe the second order behavior for this "resonant" case.

$$T_2 = T_{2,h} - \frac{(x + u_2 t)\, \gamma\, \omega\, T'^2 \sin 2k(x - u_2 t)}{4 u_2}$$

where again T_{2h} is the homogeneous solution chosen to satisfy the particular boundary or initial conditions. The particular solution now grows linearly with time and eventually either a shock will form and/or this order of approximation will no longer be valid. If T_{2h} is chosen so that the initial state (t=0) is given by (II-24) then

$$T_{2,h} = \frac{(x - u_2 t)\, \gamma\, \omega\, T'^2 \sin 2k(x - u_2 t)}{4 u_2}$$

and the speed of a point of given amplitude T_1 is then found to be[59]

$$u_2 \left(1 + \gamma T_1 \right)$$

The self-scattering (i.e. distortion) coefficient γ changes sign as temperature changes. For temperatures above 1.88°K as well as the interval from 0.4°K to 0.9°K, the coefficient is negative. In the remaining temperature range, γ is positive. A graph of γ above 1.0°K

28
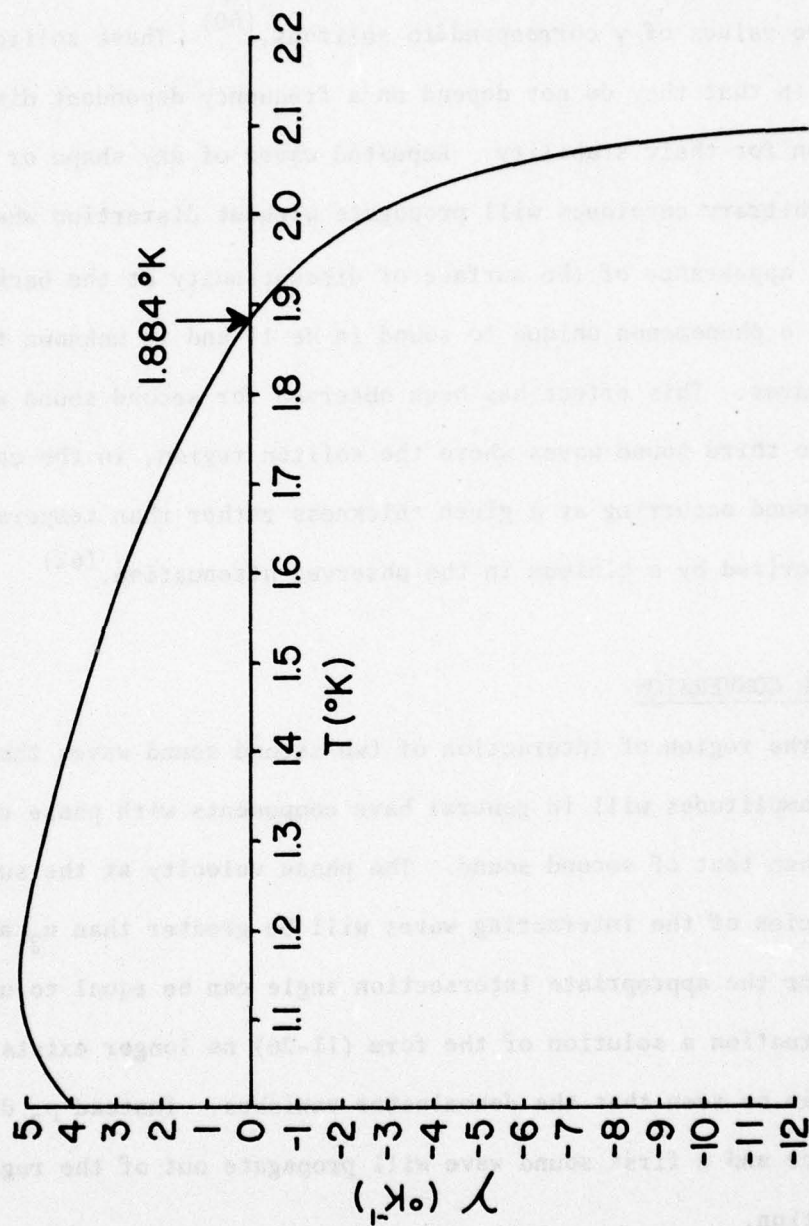
FIGURE 5. Self distortion coefficient, γ, for second sound.

is shown in Fig. 5. If a shock forms in the temperature range where γ is negative, the surface of discontinuity occurs at the <u>back</u> of the wave. For temperatures where γ is positive it arises at the front. The zero values of γ correspond to solitons.[60] These solitons are unique in that they do not depend on a frequency dependent dispersion relation for their stability. Repeated waves of any shape or packets with arbitrary envelopes will propagate without distortion when $\gamma=0$.

The appearance of the surface of discontinuity at the back of the wave is a phenomenon unique to sound in He II and is unknown for normal sound waves. This effect has been observed for second sound waves[61] and also third sound waves where the soliton region, in the case of third sound occurring at a given thickness rather than temperature, is characterized by a minimum in the observed attenuation.[62]

D. <u>MODE CONVERSION</u>

In the region of interaction of two second sound waves the product of the amplitudes will in general have components with phase velocities other than that of second sound. The phase velocity at the sum of the frequencies of the interacting waves will be greater than u_2 and, in fact, for the appropriate intersection angle can be equal to u_1. For this situation a solution of the form (II-26) no longer exists for p_2, as it can be seen that the denominator vanishes. Instead p_2 displays a resonance and a first sound wave will propagate out of the region of interaction.

If ω, $\vec{k}$ and ω', $\vec{k}$ are the frequencies and wave vectors of the two second sound waves, then the condition that must be satisfied in order that they generate a first sound resonance is

30

$$U_{ph} = \frac{\omega + \omega'}{|\vec{k} + \vec{k'}|} = U_1 \qquad (\text{II-30})$$

For the experimental situation to be described in the following chapters, the two interacting second sound waves have frequencies which are equal. To calculate the strength of a generated first sound wave in terms of the amplitude of two intersecting second sound waves of equal frequency we take

$$\vec{W_1} = W' \left\{ \left[\text{EXP} \left(i\, \vec{k} \cdot \vec{R} - i\omega t \right) \right] \hat{k} \right.$$
$$\left. + \left[\text{EXP} \left(i\vec{k'} \cdot \vec{R} - i\omega' t \right) \right] \hat{k'} \right\}$$

where $\hat{k}$, $\hat{k'}$ are unit vectors in the directions $\vec{k}$ and $\vec{k'}$. Then

$$W_1^2 = W'^2 \left\{ \text{EXP}\, 2i\left(\vec{k} \cdot \vec{R} - \omega t \right) + \text{EXP}\, 2i\left(\vec{k'} \cdot \vec{R} - \omega t \right) \right.$$
$$\left. + 2\, \hat{k} \cdot \hat{k'}\, \text{EXP}\, i\left[\left(\vec{k} + \vec{k'} \right) \cdot \vec{R} - 2\omega t \right] \right\}$$

The first two terms lead to the deformation of the separate waves as described in (II-C). The cross term is of interest here as it drives the mode conversion process. Concentrating on the cross term, (II-21) yields

$$\frac{\partial^2 P_2}{\partial t^2} - U_1^2 \nabla^2 P_2 = U_1 W'^2 \left\{ \frac{P_n P_m}{\rho}\, 2\, (\vec{k} + \vec{k'}) \cdot \hat{k}\, (\vec{k} + \vec{k'}) \cdot \hat{k'} \right.$$
$$\left. - 8\omega^2\, \hat{k} \cdot \hat{k'} \left[\frac{\partial P}{\partial (\omega^3)} + \frac{1}{2} \frac{\partial^2 P}{\partial T^2} \left(\frac{P_n U_2}{\rho S} \right)^2 \right] \right\}$$
$$\times \text{EXP}\, i\left[\left(\vec{k} + \vec{k'} \right) \cdot \vec{R} - 2\omega t \right]$$

31

When the phase velocity on the right equals the speed of first sound, p_2 will be driven at resonance. For this simplified case the resonance condition can be expressed as

$$\frac{2\omega}{|\vec{K}+\vec{K'}|}=u_1$$

or

$$\cos\frac{\theta}{2}=u_2/u_1 \qquad\qquad (\text{II-31})$$

where θ is the angle between the intersecting second sound waves.

Inserting the resonance condition into (II-30)

$$\frac{\partial^2 p_2}{\partial t^2}-u_1^2\nabla^2 p_2=-\beta K^2 u_1^2 {W'}^2 \text{EXP}\left[i(\vec{K}+\vec{K'})\cdot\vec{R}-2i\omega t\right]$$

$$\qquad\qquad (\text{II-32})$$

$$\beta\equiv 8u_2^2\left\{\frac{\rho_n\rho_s}{\rho u_1^2}\frac{u_2^2}{u_1^2}-\left(1-2\frac{u_2^2}{u_1^2}\right)\left[\frac{\partial\rho}{\partial(w^2)}+\frac{1}{2}\frac{\partial^2\rho}{\partial T^2}\left(\frac{\rho_n u_2}{\rho S}\right)\right]\right\}$$

Fig. 6 is a graph of the relevant thermodynamic terms in β as a function of temperature at the vapor pressure.

If the angle of interaction is chosen so that the resultant first sound wave travels along the x-axis and we let $p_2(x=\ )=0$, then a zero solution to (II-32) is

$$P_2=\beta K^2\frac{x\,u_1{W'}^2}{4i\omega}\text{EXP}\frac{2i\omega}{u_1}(x-u_1 t) \qquad (\text{II-33})$$

This represents a propagating first sound wave generated by the interaction of two second sound waves with an amplitude proportional to the distance from the source, the frequency and square of the amplitude of the generating second sound wave and the value of the coupling coefficient, β.

32
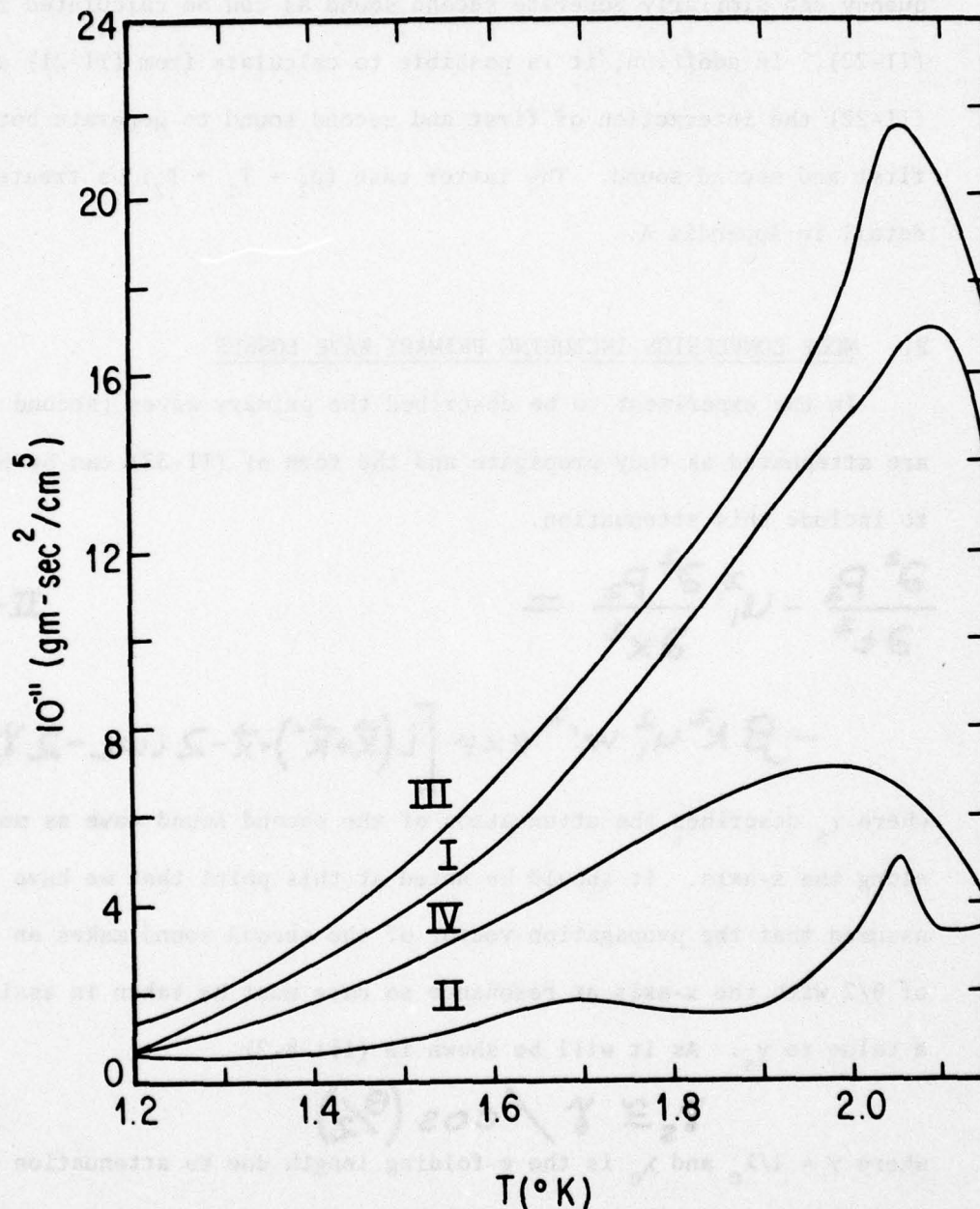
FIGURE 6. The temperature dependence at the vapor pressure of the thermodynamic quantitites determining the resonant mode conversion of second sound to first sound. (I) $\partial \rho / \partial w^2$; (II) $(1/2)(\partial^2 \rho / \partial T^2)(\rho_n u_2 / \rho s)^2$; (III) I + II. Shown for reference is (IV) $\rho_s \rho_n / \rho u_1^2$, which can play a role in the distortion of the free surface due to second sound propagation but must be multiplied by the small factor u_2^2 / u_1^2 before comparison with the other terms for the mode conversion under consideration.

33

Two first sound waves interacting through their difference frequency can similarly generate second sound as can be calculated from (II-22). In addition, it is possible to calculate from (II-21) and (II-22) the interaction of first and second sound to generate both first and second sound. The latter case $(p_1 + T_1 \rightarrow T_2)$ is treated in detail in Appendix A.

E. MODE CONVERSION INCLUDING PRIMARY WAVE LOSSES

In the experiment to be described the primary waves (second sound) are attenuated as they propagate and the form of (II-32) can be modified to include this attenuation.

$$\frac{\partial^2 P_2}{\partial t^2} - u_1^2 \frac{\partial^2 P_2}{\partial x^2} = \qquad \text{II-34)}$$

$$-\beta k^2 u_1^2 w'^2 \exp\left[i\left(\vec{k}+\vec{k}'\right)\cdot\vec{x} - 2i\omega t - 2\gamma_s x\right]$$

where γ_s describes the attenuation of the second sound wave as measured along the x-axis. It should be noted at this point that we have assumed that the propagation vector of the second sound makes an angle of $\theta/2$ with the x-axis at resonance so care must be taken in assigning a value to γ_s. As it will be shown in (III-B-2)

$$\gamma_s \cong \gamma / \cos\left(\theta/2\right)$$

where $\gamma = 1/\lambda_e$ and λ_e is the e-folding length due to attenuation of the primary wave measured along the direction of the second sound propagation vector. The value of γ_s will be treated in detail in the next chapter.

With the inclusion of dissipation in (II-34) we no longer need to

34

invoke a special "resonance" solution since the denominator no longer blows up.

$$P_2 = P_{2h} - \frac{\beta k^2 w'^2 \exp\left[i(\vec{k}+\vec{k}')\cdot\vec{x} - 2i\omega t - 2\gamma_s x\right]}{\dfrac{4\omega^2}{u_1^2} + 4\gamma_s^2 - 4i|\vec{k}+\vec{k}'| - |\vec{k}+\vec{k}'|^2} \qquad \text{(II-35)}$$

At resonance the first and last terms in the denominator cancel. Again choosing p_{2h} such that $p_2(x=0) = 0$.

$$P_2 = \frac{\beta k^2 w'^2 \exp\left[i(\vec{k}+\vec{k}')\cdot\vec{x} - 2i\omega t\right]}{-4i|\vec{k}+\vec{k}'|\gamma_s + 4\gamma_s^2} \left\{1 - e^{-2\gamma_s x}\right\} \qquad \text{(II-36)}$$

For the experimental situation of interest $|\vec{k} + \vec{k}'| \gg \gamma_s$. It can be seen that in the limit as $\gamma_s \rightarrow 0$, the solution (II-33) is recovered.

In the presence of attenuation, p_2 approaches an asymptotic value which is equal to the value given by the resonant solution (II-33) when half the e-folding length, $\lambda_s/2 = 1/2\,\gamma_s$ (see II-42), is substituted for x. This is a sensible result as it is expected that the rate of growth of p_2 should decrease as the amplitude of the primary wave decreases. The top graph on Fig. 7 shows the projection of an unattenuated second sound wave on the x-axis and below this is a representation of the linear growth of p_2 as described by (II-33). The third graph from the top represents the projection of an attenuated second wave of twice the amplitude and the lower graph shows the asymptotitc behavior described by (II-36).

The power conversion efficiency of the resonant mode conversion of second sound to first sound can be calculated from the expressions for the energy flux density of first and second sound.[67]

35
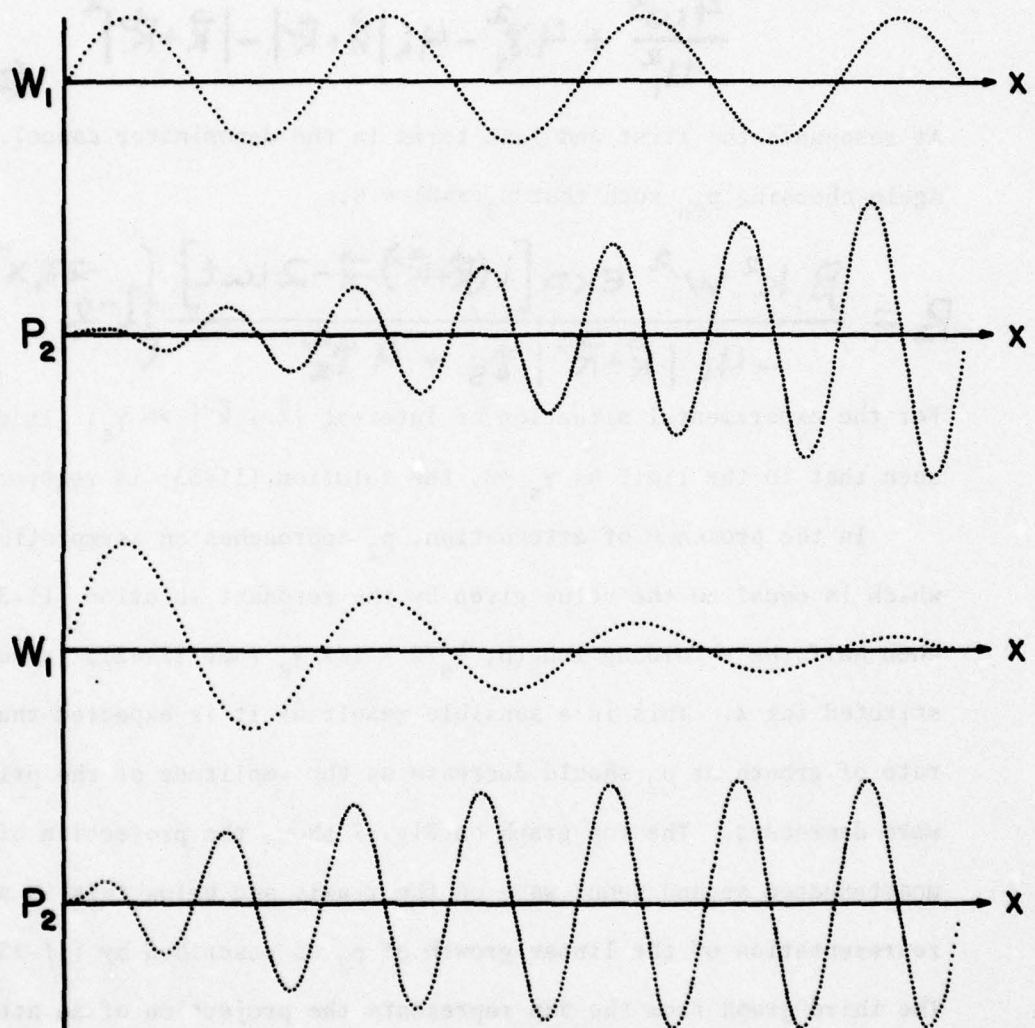
FIGURE 7. The upper two graphs schematically depict the linear growth of the mode converted signal, p_2, when driven by unattenuated second sound. The lower two show an attenuated second sound wave of twice the initial amplitude driving mode conversion toward an asymptotic limit.

$$Q_1 = \left(\rho_m N_m^2 + \rho_s N_s^2 \right) u_1 = \frac{P_2^2}{\rho u_1} \qquad (\text{II}-37)$$

$$Q_2 = \left(\rho_m N_m^2 + \rho_s N_s^2 \right) u_2 = \frac{\rho_m \rho_s}{\rho} w_1^2 u_2 \ (\text{II}-38)$$

The efficiency can be defined as the ratio of Q_1 to Q_2

$$E_{FF} \equiv \frac{Q_1}{Q_2} = \frac{\left(\frac{P_2}{W_1^2} \right) w_1^2}{\rho_s \rho_m u_1 u_2} \qquad (\text{II}-39)$$

where p_2/w_1^2 is defined by (II-36) and is a measure of the non-linear coupling of second sound to first which simultaneously takes into account the thermodynamic coupling coefficient, β (II-32); the attenuation of second sound, γ_s; and the total interaction path length, x.

CHAPTER III

EXPERIMENTAL APPARATUS

> *It has to work. After all,*
> *liquid helium is more non-*
> *linear than water.*
>
> I. Rudnick[68]

A.   UNDERLINE INTRODUCTION

The remainder of this thesis will be concerned with an experimental test of the non-linear process of resonant mode conversion of second sound to first sound as predicted by the two fluid equations (II-15-18). Based on the theoretical treatments in (II-D,E) and particularly on the intersection angle resonance condition (II-30,31) and the form of the mode converted first sound, $p_2(\beta,\lambda_s,\ k,\ w^2,\ x)$ given by (II-36), there are several features which would be advantageous in an "ideal" experiment to study the mode conversion process:

(i) Two collimated beams of high amplitude, plane wave, second sound which could interact over a distance which is comparable to their attenuation length, λ_s, and several times greater than the wavelength of the generated first sound.

(ii) A very precise way of controlling the intersection angle of the two beams.

(iii) Unidirectional propagation of both the primary and mode converted waves so complicating interference effects due to reflections need not be considered.

(iv) A means of sampling the amplitude of the mode converted signal at various distances along the interaction path.

38

(v) Transducers which can be calibrated absolutely and are sensitive only to first or second sound but not to both.

In addition, there is the physical constraint imposed by the dimensions of the dewar system which always limits the size of experiments in superfluid helium. In this laboratory the largest dewar has an inside diameter of 6 in (15.2 cm).

The use of a waveguide of rectangular cross-section operating in its lowest non-plane wave mode fulfills the first two requirements of the "ideal" experiment. Coiling the waveguide into a spiral as shown in Fig. 8 allows an interaction path of up to 149 cm within the constraints imposed by the dewar dimensions. The plate also shown in Fig. 8 forms the top surface of the waveguide and contains the transducers for detecting the pressure and temperature oscillations within the waveguide. The design of a non-reflecting termination for first sound presents special problems that will be discussed in detail in Sec. D and led to the modification of the "ideal" strategy outlined above.

B.   HIGHER ORDER MODES IN A RECTANGULAR WAVEGUIDE

1. Mathematical Properties

The theory of sound propagation in a rectangular waveguide has been treated in detail by Rayleigh.[69] He separated the wave equation in a finite, three-dimensional rectangular enclosure and obtained the following form for the traveling wave solutions in a waveguide of rectangular cross-section by letting the enclosure extend to infinity in one dimension.

39
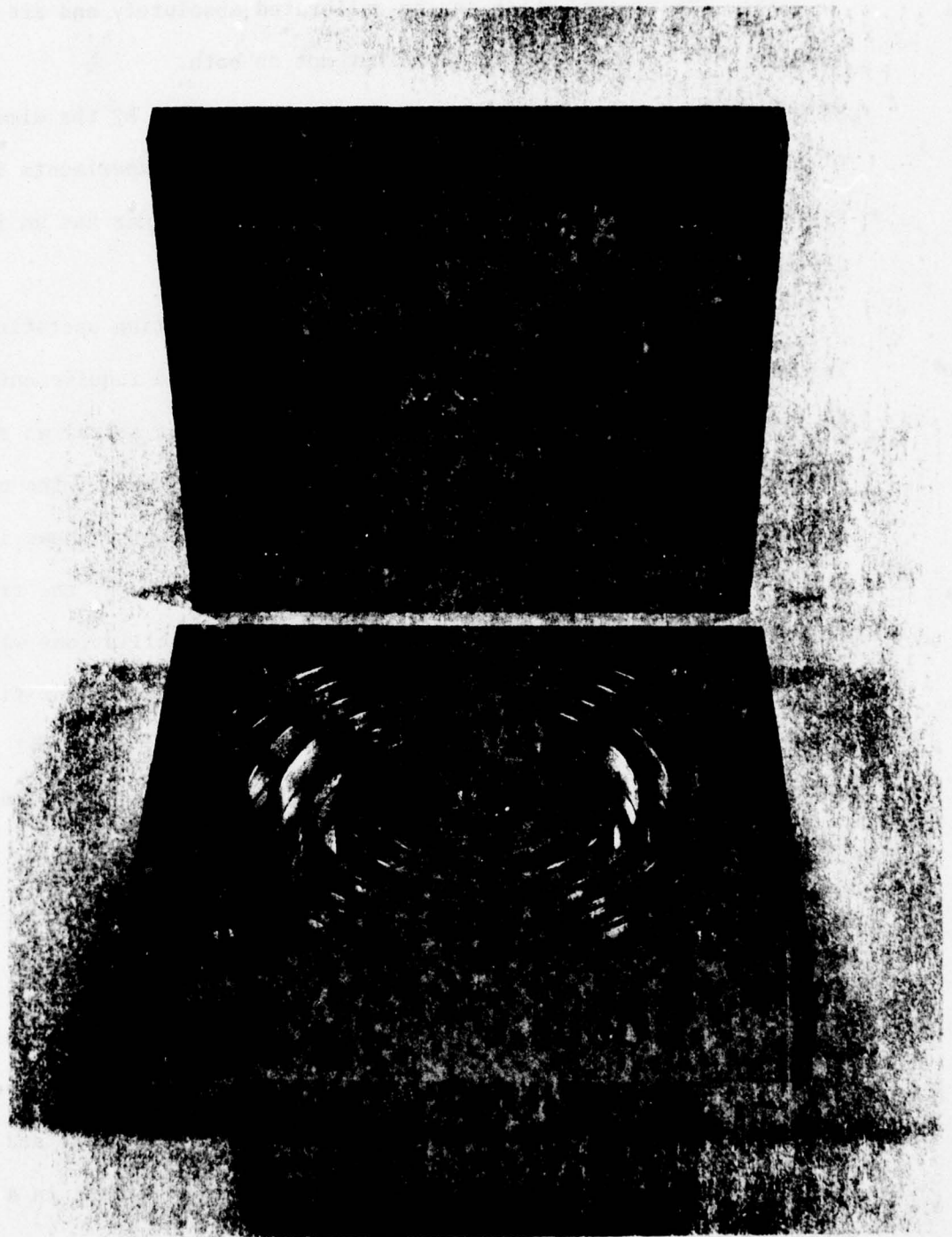
FIGURE 8.   Open view of the spiral waveguide body and transducer top-plate.

$$\phi = C_{n,m} \cos k_z z \cos k_y y \, e^{i(kx - \omega t)} \qquad (\text{III-1})$$

where
$$k_z = \frac{n\pi}{\ell_z}, \quad m = 0,1,2\ldots; \quad k_y = \frac{m\pi}{\ell_y}, \quad m = 0,1,2\ldots \quad (\text{III-2})$$

and
$$\frac{\omega^2}{c^2} = k^2 + k_z^2 + k_y^2 \qquad (\text{III-3})$$

The $C_{n,m}$ are constants which are determined by the amplitude of excitation of a particular mode (n,m). The above solution refers to a coordinate system shown in Fig. 9 where ℓ_z and ℓ_y are the height and width of the waveguide. In Rayleigh's treatment the scalar fields, ϕ, represented the velocity potential but for the case of interest here it will represent T_1 since (III-1) is a solution to the scalar wave equation (II-12) as long as the boundary conditions on all four of the waveguide walls are the same.

The lowest order mode represented by (III-1) is the (0, 0) mode which corresponds to a wave whose propagation vector, $\vec{k}$, is co-incident with the x-direction and has no amplitude variations in the x-plane, i.e. a plane wave propagating in the x-direction. The phase velocity, $u_{ph} = \omega/k$, = c and is independent of frequency. c is the thermodynamic sound speed of the medium within the waveguide which for this case is u_2. For this experiment variations in the y-direction do not occur (K_y = 0) so the next mode to consider is (1,0). Rewriting (III-3)

$$k^2 = \frac{\omega^2}{c^2} - k_z^2 \qquad (\text{III-4})$$

it is clear that for frequencies below a cut-off frequency defined by

$$\omega_{co}(m,0) = c k_z = \frac{n\pi c}{\ell_z} \qquad (\text{III-5})$$

the propagation vector k, is purely imaginary and the effects of this

41

FIGURE 9. Co-ordinate system used to describe propagation in a rectangular waveguide, ℓ_z and ℓ_y at the height (depth) and width of the waveguide.

mode below cut-off are confined to a region very close to the source of the disturbance at that frequency. At a frequency only 1% below cut-off (i.e. $1 - \omega/\omega_{co} = .01$) substitution of (III-4) into (III-1) shows that the disturbance falls to 1/e of its value at the source in a distance equal to $2.25\, \ell_z$.

The phase velocity of the higher order modes is given by

$$u_{ph} = \frac{\omega}{K} = C \left[1 - \frac{\omega_{co}^2}{\omega^2} \right]^{-1/2} \qquad (III-6)$$

and the direction of the propagation vector with respect to the x-axis, $\theta/2$, is given by

$$\cos \frac{\theta}{2} = \frac{K}{(K^2 + K_z^2)^{1/2}} = \left[1 + \frac{\omega_{co}^2}{\omega^2} \right]^{-1/2} \qquad (III-7)$$

Figure 10 is a graph of the phase velocity of the three lowest modes of the waveguide.

Since the second sound phase velocity and angle of incidence with respect to the x-axis are now functions of frequency, the mode conversion resonance condition (II-31) can be recast as a function of ω and ω_{co}

$$\frac{\omega_{mc}}{2\omega_{co}} = \left[1 - \frac{u_2^2}{u_1^2} \right]^{-1/2} \qquad (III-8)$$

where $\omega_{mc}/2$ is the frequency of the second sound at resonance. If we put $\omega_{mc}/2 = \omega_{co} + \Delta\omega$ and recall that $u_2^2/u_1^2 \ll 1$,

$$\frac{\Delta\omega}{\omega_{co}} \cong \frac{1}{2} \frac{u_2^2}{u_1^2} \qquad (III-9)$$
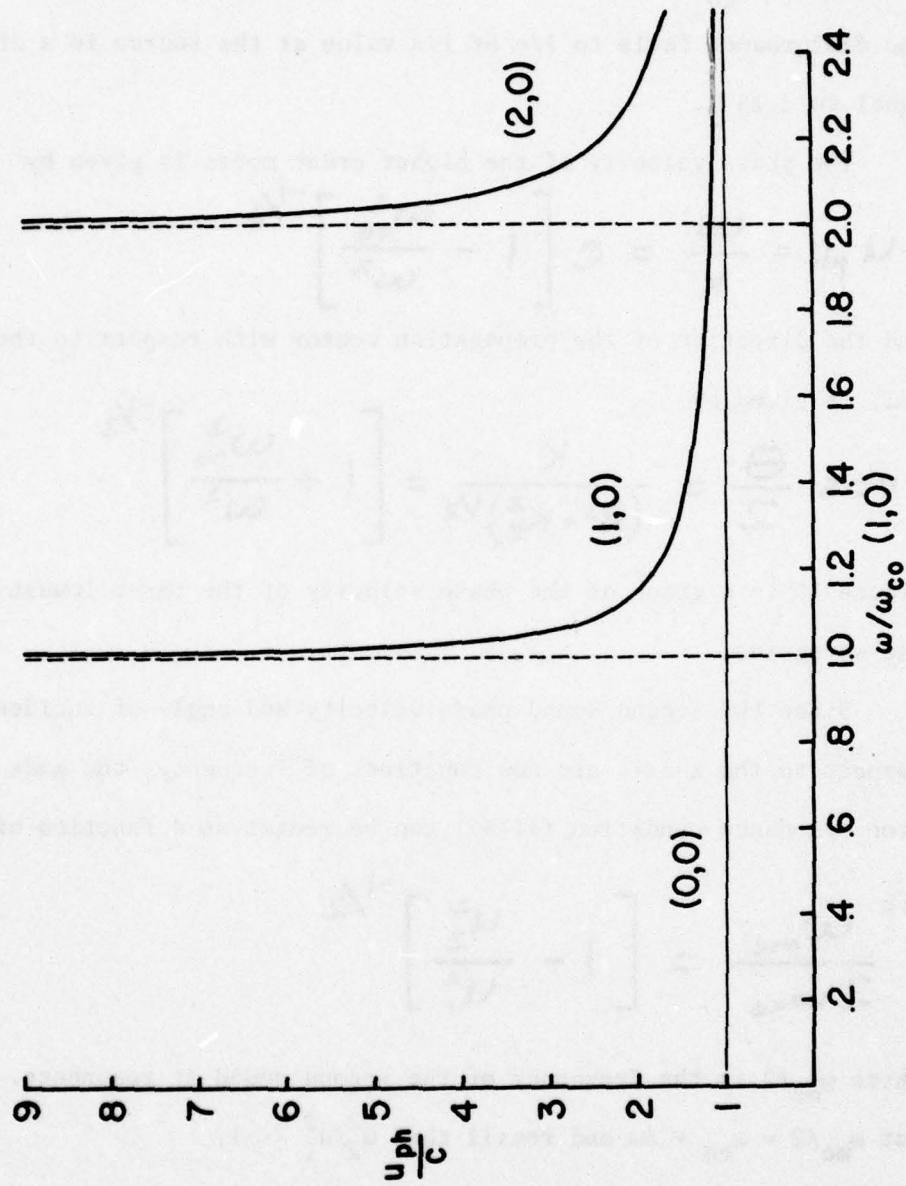
FIGURE 10. Ratio of the phase velocity, u_{ph}, to the thermodynamic sound speed, c, for the three lowest modes of the rectangular waveguide. The dashed vertical lines represent the cut-off frequencies, ω_{co}, of the first two non-planewave propagating modes.

In the region of experimental interest ($u_1/u_2 \simeq 12$), $\Delta\omega/\omega_{co} \simeq 0.35\%$ and the resonance condition is satisfied in a waveguide at about 0.35% above cut-off for the (1,0) mode. The fact that mode conversion occurs so close to cut-off places severe restrictions on the tolerable variability of the dimensions of the waveguide as will be shown in (III-B-3). Plugging (III-9) into (III-7) and dropping terms proportional to $(\Delta\omega)^2$ it can be seen that the angle of intersection condition ($\cos\theta/2 = u_2/u_1$) is also satisfied in the waveguide at the same frequency, $\omega_{mc}/2$.

The mathematical formalism in (II-D,E) was developed for two plane waves in an unconfined geometry. It is easy to show that the (1,0) mode has the same form as two intersecting infinite plane waves if the cosine term in (III-1) is expanded as the sum of complex exponentials.

$$\Phi = C_{10} \cos k_z z \, e^{i(k_x - \omega t)}$$

$$= C_{10} \frac{e^{ik_z z} + e^{-ik_z z}}{2} e^{i(k_x - \omega t)}$$

$$= \frac{C_{10}}{2} e^{i(k_x + k_z z - \omega t)} + \frac{C_{10}}{2} e^{i(k_x - k_z z - \omega t)}$$

The last line is just the representation of two infinite plane waves making an angle of $\theta/2$ with the x-axis as treated in (II-D,E), if $C_{10}/2$ is identified as w'. Figure 11 gives a schematic representation of the two plane wavefronts propagating to the right in the waveguide.

45
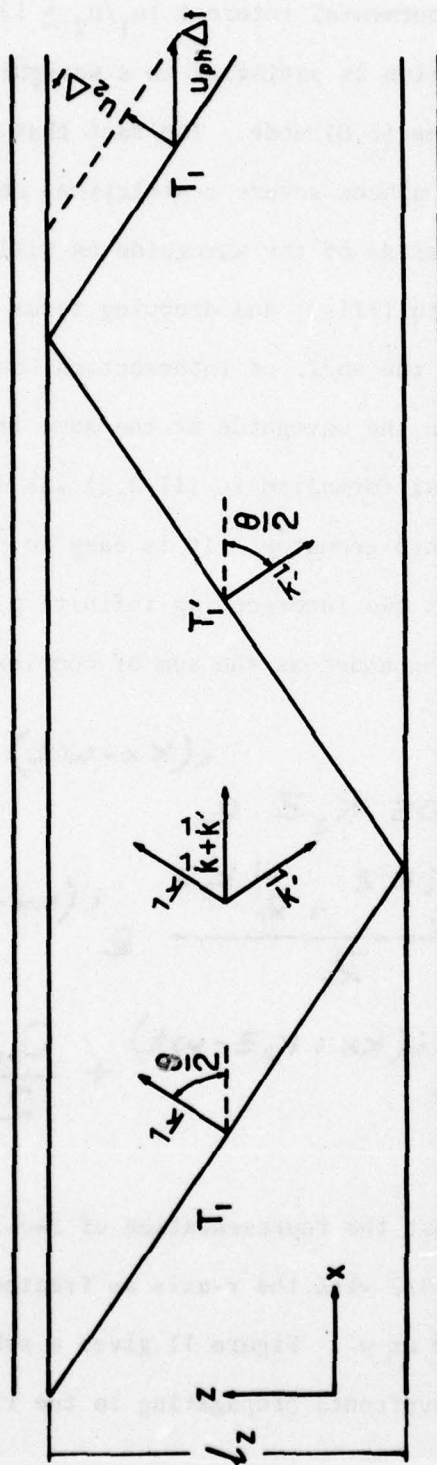
FIGURE 11. Schematic representation of two plane wavefronts, T_1 and T_1', and their wavevectors $\vec{k}$ and $\vec{k}'$, making an angle $\theta/2$ with the axis. At the center is shown the sum of the wavevectors and at the right the wavefront of T_1 is shown as a dashed line at a time Δt later than the rest of the wavefronts in the diagram. In the time Δt the wavefront has progressed a distance $u_2\Delta t$ in the direction of its wavevector. In the same time span the surface of constant phase (i.e. wavefront) has moved a distance $u_{ph}\Delta t$ along the x-direction.

2. Attenuation of the (1,0) Mode due to Viscous Losses at the Waveguide Walls

When first or second sound propagates in a waveguide, the presence of the wall surfaces introduces both attenuation and dispersion because both the normal and tangential components of the velocity of the viscous normal fluid must vanish at those surfaces. The immobilization of the normal fluid near the wall gives rise to an increase in the effective mass of the normal fluid and thus causes the velocity of second sound to decrease. Because of the waveguide dimensions and range of temperatures, this dispersion will not play a significant role in the experimental observation of resonant mode conversion. The attenuation introduced by the wall surfaces, on the other hand, is the dominant loss mechanism for the primary waves, being typically four orders of magnitude greater than the measured bulk attenuation[70] at the frequency of second sound used to produce mode conversion.

The normal fluid velocity decays exponentially to zero at the waveguide walls as a viscous diffusion wave in a characteristic distance, δ_v, given by [71]

$$\delta_v = \left[\frac{2\eta}{\rho_n \omega} \right]^{\frac{1}{2}} \qquad (\text{III-10})$$

where η is the viscosity of the normal fluid component. At $1.4°K$, $\rho_n = 0.011 \ gm/cm^3$ and if $\omega = 2\pi \times 668 \ sec^{-1}$, $\delta_v = 8.1 \ \mu m$. This effect is completely analogous to the well-known classical case of a plate executing shear oscillations in a viscous medium.[72] The presence of this viscous diffusion wave at the wall leads to gradients in the ormal fluid velocity field which, in the presence of viscosity, causes

dissipation that appears as attenuation of the primary waves.

The correct expression for the attenuation of second sound due to viscous losses at the walls of a waveguide was derived by Heiserman and Rudnick[73] for the propagation of the plane wave mode (0,0). For a rectangular waveguide of height ℓ_z and width ℓ_y their expression for the attenuation takes the form

$$\gamma = \frac{\ell_z + \ell_y}{2\,\ell_z\,\ell_y}\ \frac{\rho_s}{\rho}\ \frac{\omega\,\delta_v}{u_2} \qquad \text{(III-11)}$$

for small dispersion. The cross-sectional area of the waveguide is $\ell_z\ell_y$ and $2(\ell_z + \ell_y)$ is its perimeter.

An expression for the attenuation of the higher-order propagating mode (1,0) of second sound as measured along the x-axis is

$$\gamma_s = \frac{(u_{ph}/u_2)\,\ell_z + \ell_y}{2\,\ell_z\,\ell_y}\ \frac{\rho_s}{\rho}\ \frac{\omega\,\delta_v}{u_2} \qquad \text{(III-12)}$$

The modification of the geometric term above from its form in (III-11) can be understood by recognizing that the distance traveled by the wavefronts in the direction of their wavevectors is (u_{ph}/u_2) times greater than the distance as measured along the x-axis (see Fig. 11). The viscous losses at the side walls of the waveguide are multiplied by u_{ph}/u_2. The projection of the shear component of the normal fluid motion on the top and bottom surfaces of the waveguide is unchanged from the plane wave case so the effective value of ℓ_y is unchanged. The attenuation at resonance is given by (III-12) when $u_{ph} = u_1$.

3. Waveguide to Depth Tolerance

It is clear from (III-6) and Fig. 10 that as the cut-off frequency is approached, the rate-of-change of the phase velocity with

48

respect to frequency diverges. If we fix our attention at some frequency just above cut-off, such as the resonance frequency for the mode conversion process, then the phase velocity at that frequency becomes strongly dependent on the depth, ℓ_z, of the waveguide through the relations imposed by (III-5) and (III-6). This fact places severe restrictions on the tolerable variability in depth, $\delta\ell_z$, of the waveguide.

To determine how large $\delta\ell_z$ can become before the resonance effect is destroyed we start by considering the first sound to be generated by the sum of the non-linear interactions occurring at each point along the interaction path. The growth of the first sound wave with increasing distance from the source at resonance can be pictured in this model as the constructive interference of each "wavelet" generated by the local non-linear interaction adding in phase with all previous wavelets along the x-axis. If the phase velocity of the interacting second sound is changed slightly due to a small change in the depth of the waveguide, then the phase of the generated wavelets will no longer be locked to the growing first sound wave and in fact, if the phase differs by π to 2π, the wavelets will start to cancel the first sound generated up to that point.

To establish a quantitative conservative criterion for the limitation this effect places on the tolerable variability in waveguide depth, let θ be the phase advance of the mode converted first sound wave as measured from $x = 0$.

$$d\theta = 2\pi \frac{dx}{\lambda(x)} \qquad (\text{III-13})$$

49

$$\lambda(x) = \frac{u_{ph}(x)}{f_{mc}} \qquad (III\text{-}14)$$

where $\lambda(x)$ is the local first sound wavelength at the mode conversion

frequency, f_{mc}, and $u_{ph}(x)$ is the local phase velocity of the inter-

acting second sound determined by the local depth, $\ell_z + \delta\ell(x)$, and

equations (III-5,6). Since the effect of the second sound waves which

drive the non-linear interaction becomes small after a distance $\lambda_s =$

$1/\gamma_s$, the total phase advance up to that distance can be expressed

as

$$\theta = 2\pi \int_0^{\lambda_s} \frac{f_{mc}\, dx}{u_{ph}(x)} \qquad (III\text{-}15)$$

Assuming $u_{ph}(x)$ to be a slowly varying function of position along the

waveguide

$$u_{ph}(x) = u_1 + \left(\frac{\partial c}{\partial x}\right) x \qquad (III\text{-}16)$$

Substituting the above into (III-15) and evaluating the integral gives

the following expression for $\delta\theta$, which is the excess phase accumulated

in a distance λ_s over the amount of phase advance that would normally

occur if $(\partial c/\partial x) = 0$

$$\delta\theta = \frac{\omega_{mc}}{2u_1^2}\left(\frac{\partial c}{\partial x}\right)\lambda_s^2 \qquad (III\text{-}17)$$

The last expression can be used to set a somewhat arbitrary limit

to the rate-of-change of velocity with respect to distance along the

waveguide $(\partial c/\partial x)$ by requiring a phase shift of $\pi/2$ (90°) or less occur

50

in a distance equal to the attenuation length, λ_s, of the primary waves.

$$\frac{\partial c}{\partial x} \lesssim \frac{u_1^2}{2 f_{mc} \lambda_s^2} \tag{III-18}$$

It has been assumed that

$$\left(\frac{\partial c}{\partial x}\right) \lambda_s \ll u_1$$

The rate-of-change of u_{ph} with respect to ℓ_z can be found directly by differentiating (III-6) with respect to ℓ_z.

$$\frac{\partial u_{ph}}{\partial \ell_z} = - f_{mc} \left[\frac{u_2}{2(f_{mc} \ell_z - u_2)}\right]^{3/2} \tag{III-19}$$

The value of $\partial u_{ph}/\delta \ell_z$ is typically -2×10^6 (cm/sec)/cm. The tolerable rate-of-change of the waveguide depth per unit length in the x-direction, which will give an accumulated phase change of $\pi/2$ or less in one e-folding length of the primary second sound, can be found from (III-18, 19)

$$\frac{\partial \ell_z}{\partial x} \lesssim \frac{\left(\frac{\partial c}{\partial x}\right)}{\left(\frac{\partial u_{ph}}{\partial \ell_z}\right)} = \frac{u_1^2}{2 f_{mc}^2 \lambda_s^2} \left[\frac{u_2}{2(f_{mc} \ell_z - u_2)}\right]^{-3/2} \tag{III-20}$$

The total change in depth of the waveguide over a distance λ_s which satisfies the above criteria is given by

$$\Delta \ell_z \lesssim \frac{d \ell_z}{d x} \lambda_s \tag{III-21}$$

$\Delta \ell_z$ is plotted along with λ_s as a function of temperature in

51
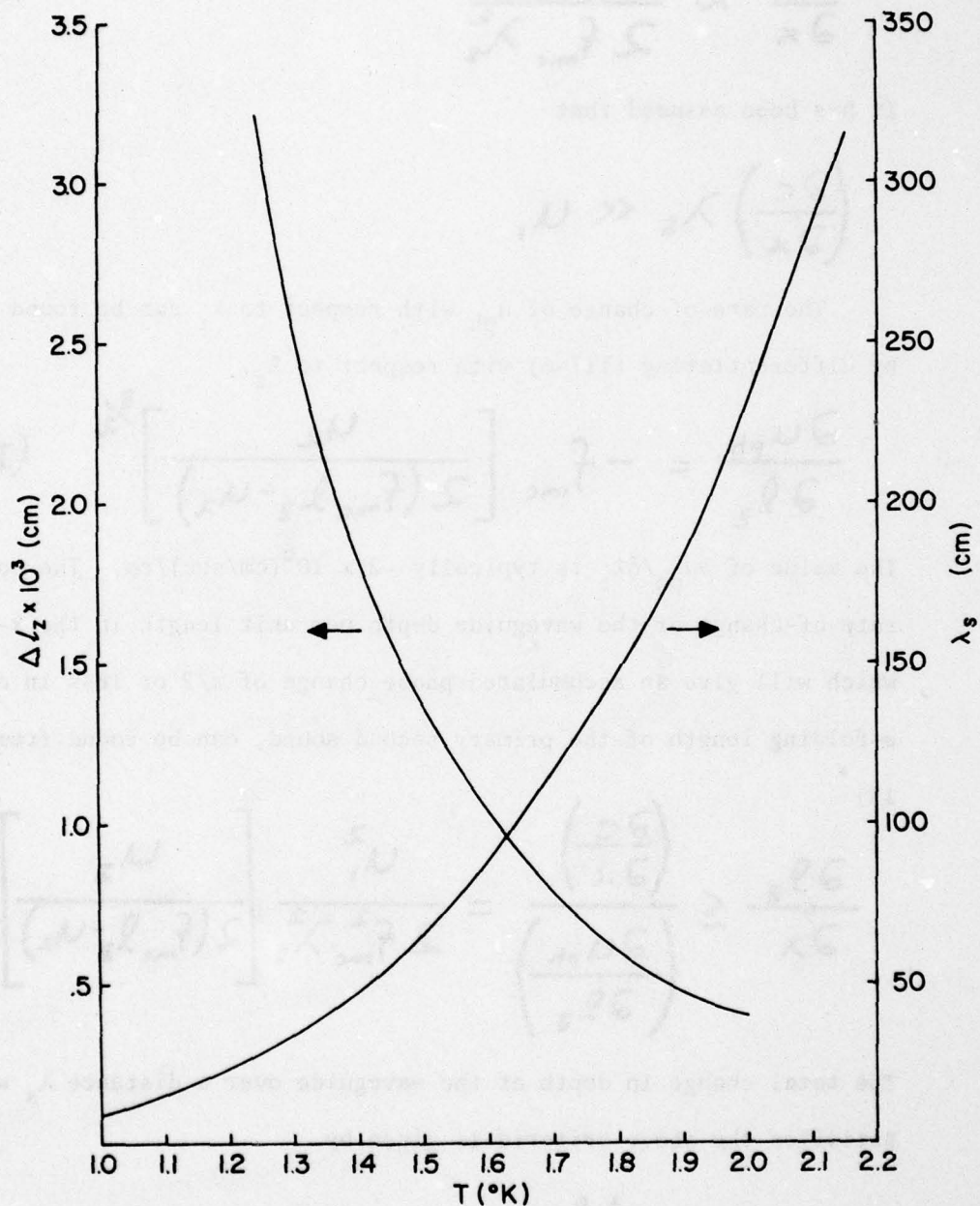
FIGURE 12. Waveguide depth tolerance, $\Delta \ell_z$, and second sound e-folding length at $f_{mc}/2$, λ_s, as a function of temperature. The vertical scale at the left refers to the curve which decreases with increasing temperature. The vertical scale on the right refers to the curve which increases with temperature.

52

Fig. 12 for the dimensions of the waveguide used in these experiments (see III-C-1). Referring to Fig. 12 it can be seen that in order to work at temperatures up to about 1.7°K the total systematic change in the depth of the waveguide, $\Delta \ell_z$, can only be of the order of 0.8×10^{-3} cm (.0003 in) over a distance of 115 cm. Local r.m.s. deviations in the depth should also be less than 8 μm. At lower temperatures the restriction is less stringent since the useful interaction length is shorter and the Q is lower (see III-B-4) due to the increasing attenuation of second sound with decreasing temperature. For 1.3°K, $\Delta \ell_z = 2.5 \times 10^{-3}$ cm (.001 in) over a distance of 34 cm.

4. Quality Factor of Resonant Mode Conversion in the Waveguide

To determine the quality factor of the mode conversion resonance in a waveguide, the following expression is obtained by setting the square modulus of the real part of the denominator of (II-35) equal to the square modulus of the imaginary part.

$$\frac{2\omega_{\pm}}{u_1} = |\vec{k} + \vec{k}'| \left(1 \pm \frac{4\gamma_s}{\vec{k} + \vec{k}'} \right)^{1/2}$$

$$\cong |\vec{k} + \vec{k}'| \left(1 \pm \frac{2\gamma_s}{\vec{k} + \vec{k}'} \right) \tag{III-22}$$

where it is assumed that $\gamma_s \ll |\vec{k} + \vec{k}'|$ and ω_+ and ω_- are the frequencies at which the mode converted first sound intensity has decreased by 3 dB. $|\vec{k} + \vec{k}'|$ and γ_s are both functions of ω_{co}/ω in a waveguide and this must be taken into account explicitly in the calculation of the quality factor for resonant mode conversion in a waveguide.

From the resonance condition (II-31) and the expression for the phase velocity (III-6), the magnitude of the sum wave-vector is

$$|\vec{k} + \vec{k}'| = \frac{2\omega}{u_2}\left(1 - \frac{\omega_{eo}^2}{\omega^2}\right) \qquad \text{(III-23)}$$

The expression for attenuation in the waveguide, γ_s (III-11), can be re-written as

$$\gamma_s = \Gamma\, u_{ph}\, \ell_z \left(\frac{\omega_{mc}}{2}\right)^{1/2}$$

$$\Gamma \equiv \frac{(\rho/\rho)}{2\, u_2^2\, \ell_z\, \ell_y}\left(\frac{2\eta}{\rho_m}\right)^{1/2} \qquad \text{(III-24)}$$

where it has been assumed that $\ell_y \ll (u_{ph}/u_2)\, \ell_z$. At the mode conversion frequency the ratio of those quantities is about 0.027.

Writing

$$2\dot\omega_\pm = \omega_{mc} \pm \Delta\omega \qquad \text{(III-25)}$$

and defining Q in the usual way

$$Q = \frac{\omega_{mc}}{2\Delta\omega} \qquad \text{(III-26)}$$

equations (III-23, 24) can be substituted into (II-22) and $\omega_\pm$ can be expanded. Discarding quantities which are second order in $\left[u_2^2/u_1^2\right]$ or $(2\Delta\omega/\omega_{mc})$ or products of those small quantities, the following expression results after sufficient algebraic manipulation.

$$\frac{2\Delta\omega}{\omega_{mc}} = \pm\, \frac{2\rho_a}{\rho}\, \frac{\delta_v}{\ell_y} - \frac{\left(\dfrac{\rho_a}{\rho}\,\dfrac{\delta_v}{\ell_v}\right)^2}{\left(\dfrac{u_2^2}{u_1^2} + \dfrac{2\Delta\omega}{\omega_{mc}}\right)} \qquad \text{(III-27)}$$

54

where δ_v is the viscous penetration depth defined in (III-10). Using the method of successive approximation the second term on the right hand side of (III-27) is neglected giving the following value for the quality factor in a waveguide

$$Q = \frac{\rho}{2\rho_s} \frac{\ell_y}{\delta_v} \qquad \text{(III-28)}$$

The validity of discarding the last term in (III-27) can now be justified if the following inequality proves true under the conditions where the above result is to be applied.

$$\frac{2\left(\frac{u_2^2}{u_1^2} + \frac{1}{Q}\right)}{\frac{\rho_s}{\rho} \frac{\delta_v}{\ell_y}} \gg 1 \qquad \text{(III-29)}$$

It is found that (III-29) has the value 8 at $1.2°K$ increasing monotonically to 42 at $2.0°K$ so (III-28) can be used to predict Q's in the range of experimental interest. At temperatures below $1.2°K$ the validity of this approximation, and more significantly, the assumption that $\gamma_s \ll |\vec{k} + \vec{k}'|$, starts to fail.

C. SPIRAL WAVEGUIDE

1. Construction and Depth

The spiral waveguide body shown in Fig. 8 is made out of a single 5.000 in (12.70 cm) square of 6061-T6 aluminum, 0.85 in (2.16 cm) thick. The groove was cut on a numerically controlled milling machine (Meister Engineering Corp., Pasadena, CA) with a 3/16 in (0.476 cm) end mill in several passes. The groove enters the block and runs for 2.50 in (6.35 cm) parallel to one edge of the block and then begins its

55

spiral to the center. At the start of the spiral the outside and inside radii of the groove are 2.250 in (5.715 cm) and 2.063 in (5.240 cm) respectively. The groove then makes seven complete rotations and the inner and outer radii decrease linearly with angle by .250 in (.635 cm) per revolution. The equations for the inner and outer radii of the groove, r_- and r_+, are given below in inches.

$$r_+ = 2.250 - 0.250 \frac{\theta}{360°}$$

$$r_- = 2.063 - 0.250 \frac{\theta}{360°} \qquad (\text{III-3b})$$

$$0° \leq \theta \leq 2520°$$

After the groove is cut into the block and the top-plate, driver and probe mounting holes are drilled and tapped, the top surface of the block is lapped until measurements of the groove depth yielded an overall r.m.s. deviation which did not exceed ±.0003 in (±8 µm). The depth measurements were made at 45° intervals along the spiral with a Lufkin #513 depth micrometer. The depth at each position was measured a minimum of three times with the foot of the micrometer rotated to a different orientation for each measurement. This procedure was repeated until it was certain that three or more readings agreed to within ±.0001 in. The zero reading of the micrometer was checked by placing it on a granite surface plate and it was found to be off by -.0003 in. Correcting for this zero offset, the average depth of the groove at room temperature is $\ell_z(T = 300°K) = 0.5798 \pm .0003$ in (1.473 ± .0008 cm). Using published values of the thermal expansion co-efficient of

56

aluminum[74], the depth at the temperatures of experimental interest was calculated to be $\ell_z(T = 0°K) = 1.467 \pm .0008$ cm. This last value of ℓ_z is used for all calculations involved in the experiment. The width, ℓ_y, is much less critical and when compensated for thermal contraction is $\ell_y(T = 0°K) = 0.474$ cm.

The most critical section of the groove is the beginning and in the first 12 cm the depth is constant to within ±.0001 in, that is, is constant to within the resolution of the measuring device.

2. Thermal Cross-talk through Waveguide Walls

The grooves in the spiral waveguide are separated by an aluminum wall which is 1/16 in (.16 cm) thick. A large amplitude temperature wave is to be sent through the waveguide. It is sensible to try to predict the amount of heat that will be transmitted through the wall separating adjacent waveguide sections that would show up as cross-talk. The thermal diffusion length can be calculated simply from the Fourier Heat Diffusion equation[75]

$$\rho C \frac{\partial T}{\partial t} = \kappa \nabla^2 T \qquad \text{(III-31)}$$

where κ is the thermal conductivity and C is the specific heat. The second sound which propagates down the waveguide acts as an oscillating temperature of frequency ω applied to the boundary since the specific heat of He II is much greater than that of the aluminum. If wavelike solutions to (III-31) are sought it is found that the temperature decays exponentially as a thermal diffusion wave in a characteristic distance, δ_T, called the thermal penetration depth.

57

$$\delta_T = \left[\frac{2\kappa}{\rho C \omega} \right]^{\frac{1}{2}} \qquad \text{(III-32)}$$

The length is completely analogous to the viscous penetration depth
(III-10) since the form of (III-31) is isomorphic to that of the
linearized Navier-Stokes equation.[75]

Using published values[74] for κ and C and $\omega = \omega_{mc}/2$, the value
of δ_T is about .56 cm between 1°K and 2°K. This calculation would
indicate that any oscillatory temperature variations imposed on one
face of the wall separating adjacent waveguide sections would reach
the other face diminished only by a factor of about 0.75. Having only
2.5 dB of isolation between waveguide sections would cause a hopelessly
jumbled second sound signal to propagate in the waveguide.

This intolerable situation is avoided by an effect which occurs
for heat transfer from a solid boundary in contact with He II and is
known as the "Kapitza Resistance".[76] P. Kapitza[77] discovered that
when heat is released in a solid body which is in contact with He II
there arises a constant temperature difference between the solid body
and the He II. It has been shown that discontinuity is localized to a
narrow boundary layer of the liquid whose thickness is less than 10^{-3}cm.
The value of the Kapitza resistance is defined as the ratio of the
temperature discontinuity to the heat flux and is found to increase
with decreasing temperature according to a cubic law.

This thermal boundary resistance is responsible for the abnormally
low value of the transmission co-efficient for second sound passing
through thin metallic foils observed by Osborne.[61] Khalatnikov[78]

58

has calculated the transmission co-efficient for second sound through a solid whose thickness is small compared to the thermal penetration depth and expresses the ratio of transmitted energy flux, U_3, to the incident energy flux, U_1, as

$$\frac{U_3}{U_1} = \frac{4KT^3}{\rho C u_2}\left(1 + \frac{4KT^3}{\rho C u_2}\right) \qquad (\text{III-33})$$

where $4KT^3 = 1/R_K$ and R_K is the Kapitza resistance. R_K is typically 1-10 cm^2 - °K/watt between 1°K and 2°K for most metals[76] and $\rho C u_2$ goes from 86 to 1210 watt/cm^2 - °K between 1.2°K and 2.0°K. For the waveguide wall $4KT^3/\rho C u_2 \ll 1$ and U_3/U_1 goes from .002 (-27 dB) at 1.2°K to .0004 (-34 dB) at 2.0°K so the cacophony predicted in the first part of this subsection based on classical heat transport does not occur when the Kapitza resistance is taken into account. For exactly the same reason, we were able to neglect thermal conduction losses in the expression for the attenuation of second sound due to the presence of the waveguide walls (III-12).

3. Transducer Top-plate and Assembly of the Waveguide

The top-plate which is pictured in Fig. 8 serves two functions: it seals the waveguide providing its top surface and it houses the pressure and temperature transducers used to detect first and second sound. The construction of the transducer "buttons" will be described here but their acousto-electric behavior (e.g. equivalent circuits, sensitivity, biasing, calibration, etc.) will be treated in later sections devoted specifically to transduction.

The top-plate is made from a 5.00 in (12.70 cm) square plate of

59

6061-T6 aluminum 0.50 in (1.27 cm) thick. Five holes for fastening

screws and a vent hole which is located above the end of the spiral are

drilled through the top-plate. The transducers are made by milling

.25 in (.63 cm) deep depressions in the top-plate at the desired

location and drilling and tapping to 10-32 a hole which is centered in

the depression. Fig. 13 is an exploded view of a typical transducer

and the associated "tower" which serves to make positive electrical

connection to the grounded top-plate, B, and the electrically hot

"button" A. The button is epoxied[79] into the depression and care is

taken to assure that the button is electrically insulated from the

top-plate and the epoxy does not fill the grooves of the 10-32 tapped

hole. When the epoxy has cured, the surface of the top-plate which

faces the grooves is faced-off on a lathe. Holes are drilled concentric

to the existing 10-32's into the button but not through it and tapped

to accept a 1-72 machine screw. The faced-off surface of the top-plate

is then hand-lapped to flatness with #600 grit silicon carbide coated

abrasive sheets placed on a granite surface plate. The entire top-plate

is then masked, with the exception of the button faces, which are

lightly sandblasted to improve their sensitivity when they are used as

the hot electrode in an electret microphone consisting of the button as

a backplate and aluminized teflon as the pressure sensitive diaphragm.

The electrical connections to the button and top-plate are made

by the "tower" assembly indicated in the exploded view in Fig. 13 as

parts C through G. G is a standard Microdot[80] 50-ohm bulkhead

receptacle (031-0050-0001) and F is a back-up nut. E is a 1/2 in long

brass 1-72 machine screw with the head removed and a small, 1 mm deep,

60
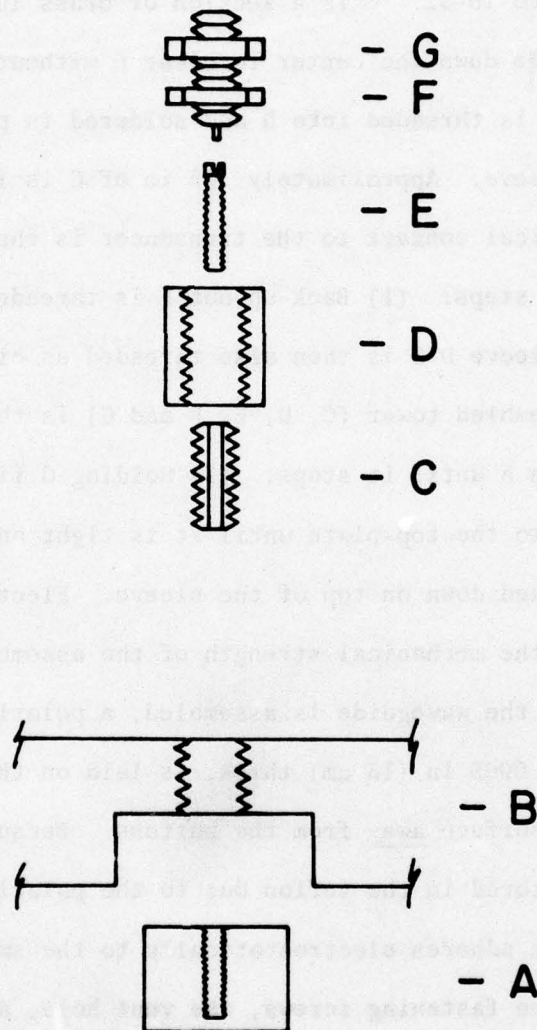
FIGURE 13. Exploded view of transducer "button" (A, B) and electrical "tower" (C, D, E, F, G) used to make electrical contact to pick-up transducer.

61

depression in the top to accept the center conductor pin of G to which it is soldered. D is a 1/4 in dia. brass rod 5/16 in. in length drilled and tapped to 10-32. C is a section of brass 10-32 threaded stock with a 1/8 in hole down the center to clear E without making electrical contact. C is threaded into D and soldered in place to make D-C into a single sleeve. Approximately 1/8 in of C is left exposed.

Electrical contact to the transducer is then made by the following sequence of steps: (1) Back-up nut F is threaded all of the way up on G and the sleeve D-C is then also threaded as close to F as possible. (2) The assembled tower (C, D, E, F and G) is then screwed into the 1-72 hole in A until it stops. (3) Holding G fixed, the sleeve D-C is threaded into the top-plate until it is tight and then the back-up nut F is tightened down on top of the sleeve. Electrical contact is excellent as is the mechanical strength of the assembled connector.

Before the waveguide is assembled, a polarized sheet of aluminized teflon,[81] .0005 in (13 μm) thick, is laid on the top-plate with the aluminized surface <u>away</u> from the buttons. Because a strong electric charge is stored in the teflon due to the polarization process,[82] the teflon sheet adheres electrostatically to the smooth top-plate surface. Holes for the fastening screws, the vent hole, and the second sound pick-up transducer are cut in the teflon with a scalpel and the sandwich consisting of the spiral waveguide body, teflon electret and top-plate is closed by tightening the five 8-32 fastening screws. Fig. 14 is a photograph of the assembled waveguide with the electrical towers in place.

62
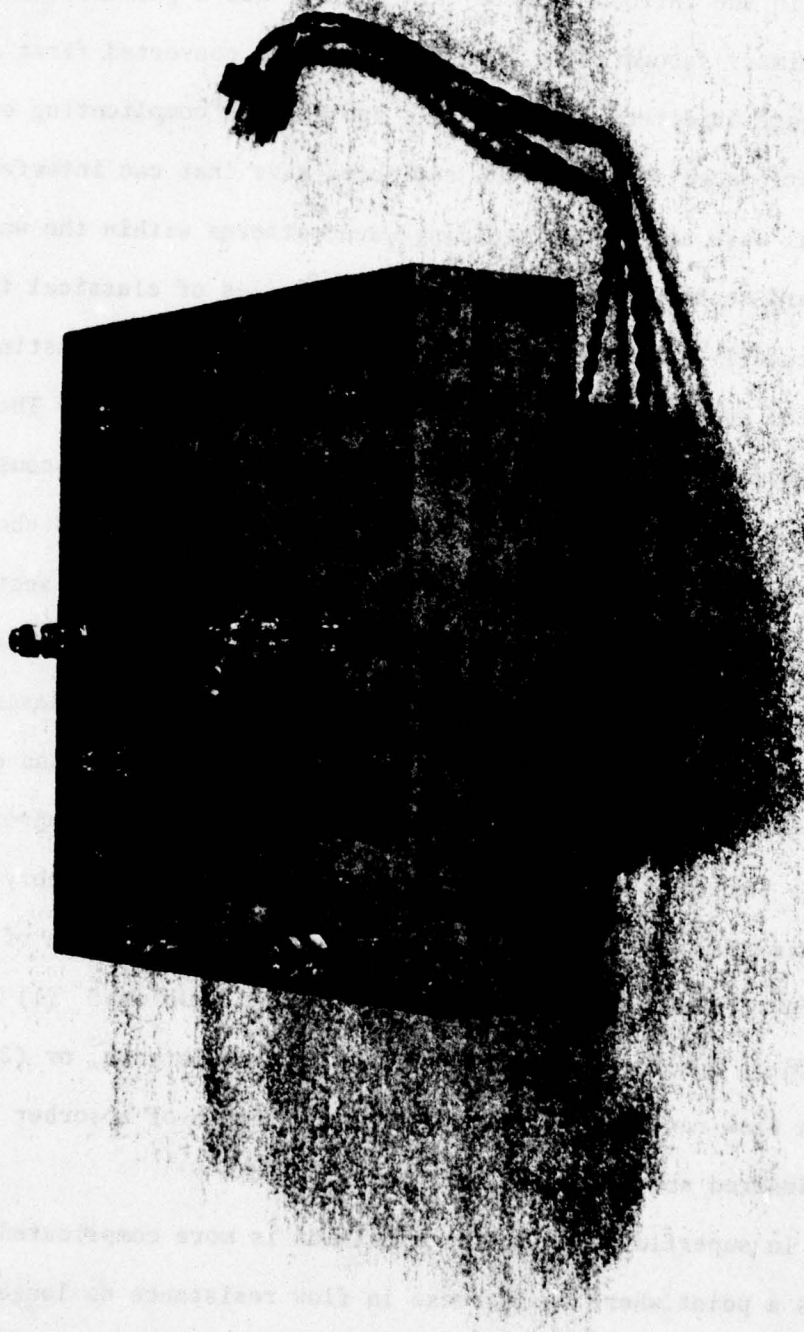
FIGURE 14. Assembled waveguide with dipole driver and "towers" in place.

63

4. Non-Reflecting Termination

One of the desirable features of the "ideal" experiment out-lined in the introduction to this chapter was a geometry in which both the primary second sound waves and the mode converted first sound waves propagate unidirectionally. This avoided the complicating effects which are introduced if there is a reflected wave that can interfere with the initial wave and create standing wave patterns within the waveguide. A standard technique used in acoustical studies of classical fluids, particularly in tubes, is the anechoic termination consisting of a wedge of porous material placed at the end of the tube. The wedge dissipates the sound energy as heat generated by the viscous effects within the pores of the material.[83] The wedge shape is chosen so that the change in impedance of the medium from the unpacked section of the tube to the end of the tube completely packed with porous material is gradual, again to avoid reflections. The mathematical description of sound propagation in a porous medium is well-known[84] and depends on the porosity, flow resistance and effective mass and compressibility of the porous material/fluid system. Armed with the theory and a means of measuring[85] or modeling flow resistance, the design of an acoustic absorber reduces to one of two well defined problems: (1) for a given length of absorber, find the optimum flow resistance, or (2) for a given flow resistance, find the minimum length of absorber to produce the desired absorption co-efficient.

In superfluid helium the situation is more complicated since there comes a point where an increase in flow resistance no longer results in an increase in viscous losses. For the case of first sound, it is

possible to increase flow resistance to the point where the normal fluid component is completely immobilized but the superfluid will still flow and fourth sound will propagate. At low temperatures very little of the energy of first sound is carried by the normal component (II-37) which is the only part that can lose energy to the absorber. For first sound the problem of designing an acoustical absorber can be stated in the following way: Given the maximum theoretical limit to the attenuation in a porous medium filled with He II, what is the minimum length of absorber which will produce the desired absorption? In this experiment at low temperatures the e-folding length for absorption of first sound can be twenty times the total length of the waveguide!

The behavior of plane waves in a porous medium field with He II can be calculated to lowest order from the two fluid equations (I-3, 4, 5, 6, 7) if a dissipative term proportional to the velocity of the normal fluid component and a flow resistance, R, is subtracted from the momentum conservation equation for the normal fluid. Small corrections due to the Kelvin drag[84] of the fluid on the porous material and a reduction in the compressibility of the helium in a solid matrix are neglected since they only make a small contribution to the velocity and are not dissipative.

$$\frac{\partial \rho}{\partial t} + \rho_s \frac{\partial N_s}{\partial x} + \rho_n \frac{\partial N_n}{\partial x} = 0 \qquad \text{(III-34)}$$

$$\frac{\partial S}{\partial t} + \frac{S}{\rho} \frac{\partial \rho}{\partial t} + S \frac{\partial N_n}{\partial x} = 0 \qquad \text{(III-35)}$$

65

$$\frac{\partial v_n}{\partial t} = -\frac{\rho_s}{\rho_m} S \frac{\partial T}{\partial x} - \frac{1}{\rho} \frac{\partial p}{\partial x} - \frac{R}{\rho} v_n \qquad \text{(III-36)}$$

$$\frac{\partial v_s}{\partial t} = S \frac{\partial T}{\partial x} - \frac{1}{\rho} \frac{\partial p}{\partial x} \qquad \text{(III-37)}$$

The only expression which has not appeared before is (III-36). It is just a combination of (I-5) and (I-6) with the addition of the dissipative term $-(R/\rho)v_n$. Assuming plane wave solutions for p and T the following dispersion relation results when the determinant of the co-efficients of the four linear differential equations above is set equal to zero[86] and $\beta_p = 0$.

$$\frac{\omega^2}{k^2} = \left\{ u_1^2 \left(1 + ir\frac{\rho_s}{\rho_m}\right) + u_2^2 (1+ir) \right.$$
$$+ \left[u_1^4 \left(1 - \frac{\rho_s^2}{\rho_m^2} r^2 + 2ir\frac{\rho_s}{\rho_m}\right) + u_2^4 (1 - r^2 + 2ir) \right.$$
$$\left. - 2 u_1^2 u_2^2 \left(1 + \frac{\rho_s}{\rho_n} r^2 + ir\left(\frac{\rho_s}{\rho_n}+1\right)\right)\right]^{\frac{1}{2}} \right\}$$
$$\times \left[1 + ir\left(\frac{\rho_s}{\rho_n}+1\right)\right]^{-1} \qquad \text{(III-38)}$$

where $r = R/\rho\omega$ is a dimensionless flow resistance parameter.

In the absence of flow resistance the + solution gives $\omega/k = u_1$ and the - solution gives $\omega/k = u_2$, corresponding to the pressure mode and the thermal mode respectively. If ω is taken real and $k = k_1 + ik_2$,

it can be seen that the thermal mode (second sound) becomes a diffusive wave (i.e. $k_1 = k_2$) of vanishing velocity as $r \to \infty$, and the diffusive behaviour sets in at lower values of r as the temperature is lowered. The pressure mode, on the other hand, becomes fourth sound when $r \to \infty$, i.e.

$$\lim_{r \to \infty} \frac{\omega^2}{k^2} = \frac{\rho_s}{\rho} u_1^2 + \frac{\rho_n}{\rho} u_2^2 = u_4^2 \qquad (\text{II-39})$$

Fig. 15 is a graph of the attenuation of the pressure mode per wave number ($k_2/k_1 = \lambda\alpha/2\pi$) as a function of the dimensionless flow resistance parameter, r, for eight temperatures from $1.0°K$ to $2.15°K$. It can be seen that there is a maximum attenuation per wavelength at each temperature and as the temperature is decreased the maximum value of attenuation is also decreased. If the phase velocity of the pressure mode, ω/k_1, were plotted, it could be seen that the peak in attenuation per wavelength occurs at the point where the velocity of the pressure mode is changing over from that of first sound to that of fourth sound.

The following example illustrates why the "ideal" of unidirectional propagation is impractical in the spiral waveguide. At $1.4°K$ the theoretically maximum value of k_2/k_1 is 1.9×10^{-2} for a flow resistance parameter equal to 0.8. If it were possible to fabricate a porous material with $r = 0.8$, first sound would have to travel 8.4 wavelengths (148 cm at f_{mc}) to suffer a decrease in amplitude of 0.37 (-8.7 dB). Since the total length of the spiral waveguide is only 149 cm, a large majority of which it is hoped would be devoted to generating the mode converted first sound rather than absorbing it, another strategy was

67
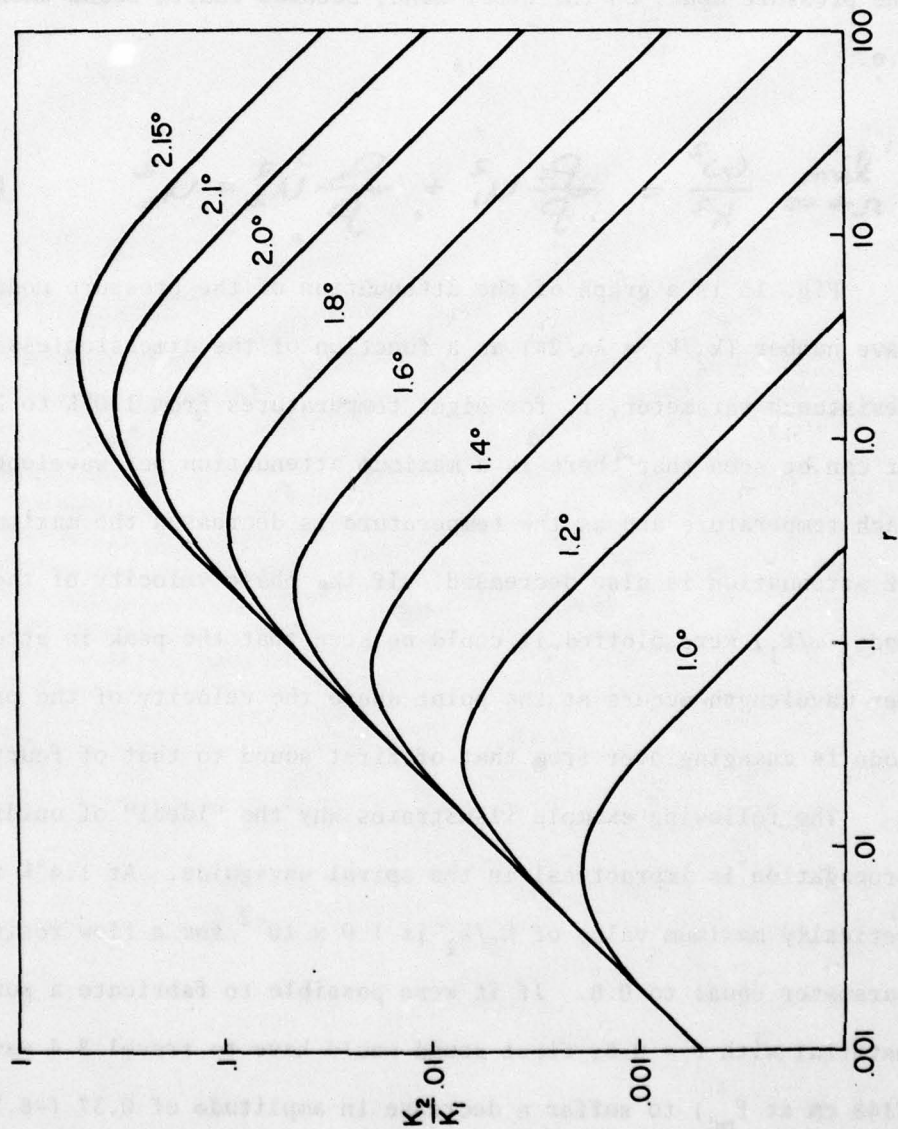
FIGURE 15. Attenuation per wavelength ($k_2/k_1 = \alpha\lambda/2\pi$) of the pressure mode (first or fourth sound) in a porous medium as a function of the dimensionless flow resistance parameter, r.

developed to allow quantitative measurement of the mode converted sound. That strategy will be described in the next section.

The absorption of second sound doesn't present the difficulties of the first sound since the attenuation length for the (1, 0) second sound mode in the waveguide, λ_s, is shorter than the length of the waveguide at temperatures and frequencies of experimental interest (see Fig. 12). Just for comparison, the attenuation of second sound at the same temperature, and in the same theoretically optimum porous material, can be calculated from (III-38). Since the frequency of second sound is half that of the mode converted first sound, the flow resistance parameter, r, is twice as large. For 1.4°K and r = 1.6, $k_2/k_1 \simeq 1$ and $\omega/k_1 = .32\ u_2 = 630$ cm/sec. This indicates that in the same medium, second sound is diffusive and has a characteristic decay length of 1 cm for a plane wave.

5. <u>If you can't beat 'em</u> ...

The theoretical treatment of the previous section was tested experimentally and the theoretical conclusions were qualitatively confirmed. The last 30 cm of the waveguide were packed with various porous materials shaped into wedges typically filling the last 15 cm of the waveguide completely and tapering out over a distance of about 15 cm. Cotton, felt, copper wool and 50 μm silicon carbide grinding compound contained in a cloth "sock" were used as porous media. Plane wave first or second sound was generated at the other end of the waveguide by transducers that will be described in subsequent sections at frequencies which were below cut-off for the propagation of any higher order modes (III-15). The amplitude of the sound field was detected

69

near the driven end of the waveguide.

Figure 16 shows raw data obtained in two separate experiments. The upper chart shows the sharp resonances of first sound at 1.40°K with a wedge absorber (50 µm silicon carbide "sock") at the end of the waveguide. The signal was detected by a pressure transducer located at 1.35 cm from the first sound driver attached to the end of the wave-guide. The vertical axis is proportional to the first sound amplitude and the horizontal axis is linear in frequency from 687 to 1749 Hz. At higher temperatures the sharpness of the resonances decreases slightly, but nothing approaching a non-reflecting termination (i.e. flat ampli-tude response as a function of frequency) was ever observed. The prospect of radiating the first sound out of the system by coupling a horn on the end of the waveguide was judged impractical due to space limitations.

The lower chart in Fig. 16 shows plane wave second sound resonances at 1.32°K, detected by a temperature transducer located at 7.4 cm from the drive in the waveguide without any porous absorbing material. The vertical axis is proportional to the second sound amplitude and the horizontal axis is linear in frequency from 474.4 to 526.1 Hz. The lower trace on the same chart is the background level received with the second sound driver turned off. With any of the porous materials in the waveguide under otherwise similar conditions, no resonant structure in the plane wave second sound signal was detectable. Thus we have an absorber which leads to progressive plane waves of second and a non-reflecting termination for higher order second sound modes. First sound, on the other hand, will be reflected except at the highest

70
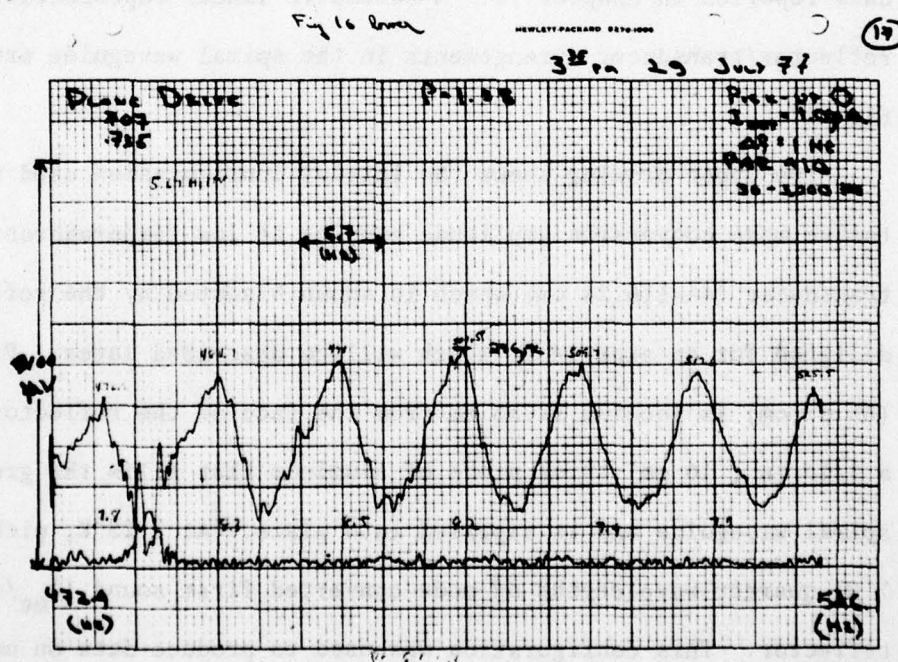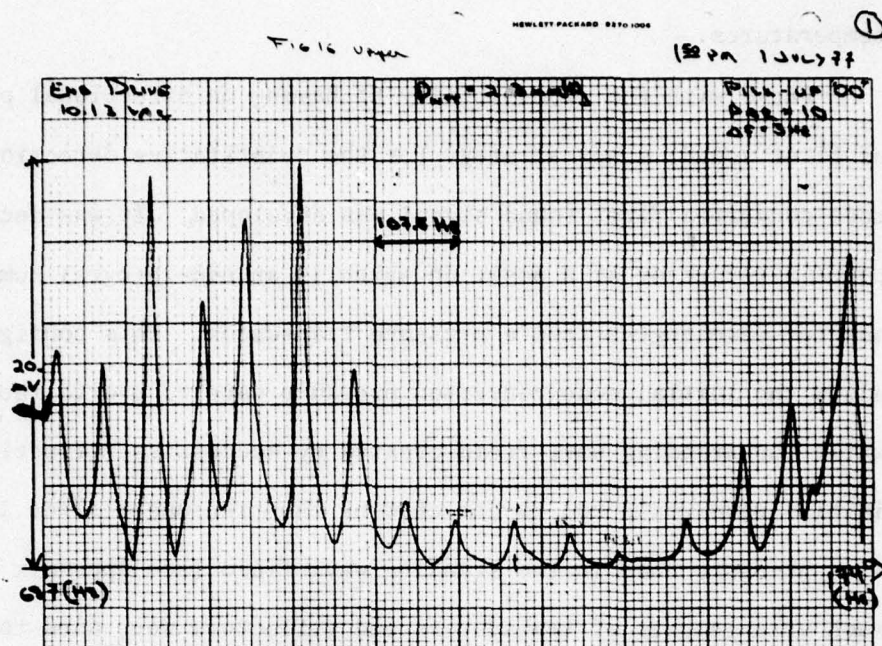
FIGURE 16. Raw data showing first sound resonances with a 50 μm silicon carbide "sock" wedge absorber at 1.4°K (upper) and second sound resonances at 1.32°K without absorber (lower).

71

temperatures.

Faced with the impossibility of having unidirectional propagation of first sound, a new strategy for the quantitative detection of the mode converted first sound signal was developed. It was decided to place a reflector at a position which is an odd-integral number of quarter-wavelengths from a pressure transducer. This configuration will allow the initial mode converted pressure wave to excite the transducer while the standing wave field created by successive reflections of the initial wave would not be detected by the transducer since it is located at a pressure node in the standing wave field (see Appendix E). Two such arrangements of transducers and reflectors were used to obtain the data reported in Chapter IV. A schematic linear representation of the reflector/transducer arrangements in the spiral waveguide are shown in Fig. 17.

The upper drawing shows the initial configuration used for quantitative mode conversion amplitude studies at low temperatures. The long transducer (4A-116.24 cm) which is shown bisected by the reflector was designed for an experiment which will be described later. Pick-up 2C (85.53 cm) is located 32.35 cm from the face of the reflector which is a 1/16 in (.16 cm) thick piece of aluminum that fills the groove in the spiral waveguide and is expoxied into place. At 1.25°K, pick-up 2C is 7.01 quarter-wavelengths of mode converted first sound ($\lambda_{mc}/4$) from the reflector. This configuration was used to produce data on mode conversion up to a temperature of 1.35°K where the location of 2C with respect to the reflector is 7.22 $\lambda_{mc}/4$.

A later version of the top-plate transducer/reflector combination
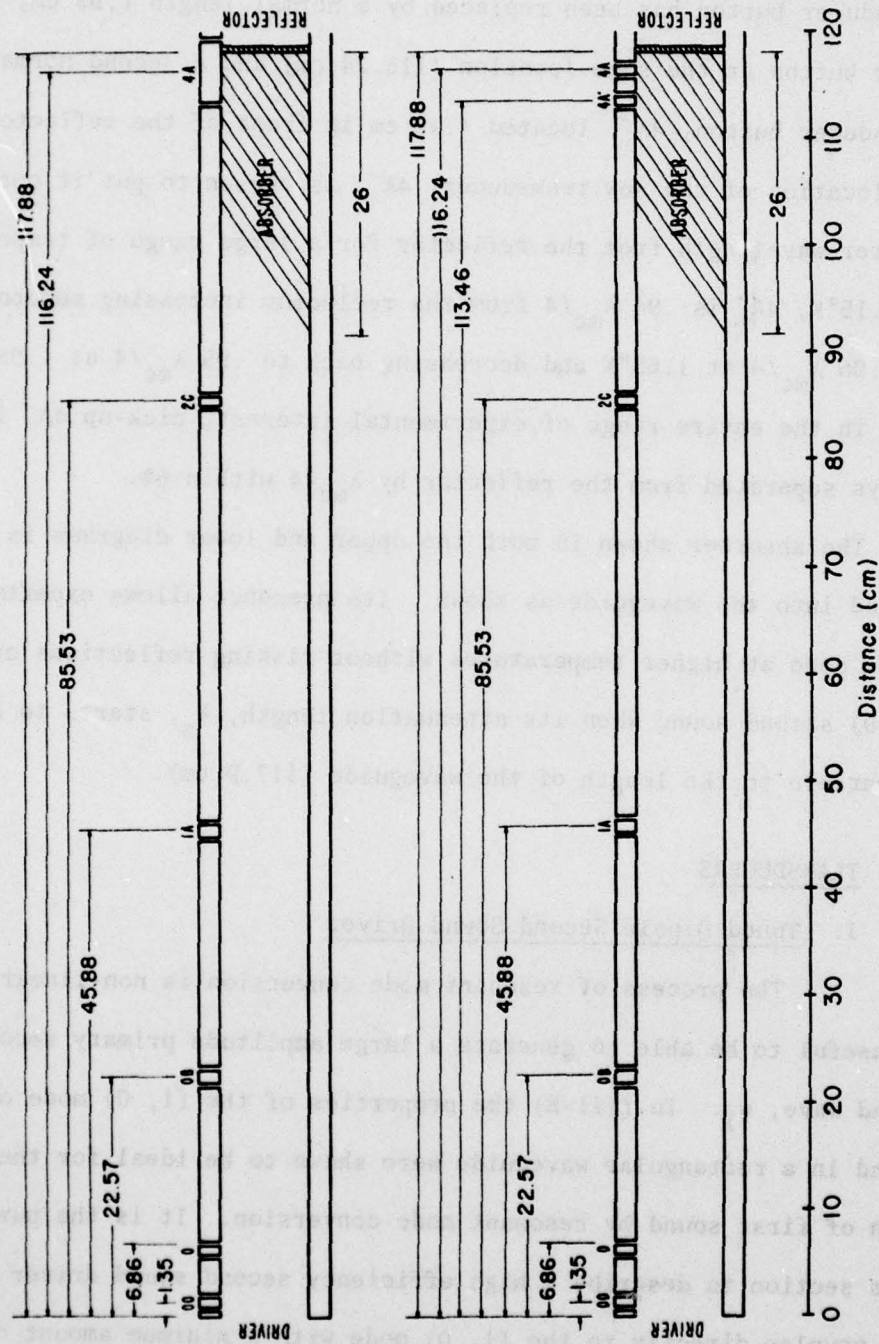
FIGURE 17. Schematic linear representation of the spiral waveguide with absorber, reflector and two different top-plate transducers. All dimensions are in centimeters.

73

is shown in the lower half of Fig. 17. Here the long (5.8 cm) 4A transducer button has been replaced by a normal length (.95 cm) transducer button at the same location (116.24 cm) and a second normal transducer button, 4A´, located 4.42 cm in front of the reflector. The location of the new transducer, 4A´, is chosen to put it one quarter-wavelength from the reflector for a large range of temperatures. At 1.15°K, 4A´ is .94 $\lambda_{mc}/4$ from the reflector increasing monotonically to 1.06 $\lambda_{mc}/4$ at 1.65°K and decreasing back to .95 $\lambda_{mc}/4$ at 1.95° so that in the entire range of experimental interest, pick-up 4A´ is always separated from the reflector by $\lambda_{mc}/4$ within 6%.

The absorber shown in both the upper and lower diagrams is cotton packed into the waveguide as shown. Its presence allows experiments to be done at higher temperatures without risking reflections of the (1, 0) second sound when its attenuation length, λ_s, starts to become comparable to the length of the waveguide (117.9 cm).

D.   TRANSDUCERS

1.   Tuned Dipole Second Sound Driver

The process of resonant mode conversion is non-linear so it is useful to be able to generate a large amplitude primary second sound wave, w_1. In (III-B) the properties of the (1, 0) mode of second sound in a rectangular waveguide were shown to be ideal for the generation of first sound by resonant mode conversion. It is the purpose of this section to describe a high efficiency second sound driver which (1) couples directly to the (1, 0) mode with a minimum amount of plane wave generation and (2) is tuned to give the maximum second sound amplitude in the +x direction for a given power input, since critical

74

velocities[87] at the heater element put a limit on the amount of power that can be put into the heaters.

From the solution to the wave equation in the rectangular waveguide (III-1), it can be seen that the temperature distribution for the (1, 0) mode in the x-plane always has a sinusoidal profile with maxima of opposite sign at the top and bottom surfaces of the waveguide. The integral of the temperature distribution in the z -direction is zero.

$$\int_{z=0}^{z=\ell_z} \phi_{10} \cos k_z z \, e^{i(kx - \omega t)} \, dz = 0 \qquad (\text{III-40})$$

That is, there is no plane wave component. Consequently, a driver which has optimum coupling to this mode should also be dipolar along the z-axis and its amplitude should have a sinusoidal "taper" which is zero at the center and 180° out-of-phase about the center line ($z = \ell_z/2$). The driver used in all of the mode conversion experiments is an approximation to that optimum configuration and is shown on the left-hand side of Fig. 18. The photograph shows the side of the driver which faces the waveguide.

Each heater element is made from a 6 in (15.2 cm) length of .0034 in dia. (86 μm) nickle-chrome resistance wire[88] which has been folded in half and twisted. The nominal resistance of the wire is 68.7 Ω/ft (2.25 Ω/cm). The twisted wire is woven through a series of #80 holes (.034 cm dia.) in a 5 mil (.013 cm) thick sheet of mylar that is slightly smaller than the waveguide groove dimensions. The #80 holes are drilled in an approximately sinusoidal pattern. The mylar sheet with the heater wire is contained in the driver housing which was machined
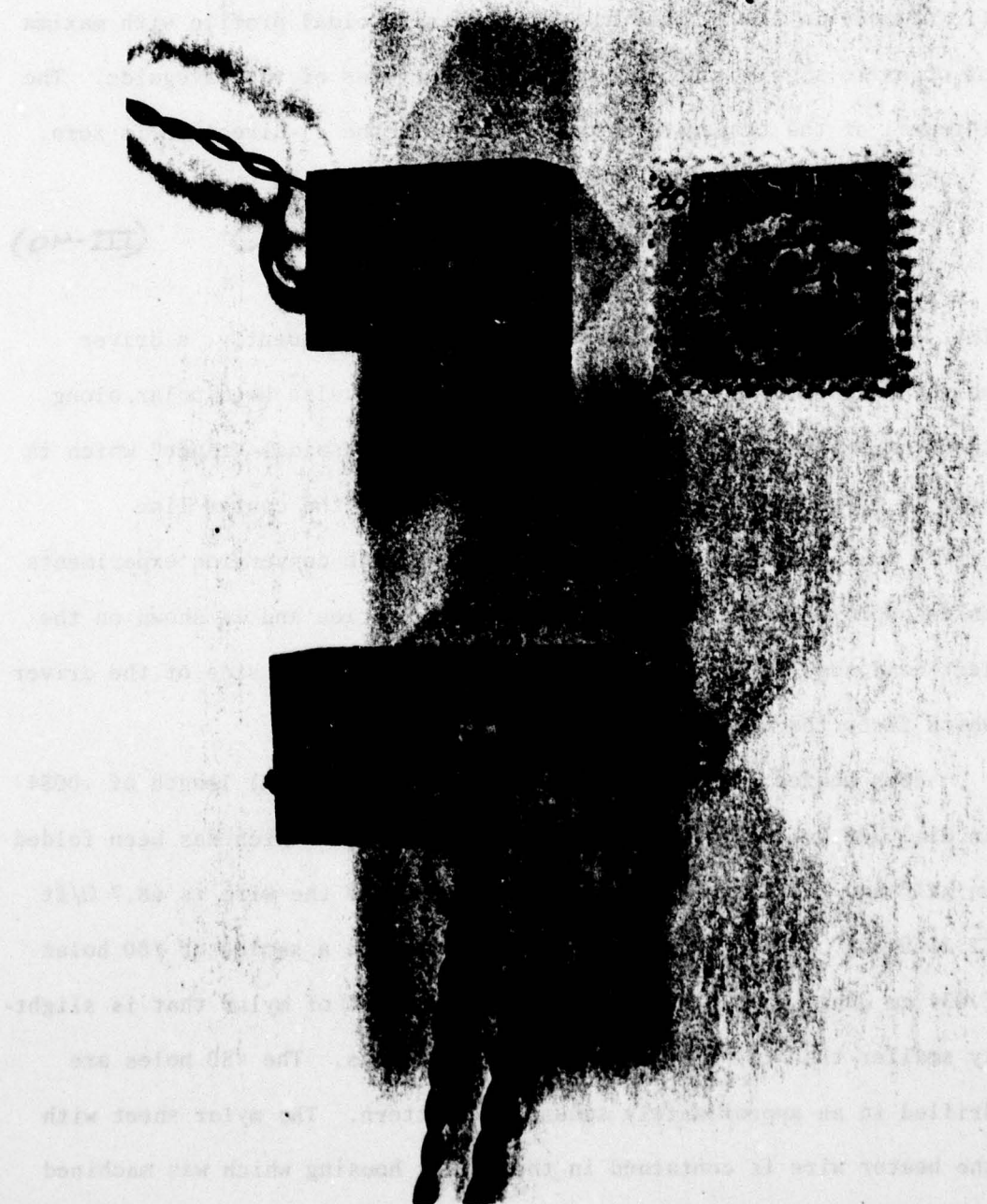
FIGURE 18. Tuned dipole second sound driver (left) and plane wave first sound driver (right).

out of a solid block of epoxy.[89] The heater wire is on both sides of the mylar sheet which is installed 0.50 cm from the place at which the driver housing joins the waveguide. The rear section of the mylar heater sheet has another 5 mil mylar sheet epoxied[79] to it and the epoxy housing which serves to divide the rear of the driver assembly into two tubes of rectangular cross-section whose length is chosen to be one quarter of a plane wave, second sound wavelength long, at the frequency of second sound that corresponds to mode conversion in the waveguide. The partition can be seen in Fig. 14. The second sound radiated off the rear of the heaters is reflected with a 180° phase reversal at the "open end" of the λ/4 tube which faces the helium bath and when it returns to the heater it adds in phase to the second sound flux in the +x direction, hence the designation, <u>tuned</u> dipole driver.

The heaters are driven by a sinusoidally time varying voltage of half the frequency of the desired second sound. One of the heaters is driven 90° out-of-phase with respect to the other. Since the heating is proportional to the square of the applied voltage (the heat flux is positive regardless of the sign of the voltage applied across the heater), the generated second sound is at twice the frequency of the applied voltage and the two halves of the dipole are 180° out-of-phase. It is clear from the trigonometric identity, $\cos^2 \omega t = (1/2)(1 + \cos 2\omega t)$, that only one half of the electrical power dissipated in the heaters goes into creating second sound at 2ω and the other half goes into d.c. heating of the fluid.

The theoretical output of the driver can be calculated from the entropy conservation equation (I-4). Since only the normal fluid

77

component can carry heat away from the driver,

$$\frac{P}{A} = N_m \rho S T \qquad (\text{III-41})$$

where P is the power dissipated in the heater and A is the area over which it is being dissipated. If the power is being dissipated uniformly over A, then v_n should be constant over the area with the exception of a thin layer near the walls of the housing within the distance of a viscous penetration depth, δ_v (III-10). For the dipole driver, the power is being dissipated over a sinusoidal profile so a power/unit length in the z-direction can be defined

$$\mu = \mu_0 \cos \frac{\pi z}{\ell_z} \qquad (\text{III-42})$$

where μ_0 is defined by the integral

$$P_{tot} = 2 \mu_0 \int_0^{\ell_z/2} \cos\left(\frac{\pi}{\ell_z} z\right) dz = \frac{2 \mu_0 \ell_z}{\pi} \qquad (\text{III-43})$$

The factor of two accounts for both heaters and P_{tot} is the total electrical power dissipated in both heaters.

The maximum power/unit area at the top and bottom of the driver is then

$$\lim_{z \to 0, \ell_z} \frac{P}{A} = \frac{\mu_0}{\ell_y} = 2.26 \frac{P_{tot}}{A} \qquad (\text{III-44})$$

Using the definition of the counter-flow velocity, $w = v_n - v_s$ and the restriction that $J = 0$ for second sound, a theoretical expression for the peak amplitude of w_1 can be expressed as

78

$$W_1 = 2.26 \frac{P_{tot}}{\rho ST} \qquad (\text{III-45})$$

where it is understood that P_{tot} is the total oscillating (not d.c.) peak (not r.m.s.) value of the electrical power dissipated in the heater.

The electrical resistance of each of the two heaters and the total resistance of the cables and probe which connect the heaters to the drive amplifiers was measured in situ using a d.c. wheatstone bridge (Leed and Northrup Co., model no. 4735) and a d.c. null volt-meter (Hewlett-Packard, model 419A). The resistance of the upper half of the driver, $R_{\ell f} = 31.5 \pm .9\Omega$, and the lower half, $R_{rf} = 30.3 \pm .9\Omega$, and the resistance of the probe and cables, $R_c = 1.9 \pm .5\Omega$. The subscripts ℓf and rf arise from the output channels of the second sound drive amplifiers (Sony, model SQR 6075) used to power the heaters: left front and right front. The total power dissipated in the lower heater is

$$P_{rf} = \frac{V_{rf}^2 \, R_{rf}}{(R_{rf} + R_c)^2} = 2.9 \times 10^5 \, V_{rf}^2 \left[\frac{ergs}{sec} \right] \quad (\text{III-46})$$

In all the experiments $V_{\ell f} = 1.05 \, V_{rf}$ so that the power dissipated in both heaters was equal.

The absolute output of the driver extrapolated back to the driver location (x = -.50 cm) was measured in the course of the mode conversion experiments by a technique to be described in a subsequent section (III-D-3) and it was found that, on the average, w_1 was proportional to

79

$V_{rf}^{1.78 \pm .14}$. Theoretically a square law would be expected on the basis of (III-45). The counter-flow velocity amplitude, w_1, for an output of 1.00 volts (r.m.s.) from the drive amplifiers connected to the heaters is plotted in Fig. 19. The circles correspond to measurements made with the second sound pick-up transducer on the older top-plate (upper drawing on Fig. 17) and the triangles correspond to measurements made using the second sound pick-up on the later top-plate (lower drawing, Fig. 17). The solid line is a least squares power law fit to all of the data points shown on the graph: $w_1 = 17.3 \ T^{-4.69}$ with a correlation co-efficient, $r^2 = .984$.[90] The dashed line is a plot of (III-45) but with a constant of 1.043 rather than the derived constant of 2.26. The lower value was obtained by finding the value of the constant which matches (III-45) to the empirical power law at 16 equally spaced points from 1.25°K to 2.00°K. The value 1.043 is the average for the 16 points and the standard deviation is .125 (12%). Based on the theoretical and measured value of the constant in (III-45) and neglecting the half of the dissipated power which went into d.c. heating, the efficiency of the dipole drive is 46%.

The dipole driver efficiency is not 100% because of some combination of the following three effects which were not considered in the efficiency calculation. First, the heating element is not a uniform surface of sinusoidal profile with a uniform heat output per unit area. It is a wire which is woven into a mylar sheet in a quasi-sinusoidal pattern. The surface area of one side of a half-heater is $.17 \pm .03 \ cm^2$. The surface area of the wire in that half-heater is only $3.5 \times 10^{-4} cm^2$. The ratio of those areas, and consequently the ratio of the average

80
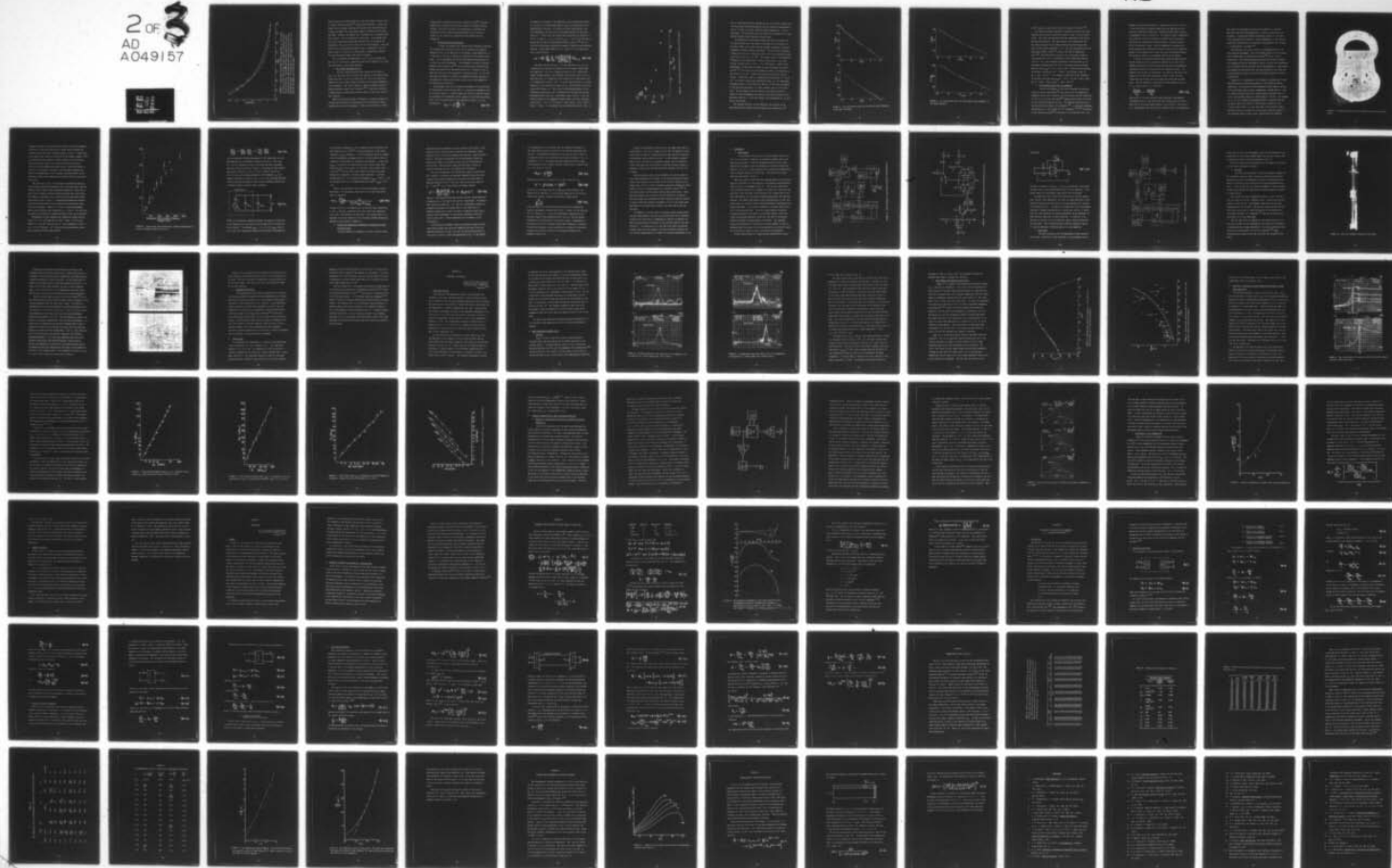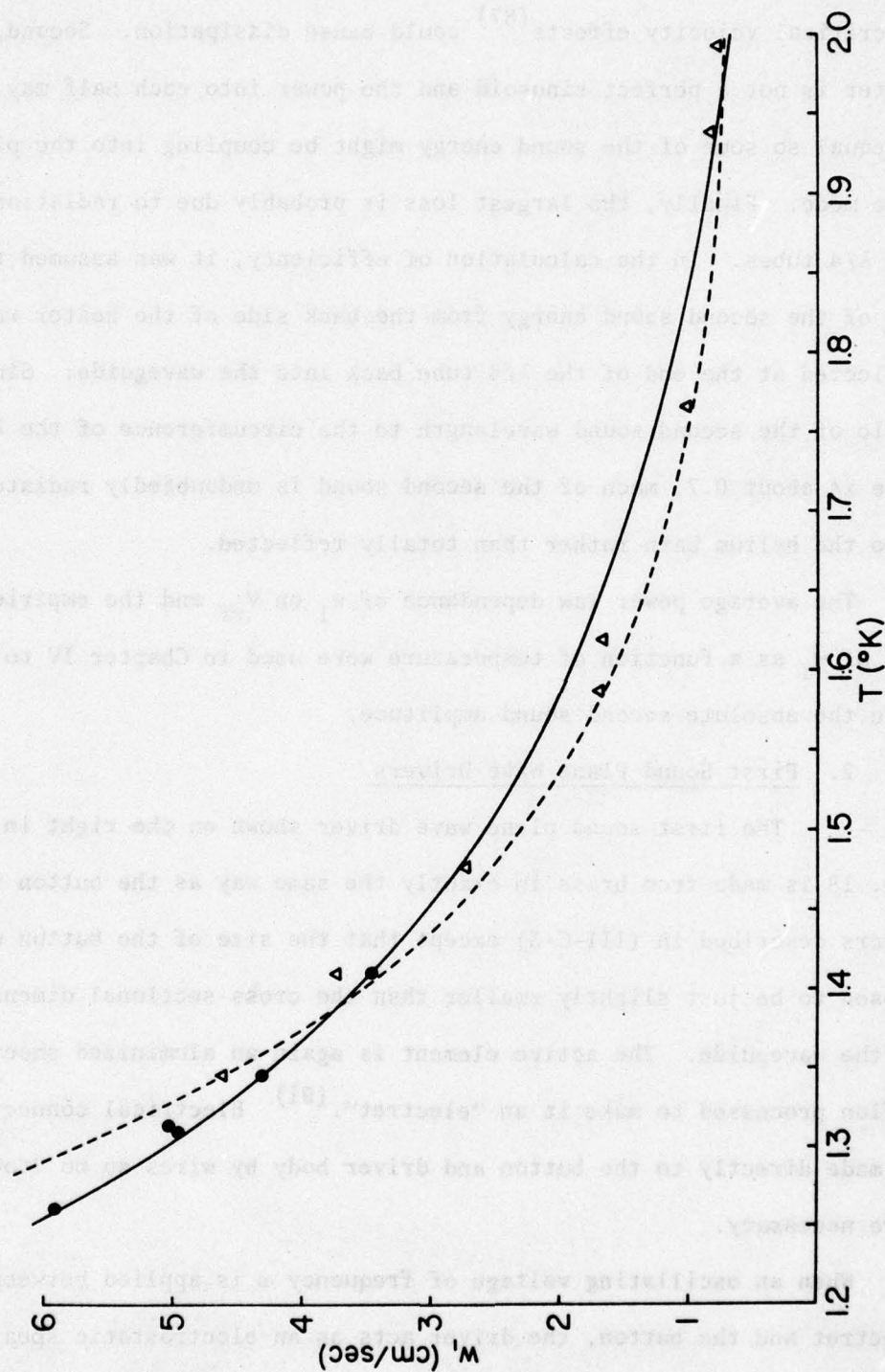
FIGURE 19. Second sound counterflow velocity amplitude, w_1, for an input of $1.00 V_{AC}$ to the dipole driver at mode conversion extrapolated back to the driver location. Circles ● represent data taken with the second sound pick-up on the older top-plate and triangles △ are data taken with the newer top-plate. The solid line is a least squares best fit to the data and the dashed line is from the theory.

81

fluid velocity to the fluid velocity at the wire surface is nearly 250, so critical velocity effects[87] could cause dissipation. Second, the heater is not a perfect sinusoid and the power into each half may not be equal so some of the sound energy might be coupling into the plane wave mode. Finally, the largest loss is probably due to radiation from the $\lambda/4$ tubes. In the calculation of efficiency, it was assumed that all of the second sound energy from the back side of the heater was reflected at the end of the $\lambda/4$ tube back into the waveguide. Since the ratio of the second sound wavelength to the circumference of the $\lambda/4$ tube is about 0.7, much of the second sound is undoubtedly radiated into the helium bath rather than totally reflected.

The average power law dependance of w_1 on V_{rf} and the empirical fit of w_1 as a function of temperature were used in Chapter IV to determine the absolute second sound amplitude.

2. First Sound Plane Wave Drivers

The first sound plane wave driver shown on the right in Fig. 18 is made from brass in exactly the same way as the button transducers described in (III-C-3) except that the size of the button was chosen to be just slightly smaller than the cross-sectional dimensions of the waveguide. The active element is again an aluminized sheet of teflon processed to make it an "electret".[91] Electrical connection is made directly to the button and driver body by wires so no "towers" were necessary.

When an oscillating voltage of frequency ω is applied between the electret and the button, the driver acts as an electrostatic speaker coupled directly into the waveguide. Since the electret has a stored

charge which is equivalent to a bias voltage 215 volts[92] the sound generated by the driver will also be ω without an external biasing voltage. The dirver was used in the experiments to determine the absorption of first sound by porous materials (III-C-5) and as a speaker in the reciprocity calibration of the pressure pick-up transducers.

3. Second Sound Pick-up Transducer

In order to determine the strength of the coupling co-efficient for resonant mode conversion, p_2/w^2, and to establish the quadratic dependence of p_2 on the amplitude of the primary second sound waves, it is necessary to be able to measure the amplitude of the primary second sound. In all experiments the second sound amplitude was measured by a carbon resistance thermometer. The thermometer was made by spraying graphite from an aerosal can[93] over the epoxy-filled insulation gap between the top-plate and transducer button "O" a distance of 6.86 cm from the driver end of the waveguide as indicated in Fig. 18. The area over which the graphite is applied was sandblasted before spraying on the graphite to increase the contact surface area of the graphite to the button and the top-plate.

The principle used in the resistance thermometer for the detection of second sound is that the resistance is a function of temperature and if a constant current, I, passes through the resistor, then the changes in resistance with temperature, $\partial R/\partial T$, appear as an oscillating voltage, $\delta V(t)$, which is proportional to the temperature swings, T_1, in the following way:

$$\delta V = I \frac{\partial R}{\partial T} T_1 \qquad (III-47)$$

83

The quantity of interest is the amplitude of the counter-flow velocity, w_1, for the (1, 0) second sound mode at $\omega_{mc}/2$ at the position of the heater/dirver a distance 7.4 cm from the second sound pick-up. The value measured at the pick-up can be extrapolated back to the heater plane (x = -.50 cm) since the second sound attenuation co-efficient of the (1, 0) mode, $\gamma_s = 1/\lambda_s$, is known at $\omega_{mc}/2$. See (III-12) and Fig. 12. Taking into account the relationship between T_1 and w_1,[54] and the fact that the electronic measurement apparatus (Hewlett-Packard Spectrum Analyzer - model 3580A) measures r.m.s. values of δV, the expression for w_1 can be written

$$w_1 = \sqrt{2}\,\frac{\rho}{\rho_m}\,\frac{S}{u_2}\,\frac{\exp\left(7.4/\lambda_s\right)}{I\left(\partial R/\partial T\right)}\,\delta V_{r.m.s.} \qquad (\text{III-48})$$

The choice of bias current, I, is very important if w_1 is to be interpreted as an absolute determination of the primary second sound wave amplitude. Fig. 20 is a graph of received r.m.s. second sound signal voltage divided by the transducer bias current, $\delta V(r.m.s.)/I$ in arbitrary units, as a function of bias current for a fixed sound field at a temperature of about 1.25°K. It can be seen that $\delta V/I$ is a strong function of I for currents in excess of 2μA. Below 2μA the sensitivity levels off at about 1.8. This is due to self-heating effects on the differential resistivity, $R_d = (1/R)(\partial R/\partial T)$ and the Kapitza resistance mentioned earlier (III-C-2). Calibration curves, R(T) vs. T, for the newer top-plate in the temperature range between 1.2°K and 1.7°K gave values of $R_d = -.23 \pm .01$ °K^{-1} with I = 100μA and $R_d = -.63 \pm .01$μ°K^{-1} with I = 1.00μA. It is essential that the calibration curves, Figs. 21

84
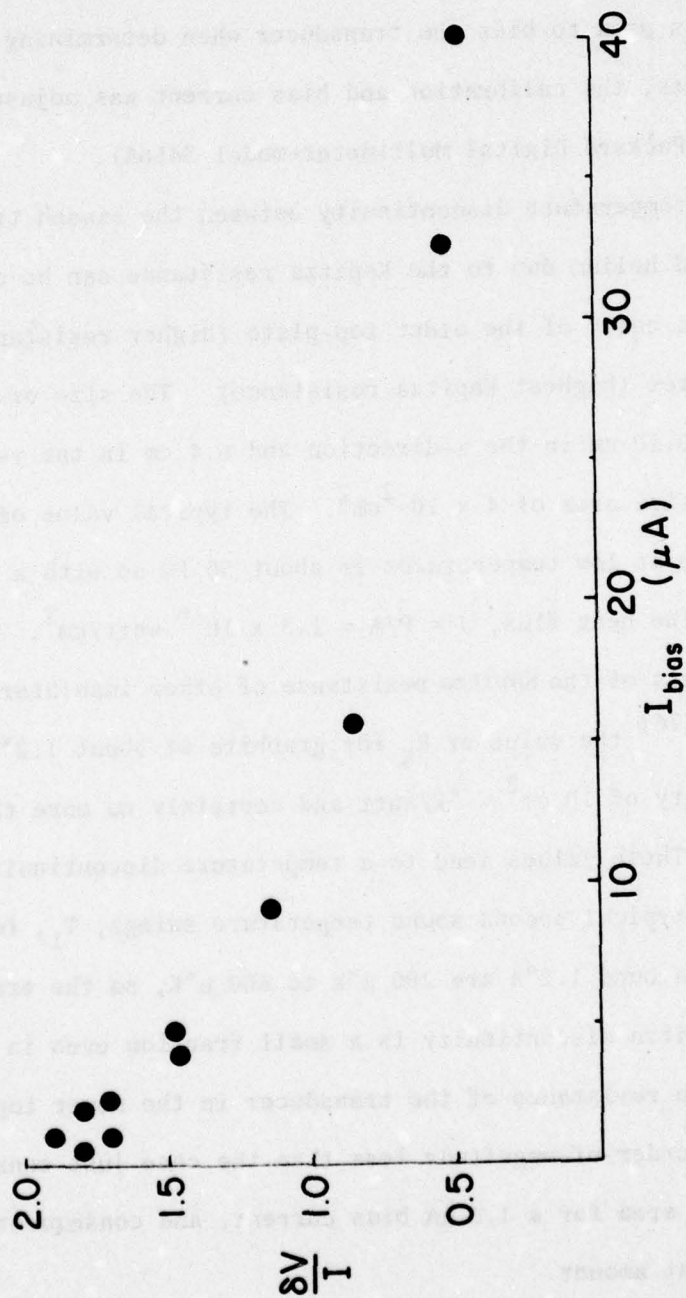
FIGURE 20. Second sound pick-up sensitivity as a function of bias current.

and 22, from which $\partial R/\partial T$ are obtained for use in (III-48), be made with the same current passing through the resistor during the measurement of R(T) as is used to bias the transducer when determining w_1. In all experiments, the calibration and bias current was adjusted to be 1.00μA (Hewlett-Packard Digital Multimeter-model 3456A).

The temperature discontinuity between the biased transducer and the liquid helium due to the Kapitza resistance can be calculated in the "worst case" of the older top-plate (higher resistance) and lowest temperatures (highest Kapitza resistance). The size of the transducer is about 0.10 cm in the x-direction and 0.4 cm in the y-direction yielding an active area of $4 \times 10^{-2} cm^2$. The typical value of the transducer resistance at low temperatures is about 50 KΩ so with a 1.0 A bias current, the heat flux, $J = P/A = 1.3 \times 10^{-6}$ watt/cm^2. Based on the measurements of the Kapitza resistance of other insulators in contact with ^{4}He,[76] the value of R_K for graphite at about 1.2°K should be in the vicinity of 10 cm^2 - °K/watt and certainly no more than 20 cm^2 - °K/watt. These values lead to a temperature discontinuity, $\Delta T \lesssim$ 10-20 μ°K. The typical second sound temperature swings, T_1, for experiments performed around 1.2°K are 250 μ°K to 800 μ°K, so the error introduced by the Kapitza discontinuity is a small fraction even in this "worst case". The resistance of the transducer in the newer top plate is almost an order-of-magnitude less than the case just considered so the power/unit area for a 1.0 μA bias current, and consequently ΔT, is also down by that amount.

The "thermal inertial" of the transducer and substrate can be neglected since the specific heat of graphite and aluminum are 10^{-4}
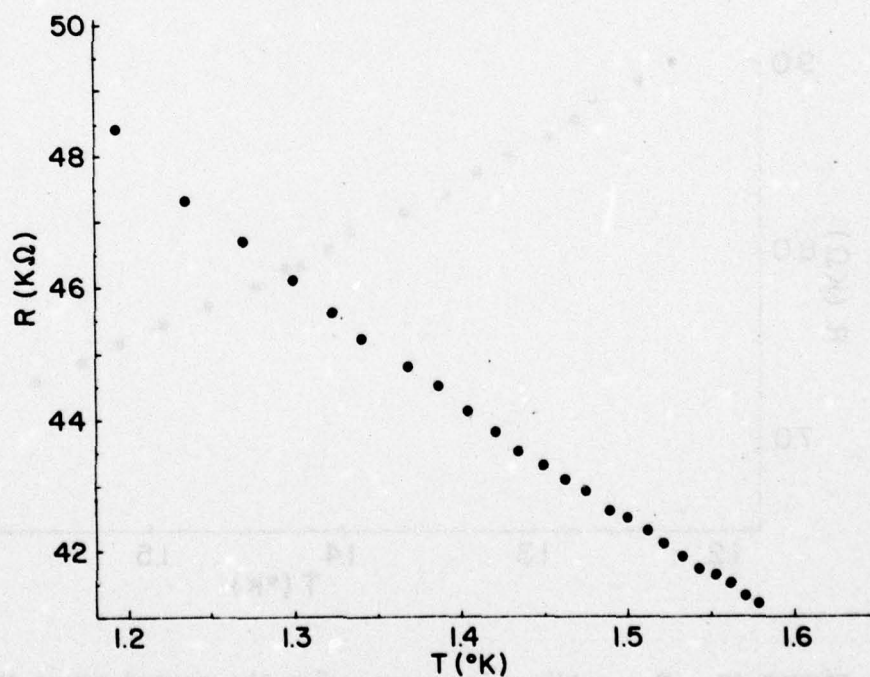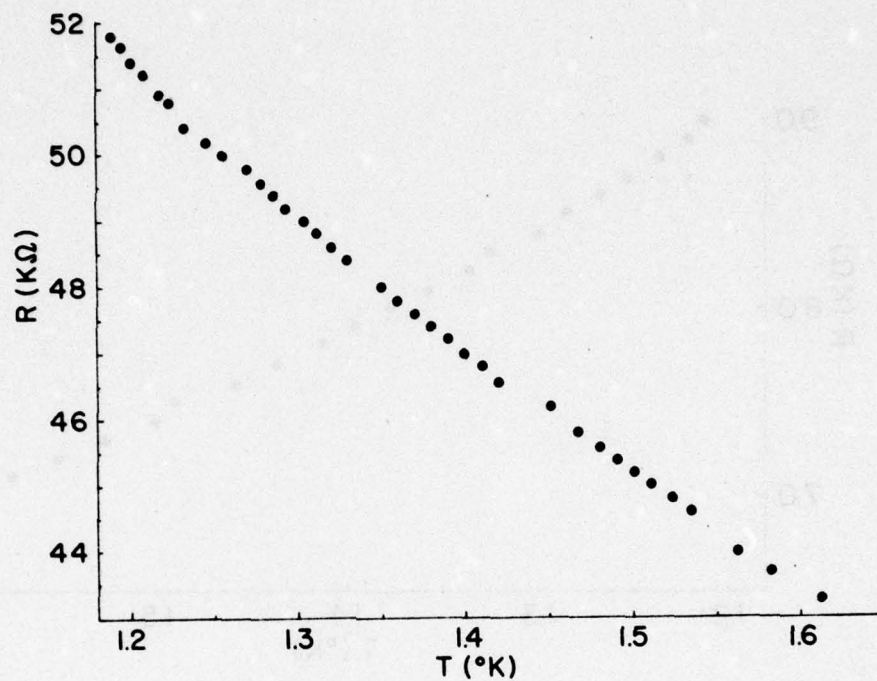
FIGURE 21. Two calibration curves for the second sound transducer in the older top-plate.
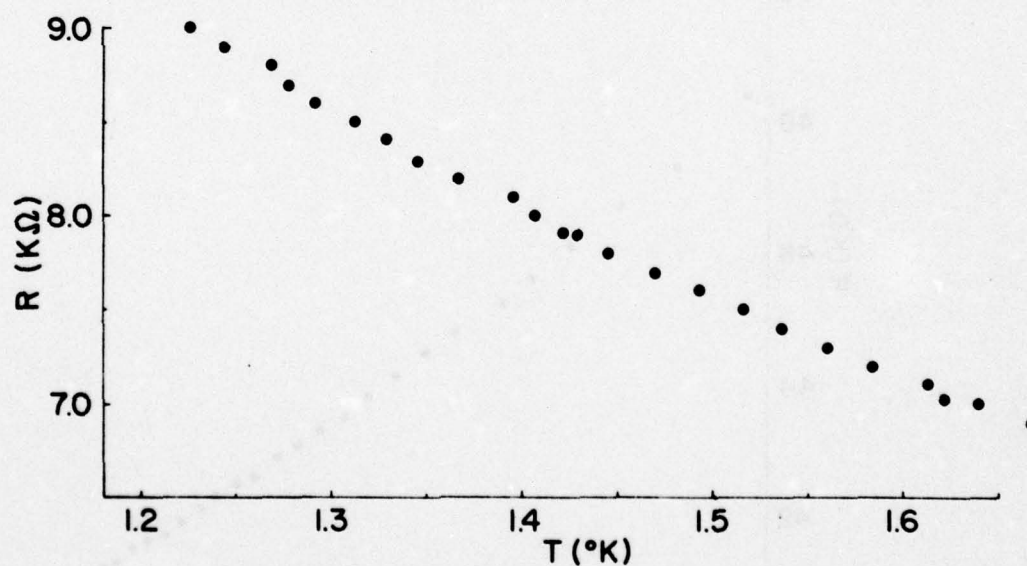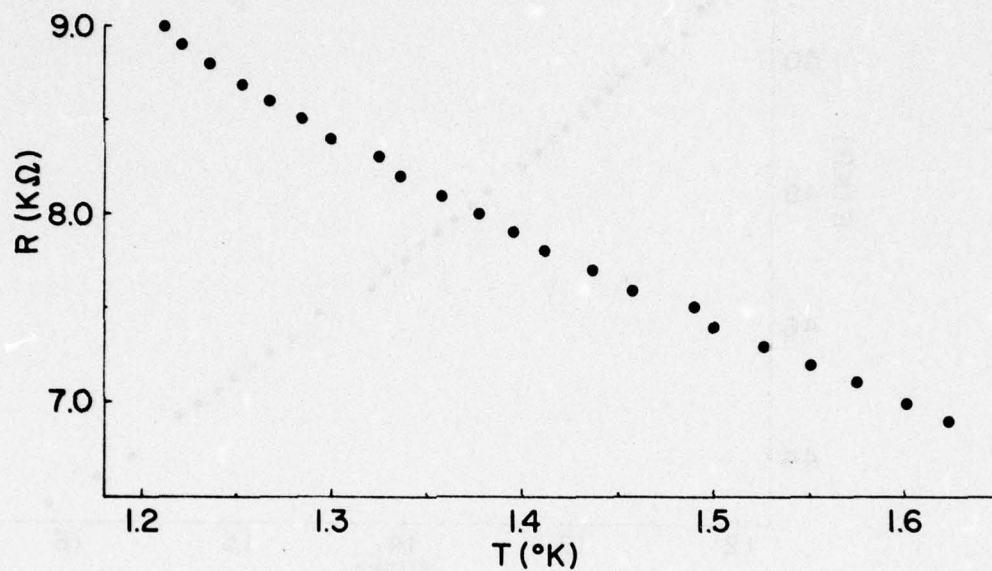
FIGURE 22.   Two calibration curves for the second sound transducer in
the newer top-plate.

to 10^{-6} times less than that of the He II between 1°K and 2°K.[74]

Two sample resistance transducer calibration curves for the older top-plate and the newer top-plate are shown in Figs. 21 and 22 respectively. The points were measured while the temperature of the helium bath was being reduced. The vapor pressure was recorded each time the digital read-out of the ohmmeter (Hewlett-Packard Digital Multi-meter - model 3476A) changed by 0.1 KΩ. The bath temperature was found from vapor pressure tables[94] based on the 1958 He temperature scale.[95] The differential resistivity was calculated by making a least square best fit to an exponential in the temperature range of 1.2°K to 1.7°K. Seven separate calibration curves were made on the resistance transducer over the span of one month giving an average best fit value $R_{old}(T) = 72 \pm 8$ exp $(-.408 \pm .018)T$ KΩ with an average correlation co-efficient of $r^2 = .9956 \pm .0013$ giving a value of $R_d = -.408 \pm .018$ °K^{-1}. Two separate calibrations of the transducer on the newer top-plate gave $R_{new}(T) = 19.15 \pm .05$ exp $(-.626 \pm .006)T$ KΩ, $r^2 = .9975 \pm .0005$, for $R_d = -.626 \pm .006$ °K^{-1}.

4. First Sound/Pressure Pick-up Transducer

Pressure disturbances in the spiral waveguide are detected using the electret microphone[96] which consists of the sandblasted transducer button that is epoxied into the top-plate and the aluminized 1/2 mil (12.7 μm) thick FEP teflon[81] membrane which covers the button in the assembled waveguide (III-C-3). The sandblasted button acts as the back-plate electrode of the microphone.[97] A large quasi-permanent charge density, σ, of the order of 10^{-7} coulomb/cm^2 [92,98] is deposited in the aluminized teflon[82] by placing it in an electric field. The

89

membrane is polarized by placing it, aluminized side up, on a 3/32 in (.24 cm) thick sheet of regular window glass and applying 6-8 KVDC across the aluminized surface and a conducting plate under the glass as diagrammed in Fig. 1A of Ref. 97. The electric field is maintained for 10-100 min. then the "electret" is removed from the glass and placed over the sandblasted electrode (button) to which it adheres due to electrostatic forces. When the waveguide is assembled the spiral waveguide body makes good electrical contact to the aluminized surface of the membrane over a large area, and the waveguide becomes the electrical contact to the membrane side of the microphone.

A voltage is generated between ground (waveguide body/top-plate) and the button when excess pressure is applied to one side of the membrane displacing it from the equilibrium position and changing the capacitance between the electrode and the aluminized surface. The charge on the electret is fixed and $Q = CV$, where $Q = \sigma S$ and S is the surface area of the button (typically .29 cm^2), C and V are the capacitance and voltage across the aluminized surface and the back-plate. When the membrane is displaced by a small amount we can let $C = C_o + \delta C(t)$, and $V = V_o + \delta C(t)$ and

$$\frac{\delta C(t)}{C_o} = \frac{-\delta V(t)}{V_o} \qquad (III-49)$$

where $\delta V(t)$ is the time varying voltage generated by the membrane displacement and V_o is the equivalent bias voltage across the trans- ducer due to the stored charge density in the electret. The value of V_o is approximately 200 volts for the electrets used in the experiments.

90

This value was determined by placing the microphone in a constant amplitude sound field and applying a d.c. biasing voltage across the microphone. Plotting the relative microphone response as a function of the additional bias voltage, a linear extrapolation of the relative response to zero determines experimentally the equivalent bias voltage, V_o, of the electret microphone.[92]

Two techniques were used to obtain the pressure sensitivity of these electret microphones. The first method involved a static measurement of $\partial C/\partial P$ using an electrostatic actuator[99] in air at room temperatures. The second determination was by the reciprocity method (see Appendix B) that was performed in the He II on the same transducers used to measure the mode converted first sound amplitudes. Surprisingly, measurements by both methods give the same sensitivity even though the actuator method was used in air and the reciprocity method was used in liquid helium.

Figure 23 is a photograph of the transducer top-plate used to make the electrostatic actuator measurements of the electret microphone sensitivity. The aluminized teflon membrane has been removed exposing five of the eight equally spaced, sandblasted, circular buttons. They are similar to those used in the spiral waveguide top-plate (Fig. 8) except they are brass and have a surface area of .197 cm^2. The aluminum arc is the "hot" element of the actuator which is separated from the top plate surface and buttons at three places by pieces of 5 mil (.032 cm) mylar sheet cut to the same shape as the actuator element. The brass screw in the center of the arc makes electrical contact to the insulated button directly below, through which the actuating

91
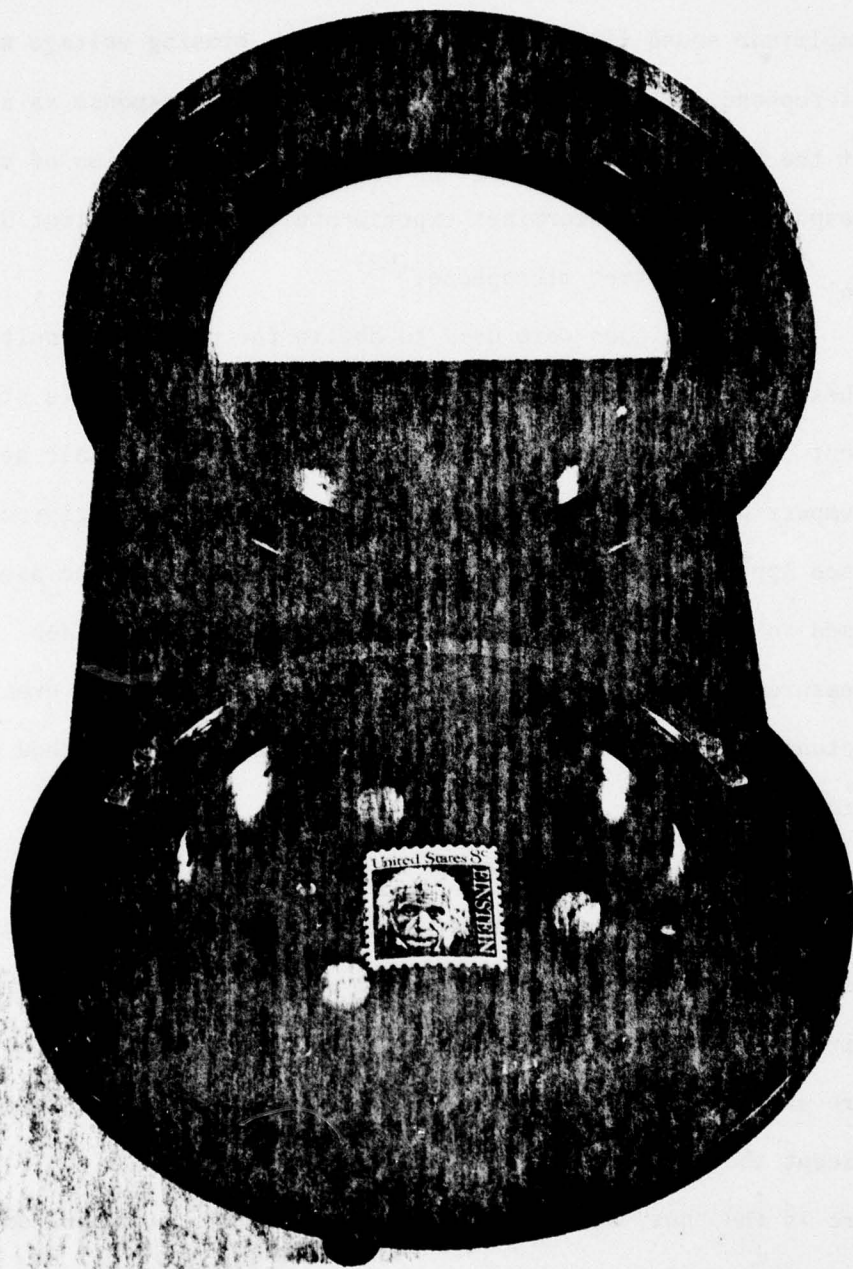
FIGURE 23. Microphone buttons with electrostatic actuator and toroidal shield.

voltage is applied to electrostatically deflect the electret membrane. The other two screws are nylon and are simply there to support the actuator and keep the mylar insulating spacers in place. A small part of the spacers are visible at either end of the actuator element. With the aluminized teflon electret in place, either of the two buttons under the actuator element can be used to measure the pressure sensitivity of the membrane/back-plate system. When the electret is in place, the top-plate is attached to the toroidal waveguide body shown in the background of Fig. 23 making the ground contact to the aluminized surface and shielding the system from electrical and acoustical noise.

The sensitivity, $\partial C/\partial P$, of the system is determined by making a three-terminal capacitance measurement of an electret/button under the actuator using a General Radio Capacitance Bridge (G.R. model 1615-A) and a lock-in detector (Princeton Applied Research Corp. model HR-8). The change in capacitance ΔC as a function of the equivalent electrostatic pressure due to the d.c. voltage applied between the actuator and the aluminized surface of the teflon was plotted and the slope, $\partial C/\partial P$ was determined. Figure 24 is a plot of typical measurements made on three different days symbolized by Δ, ∇, and 0. The error bars come from the uncertainty in reading the meter of the lock-in detector.

Measurements on five different days yielded an average value of $\partial C/\partial P = 2.0 \pm .6 \times 10^{-5}$ pf/μ bar (1 μ bar = 1 dyne - cm^{-2}) for the buttons (S = .197 cm^2) shown in Fig. 23. This corresponds to $\partial C/\partial P = 1.0 \pm .3 \times 10^{-4}$ pf/μ bar - cm^2. This can be translated into a microphone sensitivity $\partial V/\partial P$, using (III-49)

93
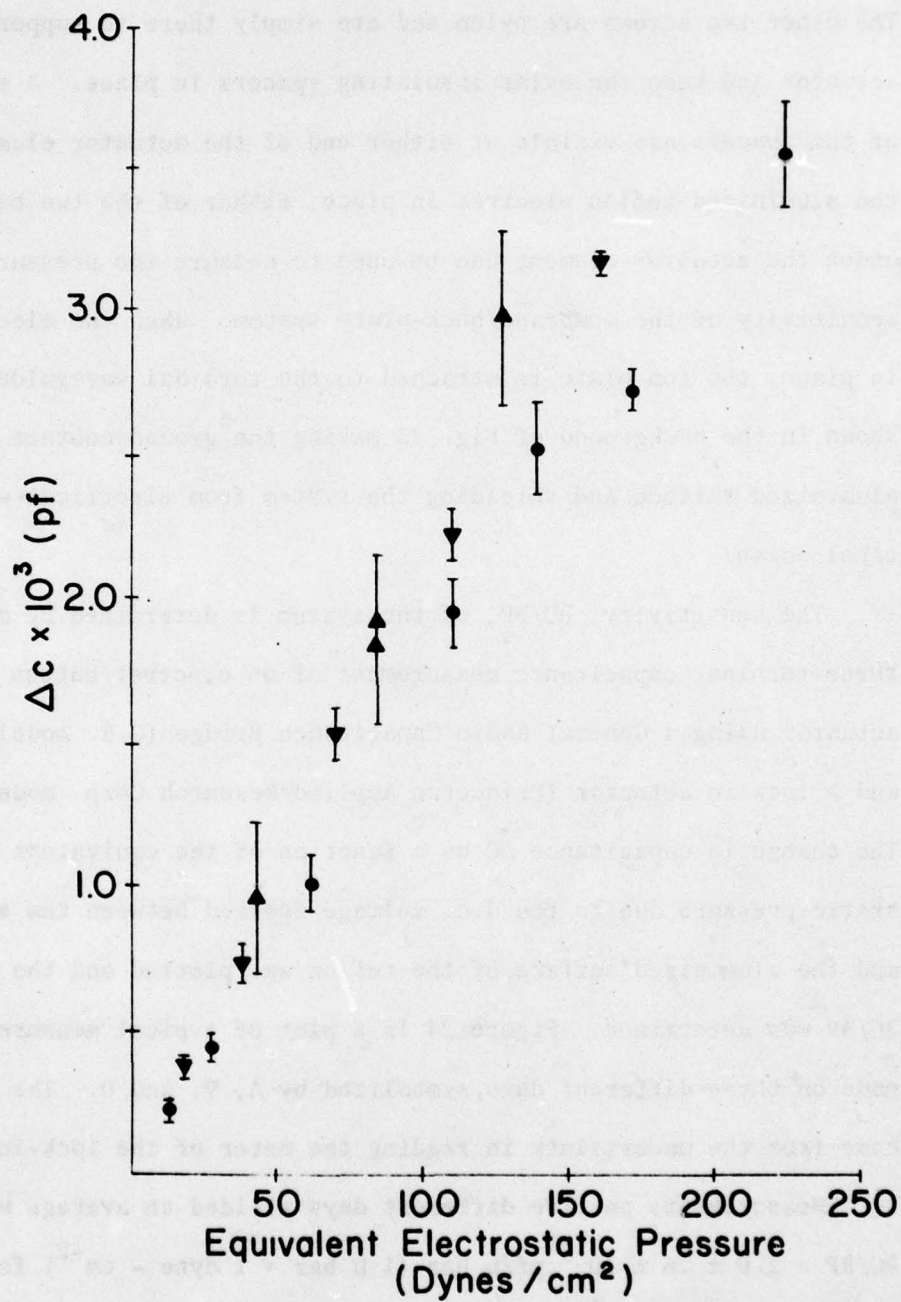
FIGURE 24. Typical data from electrostatic actuator measurements of electret microphone sensitivity in air.

$$\frac{\partial V}{\partial P} = \frac{\partial C}{\partial P}\frac{\partial V}{\partial C} = \frac{-V_o}{C_o}\frac{\partial C}{\partial P} \qquad (\text{III-}50)$$

C_o was determined by making measurements of the capacitance (as just described but by a two-terminal technique) of the six .95 cm long ($S = .29$ cm^2) transducer buttons on the older and newer top-plates with and without the electret in place. The average of those measurements give a value of $C_o = 20.6 \pm 3.7$ pf. Using a value of $V_o = 215 \pm 25$ volts, the voltage generated by the microphone, V_g, for a change in pressure of $1\,\mu$bar is $.30 \pm .11$ mV. The following equivalent circuit allows the calculation of the actual microphone sensitivities as measured remotely from the actual transducer.

$$(\text{III-}51)$$
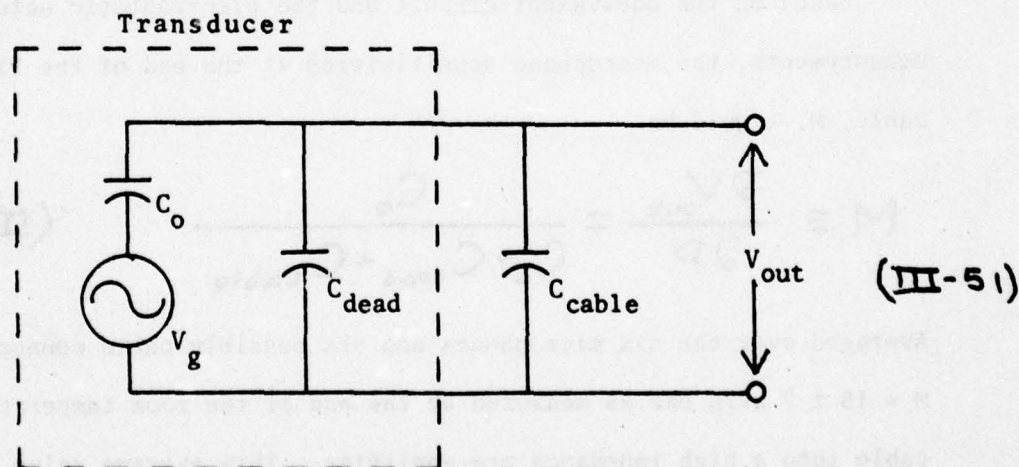
C_{dead} is the transducer capacitance without the electret in place due to the capacitance of the button to the top-plate and the capacitance of the "towers". The average $C_{dead} = 14.5 \pm 3.1$ pf. C_{cable} takes in all of the "line" capacitance between the towers and the preamplifier.

In preliminary experiments a FET pre-amplifier which functioned from room temperature to $1.0°K$[100] was attached directly to the towers eliminating C_{cable} altogether. In later experiments these low temperature FET pre-amps were abandoned since it was desireable to have all transducers be reversible for reciprocity calibrations. In that case, C_{cable} is the sum of the capacitances of the co-axial cables which attach the towers to the probe, the stainless steel co-axial cable in the probe[101] and the cables which connect the probe to the room temperature pre-amplifier (Princeton Applied Research - Low Noise Pre-Amp model 113). For calibration microphones C_{cable} = 319.5 ± .5 pF and averaged over all six microphone dedicated cables, C_{cable} = 315 ± 33 pf.

Based on the equivalent circuit and the electrostatic actuator measurements, the microphone sensitivities at the end of the final cable, M, should be

$$ M \equiv \frac{\partial V_{out}}{\partial P} = \frac{C_o}{C_o + C_{dead} + C_{cable}} \qquad (III-52) $$

Averaged over the six microphones and six possible cable connections, M = 18 ± 7 μV/μ bar as measured at the end of the room temperature cable into a high impedance pre-amplifier. This average value is in agreement with values measured by the reciprocity method described in Appendix B and discussed in Chapter IV.

5. <u>Pressure and Temperature Transducers as Detectors of First and Second Sound</u>

Although temperature transducers are used to detect second

96

sound and pressure transducers are used to detect first sound, it must always be kept in mind that first sound may have temperature swings associated with it and second sound may have pressure swings associated with it. The effect of importance for the measurement of mode converted first sound is the pressure swings that are associated with second sound. These pressure swings can arise from a variety of physical mechanisms and they are important for two reasons.

The first confrontation with the pressure swings in second sound was a proposal to calibrate the pressure transducers using the calculated pressure swings accompanying a plane wave of second sound of measured amplitude (III-D-3) that arise from the non-zero values of β_p. In bulk[54] (i.e. in the absence of boundary effects)

$$p' = \frac{\beta_p \, \rho u_1^2 \, u_2^2}{(u_1^2 - u_2^2)} T_1 \cong \beta_p \, \rho u_2^2 T_1 \qquad (III\text{-}63)$$

where p' is the pressue swing which travels with the second sound wave of amplitude T_1 in the bulk at the speed of second sound. The approximate expression assumes $u_2^2 \ll u_1^2$. When the calibration procedure was attempted using plane wave second sound, it was found that the measured pressure was at least two orders of magnitude larger than p' based on other measurements of the pressure transducer sensitivity (III-D-4 and IV-D-1). We now understand this discrepancy in the following way.

In the absence of boundary effects the pressure swings are small since both the normal and superfluid components are free to flow (in opposite directions) in such a way that the center-of-mass motion of the fluid as a whole is small and proportional to β_p. At the surface

97

of a waveguide wall, on the other hand, the tangential component of the normal fluid velocity is zero due to its viscous interaction with the wall. The superfluid component is still free to move, in fact, it is required to do so by the curl-free restriction of Landau $\nabla \times \vec{v}_s = 0$, discussed in (I-E). The compressions and rarefactions of the super-fluid components lead to dynamic pressure swings which, to lowest order in v_s, are given by (III-37)

$$-\nabla p = \rho \frac{\partial N_3}{\partial t} \qquad \text{(III-54)}$$

Assuming traveling wave solutions for v_s and p' with $\omega/k = u_2$

$$p' = \rho u_2 N_{s_1} = -\rho S T_1 \qquad \text{(III-55)}$$

The ratio of the dynamic pressure swings due to the locking of the normal fluid at the walls vs. the pressure swings due to the non-zero value of the isobaric expansion coefficient is approximately

$$\frac{S}{\beta_p u_2^2} \qquad \text{(III-56)}$$

which typically has values between 200 and 300 for the temperature range of experimental interest above 1.35°K. Clearly (III-56) diverges at 1.17°K where $\beta_p = 0$. It was the experimental observation of the pressure swings at that temperature which led us to seek the dynamic mechanism for the production of the pressure swings. Subsequently it was decided not to use a thermal (second sound) technique to calibrate the pressure transducers, and instead devise a reciprocity calibration technique that would be suitable to the waveguide geometry (see Appendix B and IV-D-1).

98

Because the attenuation coefficient for the higher order mode of second sound, γ_s (III-12) is larger near cut-off, the amplitude of the second sound is small at the positions where mode conversion pressures were measured ($\sim$100 cm from the driver). As the frequency increases above cut-off, the value of γ_s decreases rapidly and the increasing second sound amplitude could account for spurious pressure signals at frequencies greater than the mode conversion frequency (see e.g. Fig. 30 upper).

Spurious pressure peaks at the microphone can also be caused by first sound generated at the heaters in the second sound driver due to fluid velocities which are in excess of the critical velocity at the heater wires (III-D-1) or due to boundary conditions through non-linear effects (II-28), or through expansion co-efficient effects.[54] At very large values of driver power spurious peaks become large. Those peaks are probably due to critical velocity effects at the heaters. Once those peaks were observable the mode conversion pressures started to deviate from their quadratic dependance (IV-C) on the second sound amplitude and no further power increases were made and no more data was taken.

To summarize, it can be said that pressure swings arising either from the second sound or from the second sound driver do not generally interfere with the ability to unambiguously identify and measure the mode conversion peak on the output of the spectrum analyzer (see Figs. 30 and 31). The exception is in a few rare cases where the spurious pressure peaks are close enough to the mode conversion resonance and are of large enough emplitude to effect the accurate measurements of Q's.

99

E. ELECTRONICS

1. Second Sound

As discussed in the section on the tuned dipole driver (III-D-1), it is necessary to provide two sinusoidal voltages, 90° out-of-phase with each other, to the two independent heaters in the second sound driver assembly at half the frequency of the second sound being detected. Fig. 25 is a block diagram of the electronic instrumentation used to generate and detect second sound. The detection of second sound was discussed in (III-D-3).

The drive signal is taken from the tracking output of the spectrum analyzer, amplified, and then applied to the frequency halfer/quarterer whose circuitry is diagrammed in Fig. 26. The sine wave that comes into the halfer (quarterer) is changed to a square wave (7413) and then goes into a dual flip-flop (7474) which puts out a square wave at one-half (one-quarter) of the original frequency generated by the spectrum analyzer. The square wave output of the halfer/quarterer is then used as the input to a Wavetek voltage controlled generator operating in the phase-locked mode. This is done to generate a sine wave from the output of the halfer/quarterer. Since any second harmonic distortion reaching the heaters would show up as frequency doubled, plane wave second sound being radiated by the driver, the input to the heaters must be as devoid of second harmonic as possible. The sinusoidal output of the Wavetek is filtered and the second harmonic content as measured across the output of the drive amplifiers when they are loaded by the heaters is always at least -40 dB below the fundamental.

The 90° phase shifter is a simple op-amp differentiator circuit

100
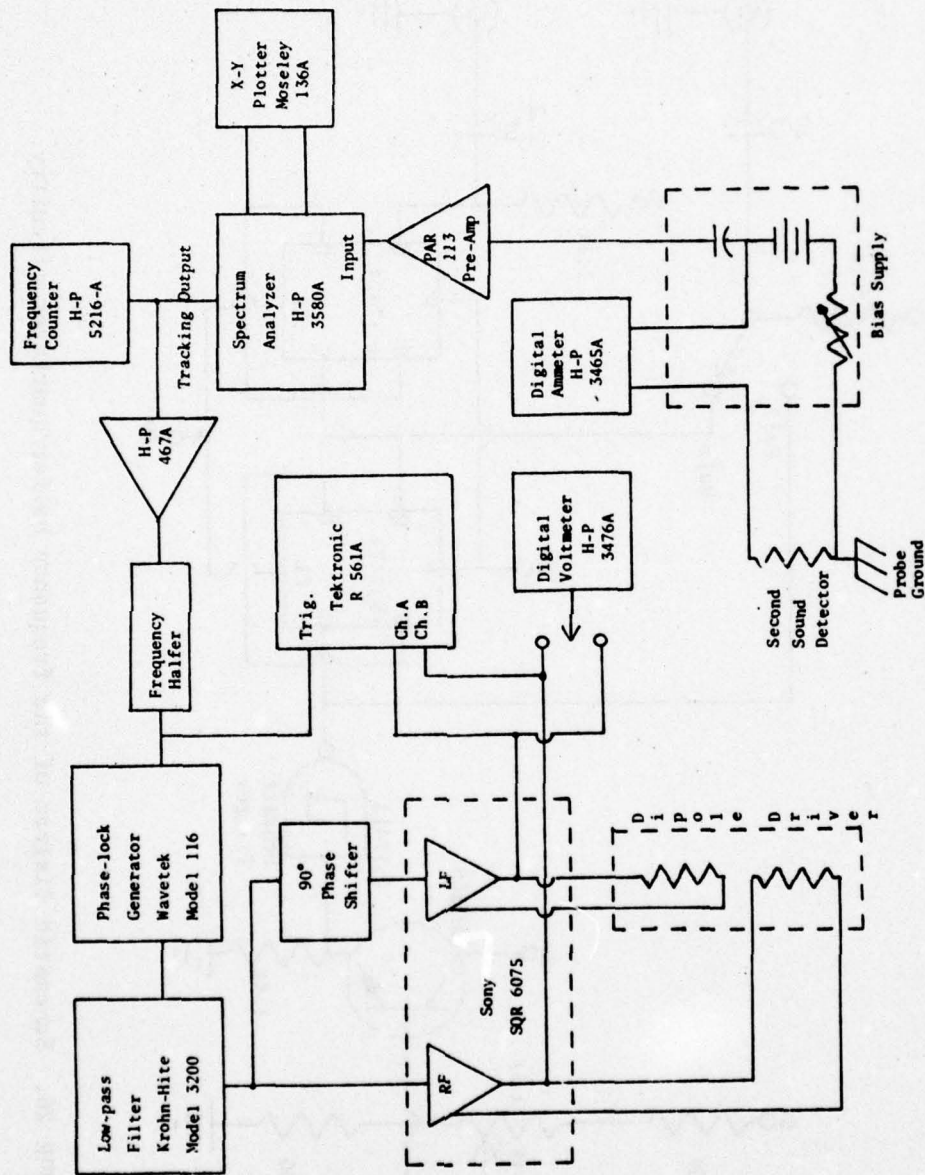
FIGURE 25. Block diagram of second sound electronic instrumentation.

101
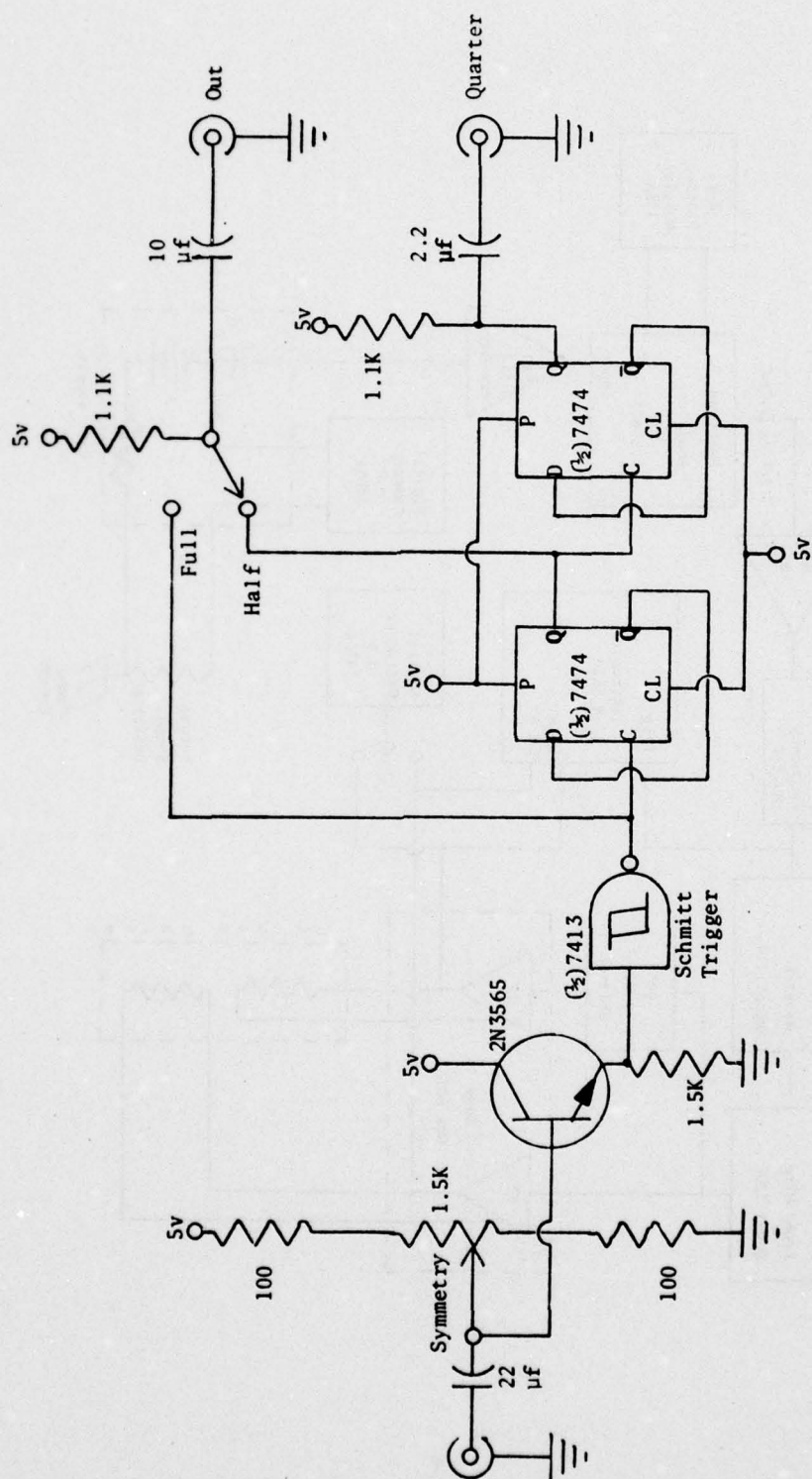
FIGURE 26. Schematic diagram of the frequency halfer/quarterer circuitry.

shown below

Gain
50 K

.02
μf

+15v

4

11

−

741C

10

In

5

6

+

90°
Out

10 K

−15v
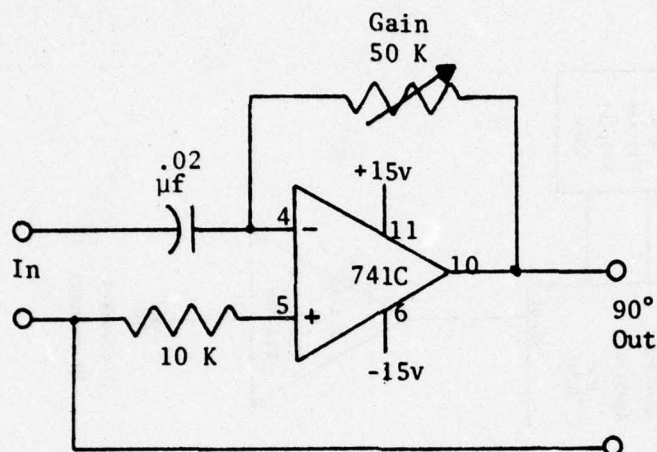
(III-57)

The gain is adjusted so that $V_{\ell f} = 1.05\ V_{rf}$ as measured by the digital voltmeter that can be switched between the two drive amplifiers. Both heater signals are continuously monitored on the oscilloscope.

The amplifiers used to drive the heaters are two of four independent, 25 watt, power amplifiers, the other two being dedicated to other purposes (monitoring helium transfer, driving transducers for reciprocity calibrations, etc.). The gain of the amplifiers can be individually adjusted or changed simultaneously by a master gain control, a feature which was very convenient for making measurements of the dependence of mode conversion amplitude on second amplitude. In addition it was possible to turn off all of the amplifier outputs without turning off the line power. This saved helium and avoided the potential hazards of "turn-on transients" affecting heaters or other apparatus.

2. First Sound

The drive electronics for the measurement of mode converted first sound is identical to that described in the preceeding section

FIGURE 27. Block diagram of first sound electronic instrumentation.

except that the mode converted signal is at twice the frequency of the second sound so the tracking output signal from the wave analyzer must be quartered instead of halved as indicated in Fig. 27.

The first sound detection electronics was described in the section on first sound transducers (III-D-4).

3. The Probe

The probe pictured in Fig. 28 provides mechanical support for the experiment inside the dewar, electrical connections between the transducers and the room temperature electronic instrumentation and a means of introducing liquid helium into the dewar and monitoring its level. It has its own built-in electret microphone so that the sounds of the helium entering the dewar can be monitored during the transfer of liquid helium.

The central tube which contains the cables is 10 mil (.025 cm) wall, one inch (2.5 cm) dia. stainless steel. The thin wall size was chosen to reduce the heat leak (thermal conduction) from the room temperature part of the probe. The tube has three heat shield assemblies that are attached to reduce the heating of the helium due to the Stefan-Boltzmann, σT^4, radiation[111] from the top plate of the probe which is at room temperature.

The two tubes which run parallel to the central tube are (1) a fill tube to guide the tube inserted into the dewar for the transfer of helium from the storage dewar and (2) a co-axial capacitative wand used as the sensing element in the level indicator[112] whose electronics are located in the small box above the top plate of the probe.

105
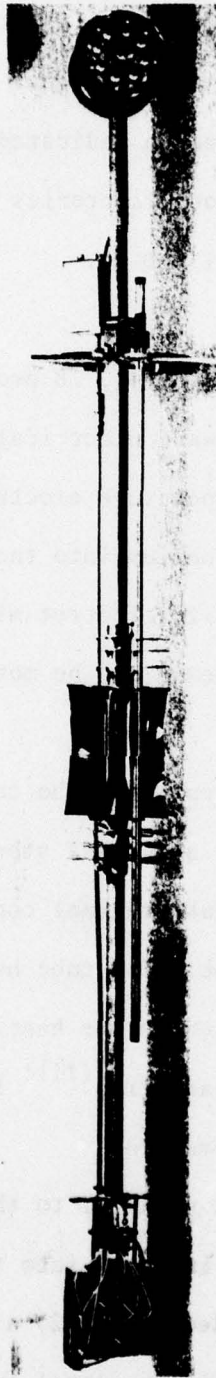
FIGURE 28.   Probe with waveguide mounted at the bottom.

The probe is wired with five twisted pairs of #30 (7 x #38 stranded) teflon insulated, stainless steel, copper clad wire which is terminated at the top of the probe in hermetically sealed BNC bulkhead receptacles mounted on a lucite face plate. At the bottom they terminate in two linear arrays of individual Amphenol pin blocks. At no point are any of the wires grounded. One pair is used to provide power to the feed-back heater in the temperature controller circuit and two pairs are used to provide power for the tuned dipole driver.

There are nine 50-ohm stainless steel co-axial cables[101] which are insulated from each other and the central tube by individual teflon sleeves (spaghetti) that run their entire length. The cables are terminated at the top end by hermetically sealed BNC bulkhead receptacles mounted on a second lucite fact plate. Eight of the nine cables are terminated at the bottom by the same type microdot bulkhead receptacles described in (III-C-3). They are mounted on a brass plate which is the primary grounding point for the probe and waveguide. The ninth cable is terminated in an electret microphone that is used to monitor the sounds of the helium gas and liquid that enter the dewar during the transfer from the storage dewar. This is a very convenient way to be sure transfer lines are not clogged and the transfer is proceeding normally. Two of the eight remaining cables are used as shielded connections to the 200Ω Allen-Bradley resistor used to monitor the temperature of the helium in the dewar and sense changes in temperature which are compensated by the output of the temperature controller to the feedback heater. The remaining six cables are used for signal from the first and second sound transducers.
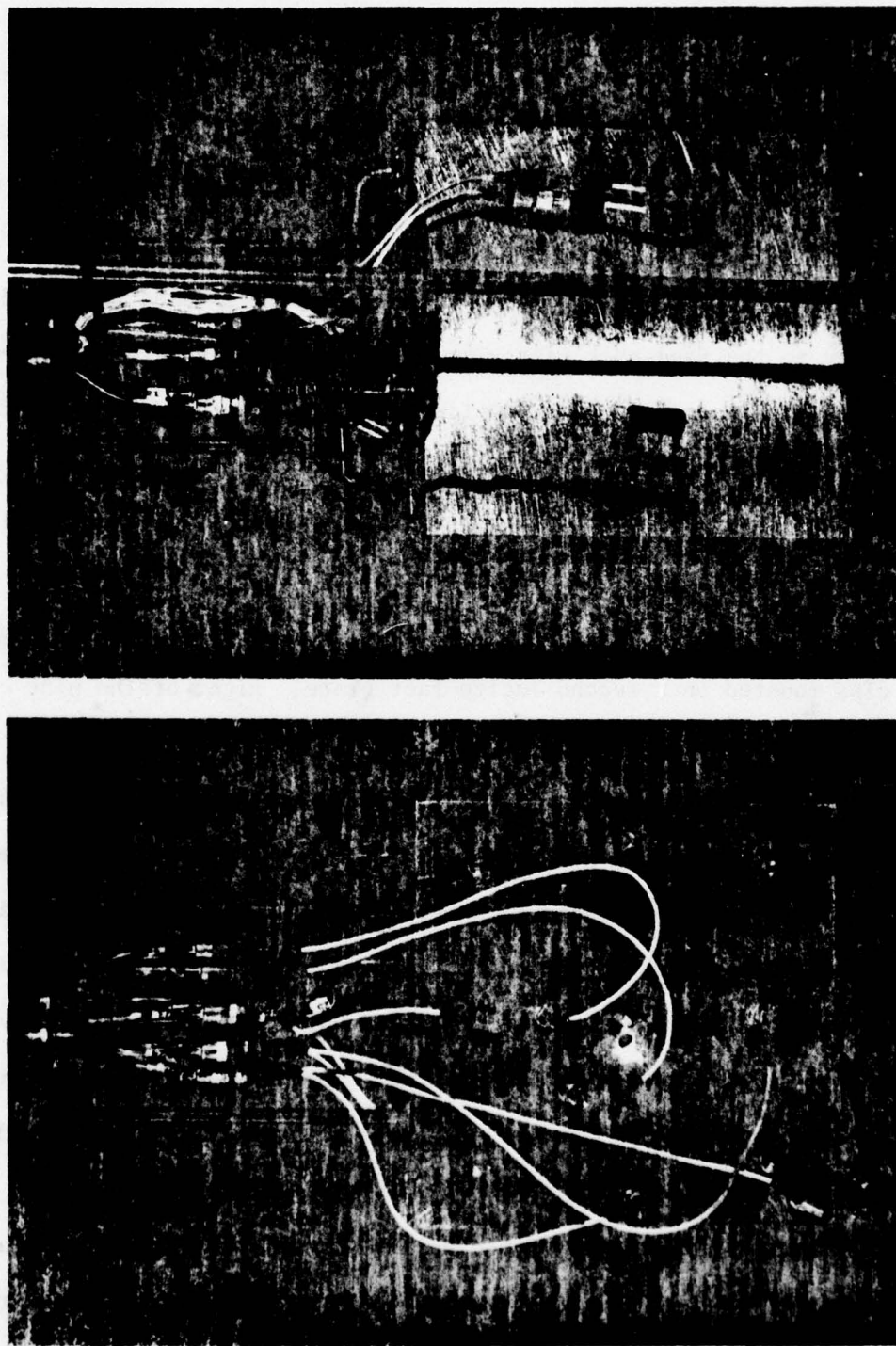
FIGURE 29. Close-up of probe bottom and the waveguide.

108

Figure 29 is a close-up view of the bottom of the probe with the spiral waveguide attached and the cables which join the transducers to the probe. The rear view shows the temperature sensing resistor and the feed-back heater. The tube is the end of the capacitive element of the level indicator.

4. Temperature Controller

The measurement of mode conversion amplitudes as a function of second sound amplitude requires that the temperature of the helium bath be held relatively constant over a large range of power inputs to the heaters in the dipole driver ($\sim$10 - 500 mW). In all experiments, except calibration of second sound transducers (III-D-3), the bath temperature was stabilized by a temperature controller modeled after a low noise bridge circuit suggested by Anderson[113] that used a ratio transformer (Gertsch model 216) and a phase-sensitive detection circuit. The off-balance signal from the detector was amplified and sent into a heater in the bath (300Ω wire wound resistor) to form a negative feedback circuit which maintained the bath temperature relatively constant without having to continually re-adjust the pumping rate as the power to the dipole driver was changed.

F. DEWAR SYSTEM

All experiments were performed in a stainless steel double dewar system (Standard Air Co., Inc., Brooklyn, N.Y.). The inner dewar diameter is 6 in (15.2 cm). The temperature of the helium bath is reduced by pumping away its vapor with a Kinney (Boston, Mass.) vacuum pump, model KC-15. The connection between the pump in an adjacent room and the bath is made by a main valve on a 4 in (10 cm) diameter

pumping line and an auxiliary needle valve parallel to the main valve. The needle valve is used for fine pumping rate regulation. A minimum temperature of 1.14°K (0.4 mm Hg) could be obtained towards the end of an experiment by using a Stokes pump (model 212) in parallel with the Kinney pump through the 4 in line.

The bath temperature is determined by measuring the vapor pressure of the helium and converting it to temperature using tables[94] based on the 1958 He temperature scale.[85] The pressure is measured by one of the following systems: (1) A Baratron capacitance manometer[114] model 170, with a 0-100 mm Hg differential pressure head and a digital readout. The reference side of the differential head was backed by a diffusion pump so the pressure reading can be regarded as absolute.

(2) A 0.50 mm Wallace and Tiernan (Belleville, N.J.) absolute pressure indicator type FA-160. The W & T gauge was found to give readings which were 196 ± 67 μm Hg higher than the Baratron system so all readings made on the Wallace and Tiernan gauge were corrected by subtracting 0.20 mm Hg.

CHAPTER IV

PROCEDURES AND RESULTS

*Things derive their being and
nature by mutual dependence
and are nothing in themselves.*

Nagarjuna[115]

A. PROCEDURES AND DATA

After making a room temperature check of the electronics and
transducers, the probe mounted experiment is placed inside the dewar
and is allowed to cool to liquid nitrogen temperature ($\sim$80°K) overnight.
The following day liquid helium is transferred into the inner dewar and
the temperature is reduced by pumping away the vapor. Upon crossing
the λ-point, measurements are made of the temperature dependence of the
resistivity of the second sound transducer as described in (III-D-3)
and of the temperature sensing resistor (II-E-4) as the temperature is
reduced to $\gtrless$1.2°K. The second sound transducer calibration curve is
plotted (see Fig. 21, 22) and fit to an exponential form, while the
temperature is being stabilized for the first mode conversion experi-
ment of that experimental run.

All of the data on the amplitudes of second sound at $f_{mc}/2$ and
the amplitude, Q, and frequency of first sound are taken from the
charts made by the X-Y plotter connected to the output of the spectrum
analyzer (see Figs. 25, 27). Before each run, the spectrum analyzer
calibration is checked against its own internal standard and full
scale on the CRT display of the analyzer is adjusted to be full scale
on the chart of the X-Y plotter. The frequency measurements are made

111

by counting, for 10 sec, the frequency of the tracking output signal
at the start and end of each sweep (±.1 Hz) and interpolating frequen-
cies linearly with distance from these end points as measured by a 12
in steel rule (satin chrome steel rule no. C305 R - L.S. Starrett Co.,
Athol, Mass.) to the closest 0.01 in (0.025 cm). Typical values of the
horizontal frequency scale on the charts are in the range of 5.3 to
5.7 Hz/in depending on the adjustment of the plotter's x-axis. On most
of the charts containing mode converted first sound peaks, the CRT
display was stored and the spectrum analyzer was reset manually to the
peak. At that point a vertical mark was made on the chart by the X-Y
plotter (see Fig. 31). The frequency assigned to that line by the
two methods (linear interpolation or direct frequency count) never
disagreed by more than 0.6 Hz and were typically within 0.3 Hz of each
other.

All charts were taken with the spectrum analyzer bandwidth set to
1 Hz and most of the sweeps were over 50 Hz and took two minutes to
complete.

B. MODE CONVERSION FREQUENCY AND Q

1. Raw Data

Figures 30 and 31 show the raw data for mode conversion
resonance peaks that were obtained by the methods described in the
previous section. The upper and lower charts in Fig. 30 were made
during preliminary runs that used low temperature FET pre-amplifiers[100]
attached directly to the "towers" so their signal-to-noise ratio is
better than that of Fig. 31 which used a room temperature pre-amplifier

112
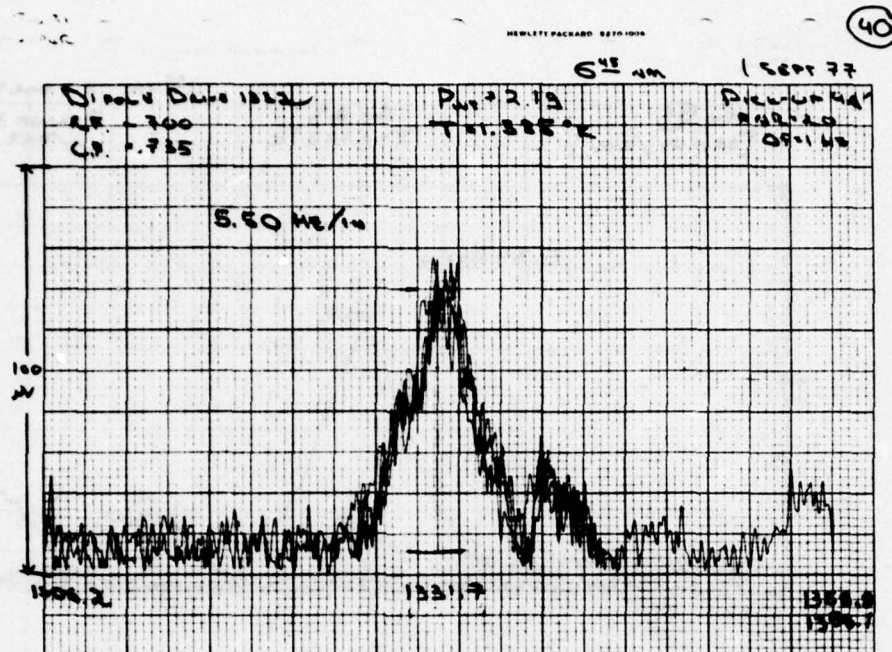
FIGURE 30. Raw mode conversion data taken with a low temperature FET pre-amplifier at 1.182°K (upper) and 1.31°K (lower).
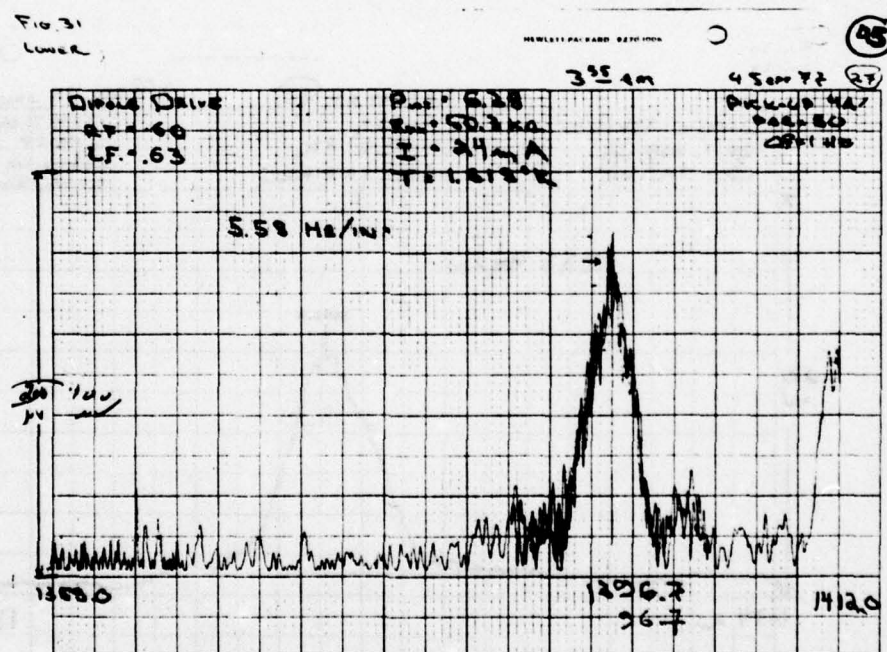
FIGURE 31. Raw mode conversion data taken with a room temperature pre-amplifier at 1.385°K (upper) and 1.619°K (lower).

(P.A.R. model 113) as shown in Fig. 27.

The upper chart in Fig. 30 was made at 1.182°K, very close to the temperature at which the expansion co-efficient, β, vanishes (1.17°K). The large central peak is resonant mode conversion at 1266.7 Hz and has a Q = 315 ± 25. The thickening of the line to the right of the peak is pen noise in the X-Y plotter. The causes of the two smaller peaks to the right of the mode converted peak were discussed in (III-D-5). One of the two lower traces on the same chart was taken without any power to the heaters in the dipole driver to establish a noise baseline. The other trace was made with the same power to both heaters as was used to measure mode conversion (20 mW/heater), except one of the drive signals was not phase shifted by 90° so that the dirver radiated plane wave second sound (0, 0) rather than the higher order dipole (1, 0) mode. This clearly demonstrates that the second sound must have the proper phase velocity (i.e. intersection angle, θ) to produce first sound by this resonant, non-linear process. The lower chart in Fig. 30 is another mode conversion peak at a higher temperature, 1.31°K.

f_{mc} = 1303.5 Hz and Q = 395.

The upper chart in Fig. 31 shows a mode conversion peak at 1.385°K at a frequency of 1332 Hz and Q = 490 ± 50. The chart contains four separate traces which were repeated to average, in a sense, over the additional noise. The noise is due to the losses imposed by the line capacitance, C_{cable} (III-51), that is present when the pre-amp is at room temperature instead of directly on the transducer at helium temperature. The lower chart is similar except it is taken at a still higher temperature, 1.619°K. The frequency of the mode conversion

resonance is 1396.7 Hz and Q = 680 ± 100, and again the peak was
retraced three times to average over the noise.

2. Data Summary and Comparison with Theory

Figure 32 is a graph of the measured mode conversion frequen-
cy as a function of temperature. The 55 solid circles represent any-
where from one to fourteen separate determinations of a measured mode
conversion resonance peak at the indicated temperature with the average
number of independent determinations per point being 2.7. The experi-
mental error is about the size of the circle. The solid line represents
the prediction of the theory (III-5, 8) with no adjustable parameters
using published[116] values of first and second sound speeds (see
Appendix C) and the depth of the waveguide as discussed in (III-C-1).
The dotted line uses the extrapolated values of second sound speed.
The cumulative error in the theoretical line is due primarily to the
values of second sound speed which are accurate to ±.1 to .2% in the
temperature range plotted. This uncertainty in second sound speed
corresponds to a vertical shift in the line of no more than ±2 Hz. It
can be seen that the agreement with theory is excellent.

Figure 33 is the measured quality factor of the mode conversion
resonances. The circles represent single determinations of Q's and
the bars represent the highest to lowest values of Q at a single
temperature when two or more determinations were available. The
line is the theory (III-28), again without any adjustable parameters.
Although the data shows the proper trend (i.e. Q increases with
temperature) and the values are of the correct magnitude, there is not
precise quantitative agreement. The fact that the points are not

116
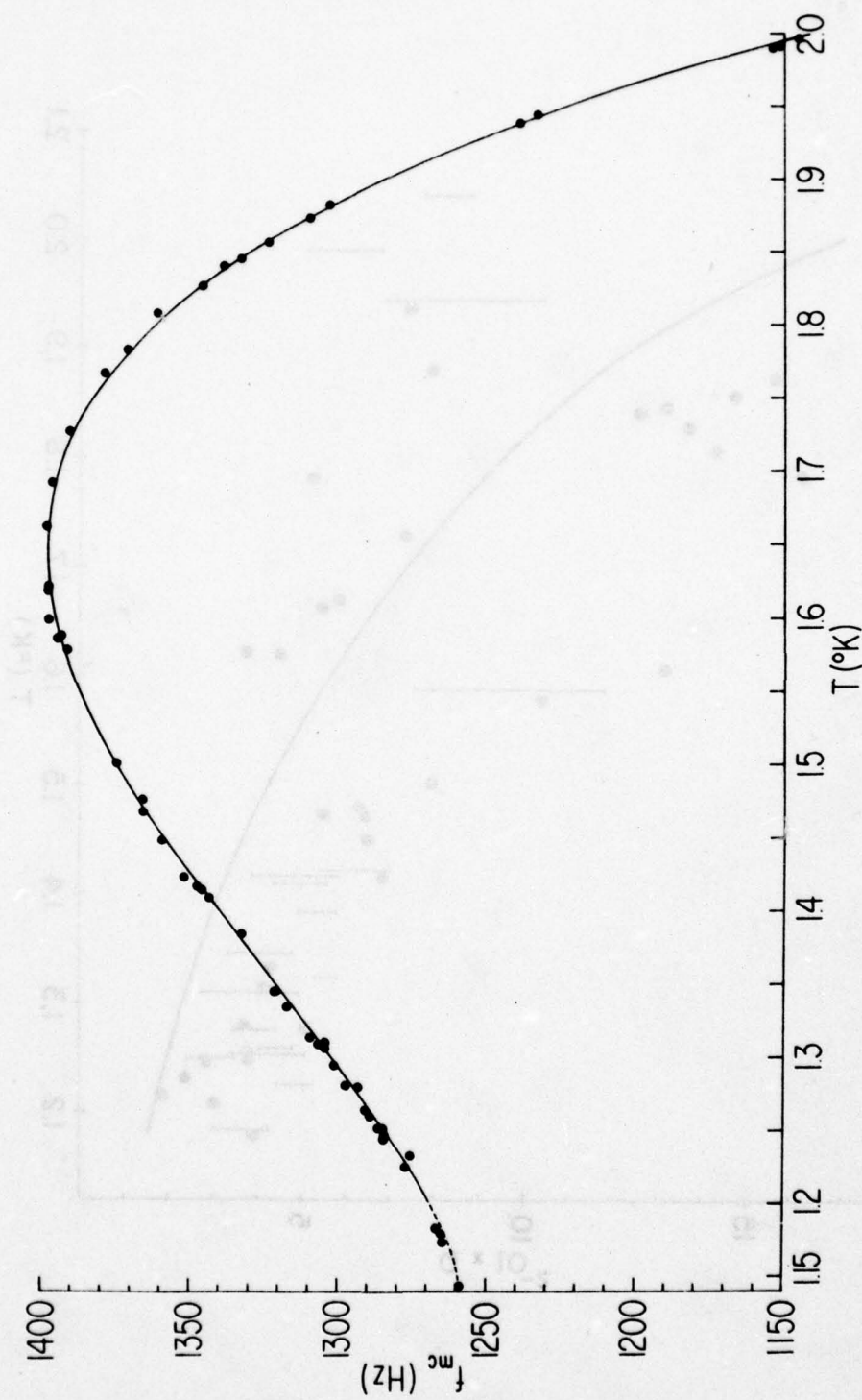
FIGURE 32. Measured mode conversion frequencies. The solid line is from the theory with no adjustable parameters.

117
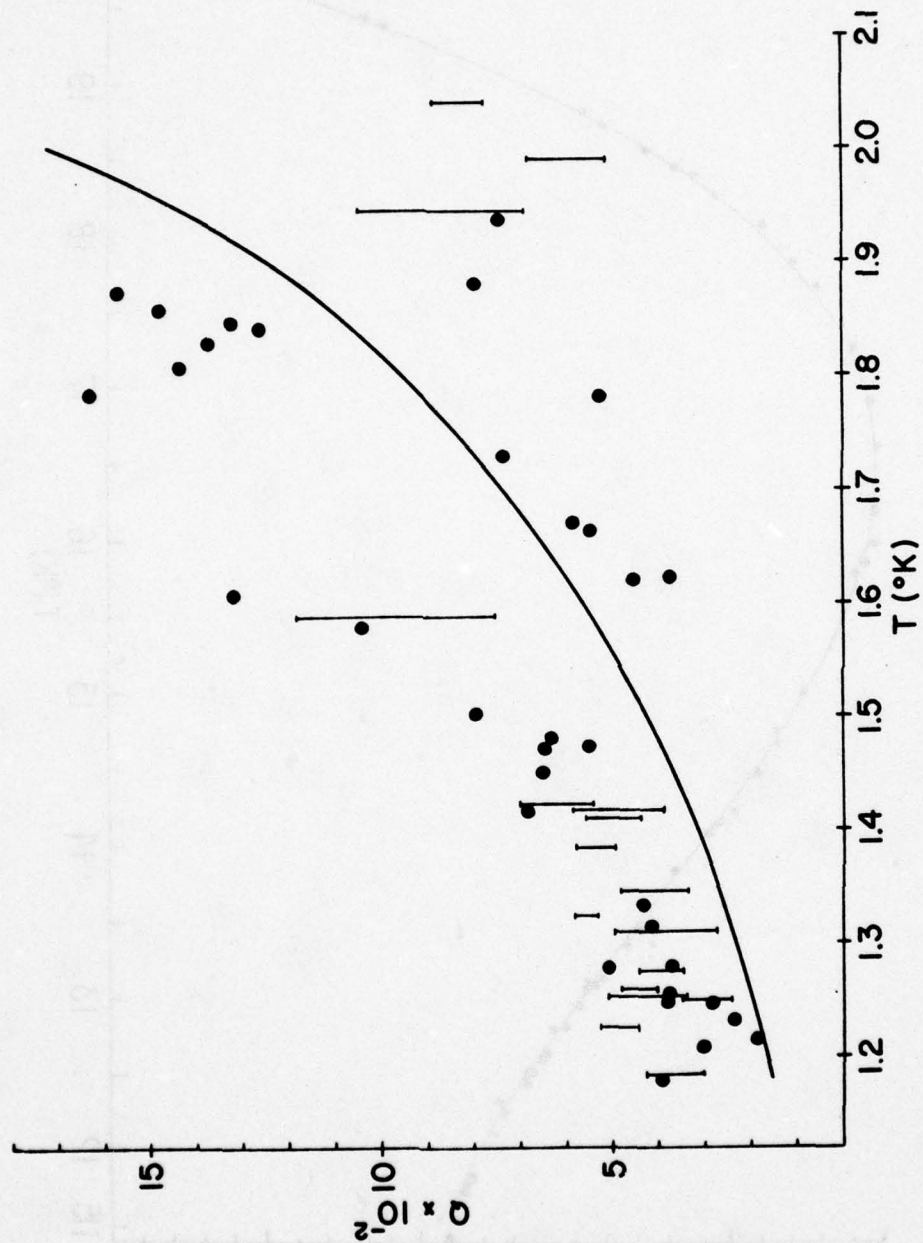
FIGURE 33. Measured mode conversion quality factors. Solid line from the theory with no adjustable parameters.

118

statistically distributed about the line suggests that there be some unidentified source of systematic error.

C. QUALITATIVE DEPENDENCE OF MODE CONVERSION AMPLITUDE ON SECOND SOUND AMPLITUDES

The amplitude dependence of mode converted first sound at f_{mc} and the amplitude of second sound at $f_{mc}/2$ were measured simultaneously. Using the electronic instrumentation diagrammed in Fig. 25, charts were made of the output of the second ousnd transducer, V_o, as a function of frequency at a fixed temperature. Figure 34 gives two samples of such measurements; the rise of the second sound amplitude above the cut-off frequency is clear. The upper chart shows four traces from the transducer in the older top-plate, each taken twice at increasing voltages, V_{rf}, applied across the heaters. The wiggles in the flat region to the right of the peak in the transducer output on all four traces is due to interference with the eleventh harmonic of the power line frequency. The lowest chart shows a trace taken twice for only one drive voltage using the transducer in the newer top-plate. Most of the second sound amplitude measurements were taken one at a time like the lower chart. The power line interference can be seen to the left of the response peak.

The amplitude of the second sound at $f_{mc}/2$ was determined by drawing a vertical line at the measured $f_{mc}/2$ interpolated from the endpoint frequencies as described in the previous section. The amplitude of the second sound was determined at the point where the line intersects the second sound signal as shown in Fig. 34. The

119
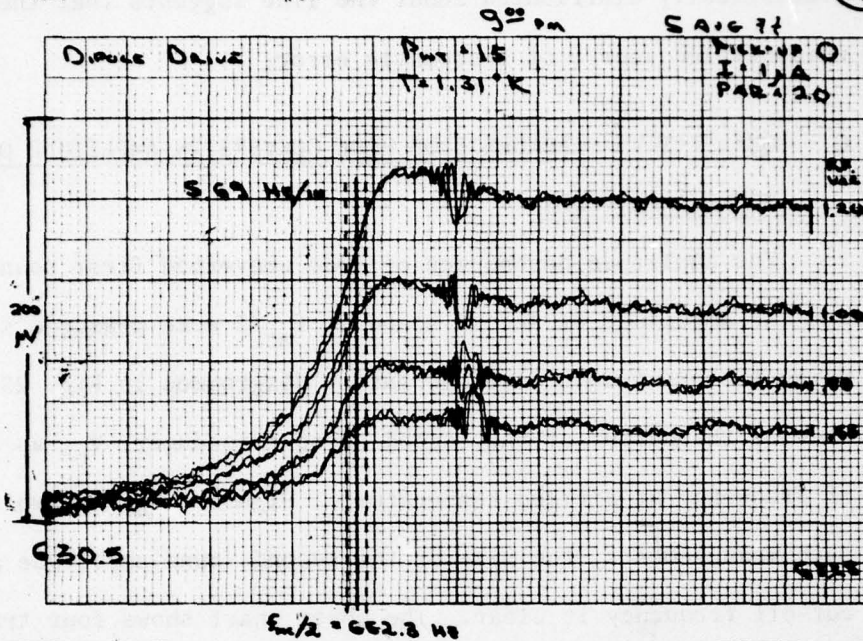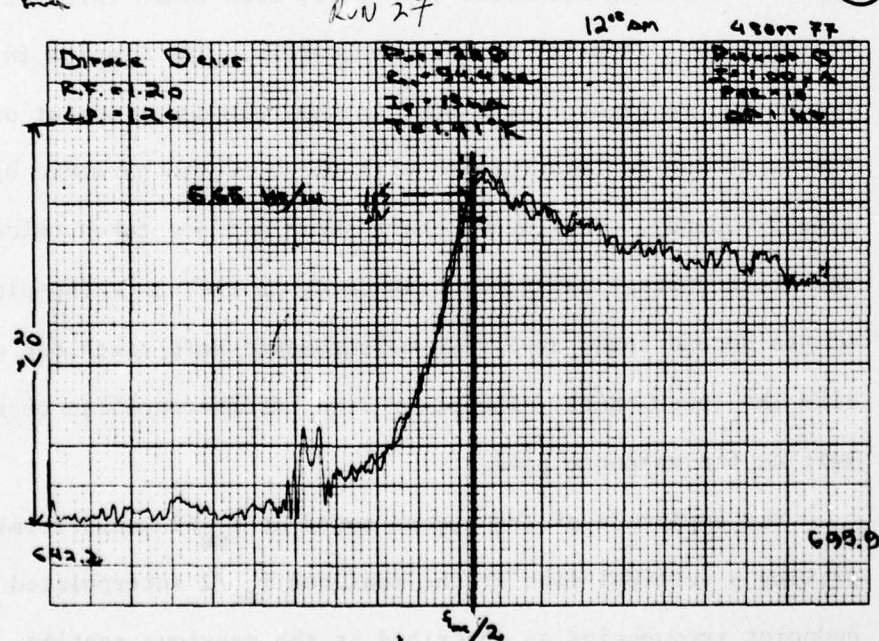
FIGURE 34. Raw second sound data around cut-off from the older (upper)
and newer (lower) top-plates.

uncertainty in the mode conversion frequency is shown by the dashed vertical lines and is reflected as an uncertainty in the amplitude of the second sound signal. Figure 35 is a logarithmic graph of the amplitude of the received signal, V_o, in r.m.s. microvolts at $f_{mc}/2$ as a function of the voltage applied to the heaters in the dipole driver for a run at 1.41°K. The solid line is a least squares power law fit to the nine points giving $V_o = 1.24 \ (V_{rf})^{1.80}$. This graph is typical of seventeen such graphs made in the course of the experiment. The average power law dependence of second sound amplitude on drive voltage was $V_{rf}^{1.78 \pm .14}$.

Figure 36 is a logarithmic plot of the output of the first sound microphone 4A´ (see Fig. 17 lower) to the room temperature pre-amplifier, $V_{4A´}$, in μV(r.m.s.), as a function of the measured output of the second sound transducer, V_o, in μV(r.m.s.) at the same nine values of driver voltage shown previously in Fig. 35. The error bars reflect the uncertainty in the first sound amplitude measured from the charts. The straight line is a least squares power law fit to the raw data shown, giving $V_{4A´} = 13.9(V_o)^{2.13}$. This is very close to the expected square law dependence.

Figure 37 shows the final stage of the data reduction for the same nine points. Using the empirical fit of the counterflow velocity, w_1, for an input of 1.00 VAC to the heaters as a function of temperature (see III-D-1 and Fig. 19) and the average power law dependence of second sound amplitude on drive voltage, the points representing the mode converted first sound are plotted logarithmically against the square of the counterflow velocity, w_1^2. The line is a least squares

121
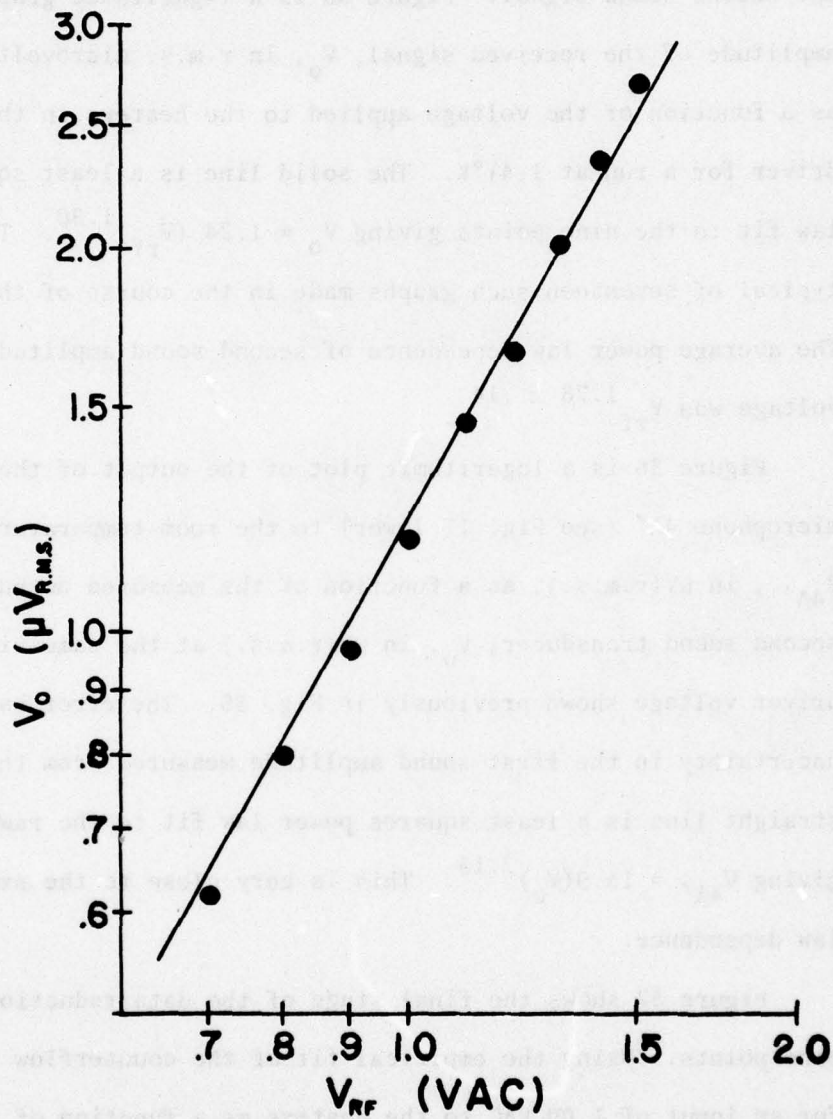
FIGURE 35. Second sound microphone output, V_o, as a function of the voltage, V_{rf}, applied across the dipole driver at 1.41°K.

122
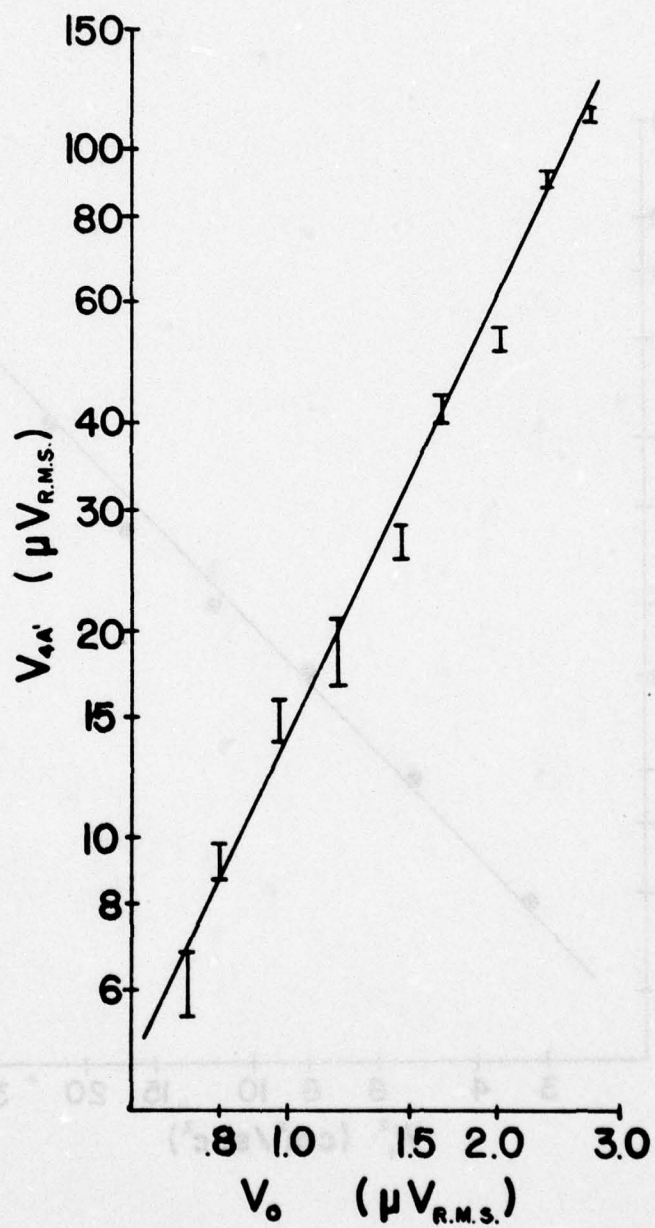
FIGURE 36. First sound microphone output, $V_{4A'}$, as measured at the room temperature pre-amp vs. second sound transducer output, V_o, at 1.41°K.

123
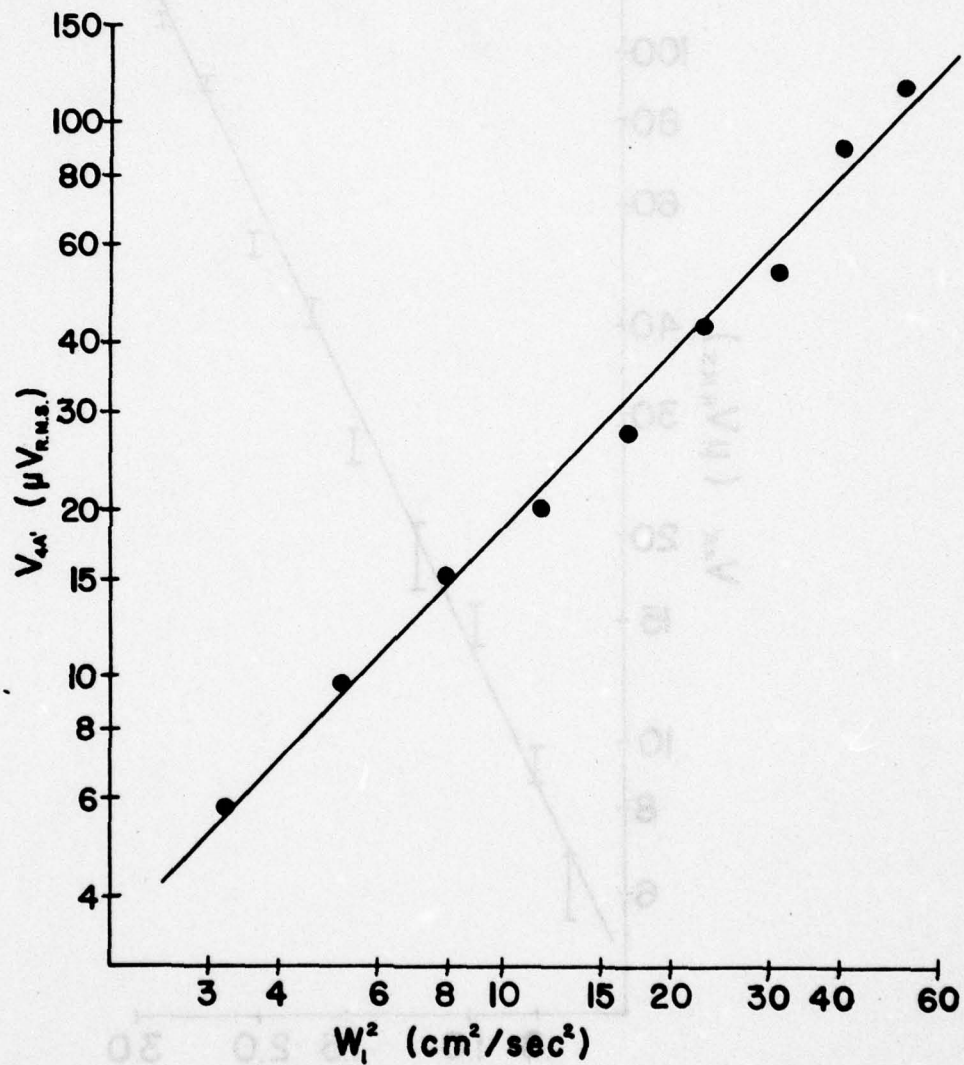
FIGURE 37. First Sound output V_{4A} as measured at the room temperature pre-amp vs. counter-flow velocity squared, w_1^2, at 1.41°K.

124

w_1^2 (cm^2/sec^2)

$V_{4A'}$ (μV r.m.s.)

1.206°

1.477°

1.938°

1.992°

2.04°
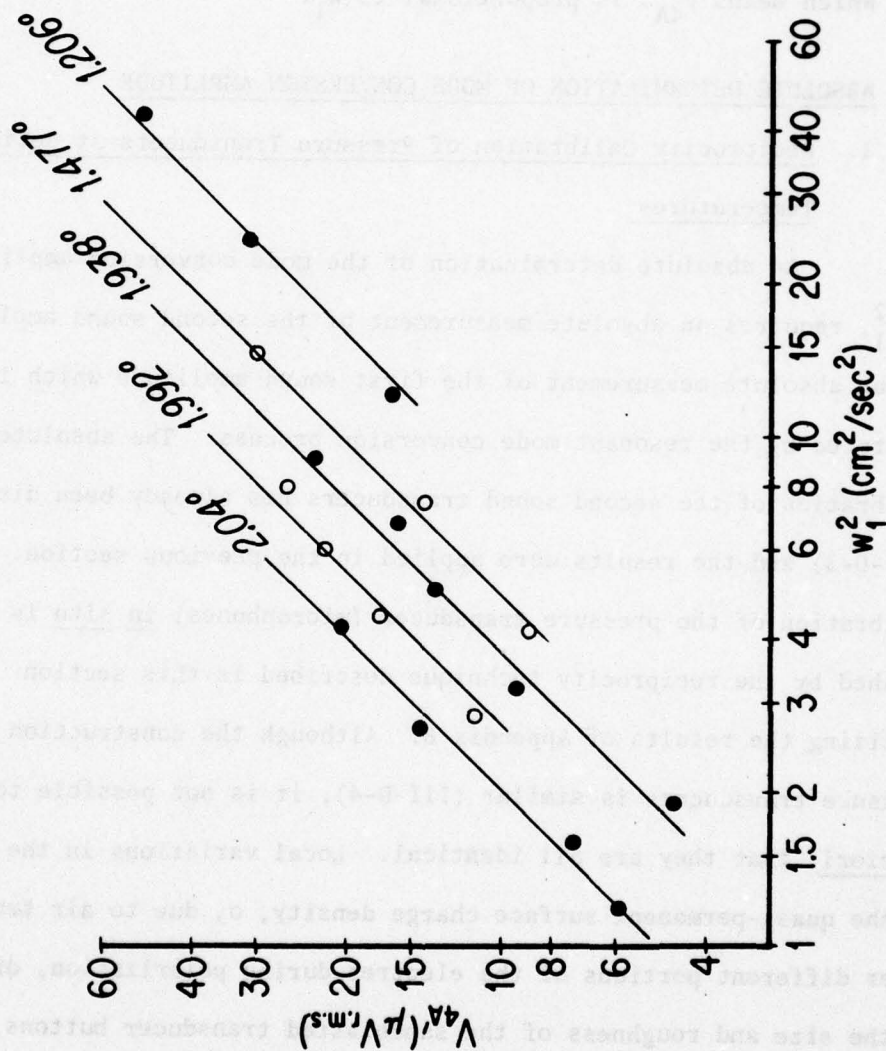
FIGURE 38. First sound transducer output, $V_{4A'}$, at five temperatures.

power law fit giving $V_{4A^-} = 1.61\left[w_1^2\right]^{1.06}$. Figure 38 shows similar plots for five other temperatures using the same transducer, clearly establishing the second-order nature of the mode conversion effect to within the accuracy of the experiment. The solid lines have a slope of 1 which means V_{4A^-} is proportional to w_1^2.

D.   ABSOLUTE DETERMINATION OF MODE CONVERSION AMPLITUDE

   1.   Reciprocity Calibration of Pressure Transducers at Helium
        Temperatures

        An absolute determination of the mode conversion amplitude p_2/w_1^2, requires an absolute measurement of the second sound amplitude and an absolute measurement of the first sound amplitude which is being generated by the resonant mode conversion process. The absolute calibration of the second sound transducers has already been discussed (III-D-3) and the results were applied in the previous section. The calibration of the pressure transducer (microphones) in situ is accomplished by the reciprocity technique described in this section utilizing the results of Appendix B. Although the construction of all pressure transducers is similar (III-D-4), it is not possible to assume, a priori, that they are all identical. Local variations in the strength of the quasi-permanent surface charge density, σ, due to air trapped under different portions of the electret during polarization, differences in the size and roughness of the sandblasted transducer buttons, and/or variations in the tension of the electret caused by unequal tightening of the screws which join the spiral waveguide body to the top-plate, might lead to differing sensitivities for each microphone. With this

126

possibility in mind, the following strategy was used to calibrate microphones using (B-51) without requiring that the resonator be terminated in two identical reversible transducers.

The upper diagram in Fig. 17 will be used to discuss the calibration procedure. As pointed out in (III-C-4), because of a small absorption coefficient for first sound the presence of the absorber in front of the reflector can be neglected for first sound if we restrict our attention to the calibration at low temperature (i.e. $\leq 1.4°K$). The waveguide can be considered as a rigid walled, plane wave resonator whose cross-sectional dimensions are small compared to the wavelengths of the first sound being considered. The lowest height (z-axis) resonance occurs at 8 kHz. For the present discussion it is only necessary to consider the transducer labeled 4A which will be used as the reversible transducer to be calibrated, 2C which need only function as a microphone, and 00 which is only used as a sound source (speaker). If 4A is driven by a voltage which is swept in frequency and fixed in amplitude, a resonance structure similar to that shown in the upper chart of Fig. 16 will be detected at the microphone 2C using the instrumentation in Fig. 39. The absolute calibration of 4A is accomplished by choosing a resonance peak at a frequency which makes the distance from 2C to the reflector (32.35 ± .2 cm) an integral number of first sound half-wavelengths. When such a resonance is found, then the acoustical environments of both 4A and 2C (i.e. the amplitudes at both locations) are identical and the following procedure is used to find the sensitivity of 4A as a microphone by the reciprocity method. The sensitivity of 2C as a microphone is determined by

127
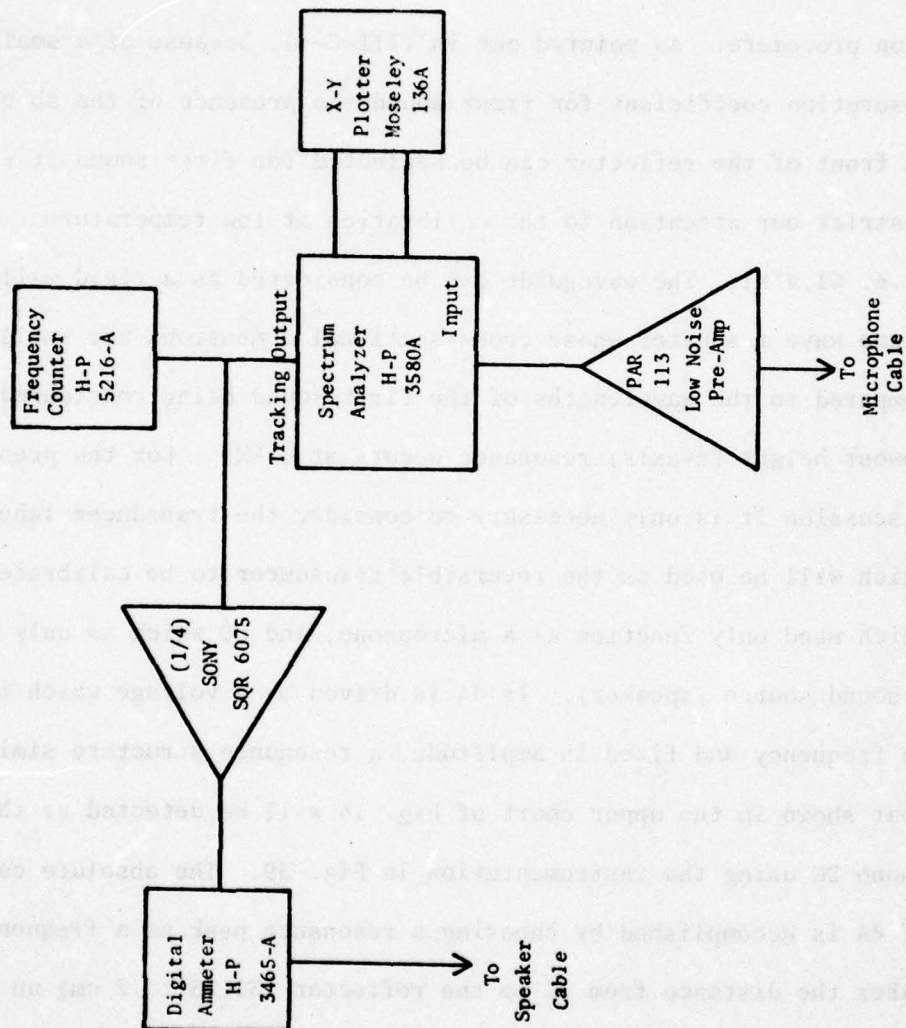
FIGURE 39. Block diagram of reciprocity calibration electronic instrumentation.

comparison with 4A. Since this method is independent of what is placed
at the "driver" end of the waveguide, except to the extent that the
termination effects the quality factor of the resonance, the calibra-
tion can be done as part of the same experiment made to observe the mode
conversion effect. If this is done, then there is no question about the
sensitivity being changed by the drastic change in temperature and
humidity when the waveguide is brought back to room temperature in air
then replaced in the dewar and bought back to liquid helium temperature.

Once a resonance is located that places 2C an integral number of
half-wavelengths from the reflector, a trace of the resonance amplitude
vs. frequency is made over typically 50 Hz, using the instrumentation
in Fig. 39, by driving 4A and using 2C as a microphone. The current
into 4A at the resonance frequency is measured and recorded. Remaining
at the resonance frequency, the drive amplifier is removed from the
reversible transducer, 4A, and connected to the speaker, in this case,
00. Monitoring the level of the input to the spectrum analyzer, the
amplitude of the drive voltage is carefully adjusted until the amplitude
of the signal received from 2C is equal to the value measured when the
resonance was driven by 4A. A second chart is then made over approxi-
mately 50 Hz as before but with the resonance excited by the speaker.
Finally with the drive amplifier still connected to the speaker, a
chart is made of the output of the reversible transducer, this time
being used as a microphone. The intermediate step of recreating the
sound field generated by the reversible transducer using the auxiliary
speaker and then using the reversible transducer to measure the sound
field allows the expression for the calibration of identical transducers

129

in a plane wave resonator (B-51) to be used since 4A is unquestionably identical to itself.

Figure 40 shows a series of three charts taken at 1.30°K as described in the preceding paragraph. The upper chart gives the response of the microphone (2C) to the reversible transducer (4A) driven with a current of 13.4 μA (r.m.s.) at resonance. The middle chart shows the same response of 2C when the resonance is excited by the speaker (00) with 15.1 VAC applied across its terminals. The bottom chart is the output of the reversible transducer (4A) to the same sound field as in the other two charts. The resonant frequency is 1069.6 ± .3 Hz and it is the eleventh (n = 11 ± 1) plane wave mode of the resonator. The microphone is 2.93 ± .02 first sound half-wavelengths from the reflector. Q = 105 ± 6. Using the known value of S/ρc, (B-51) gives a sensitivity of 4A as a microphone from purely electrical measurements, M_{4A} = 14.2 ± .8 μV/μ bar. Comparing the response of 4A and 2C to the same sound field in the middle and bottom charts gives a relative calibration of 2C with respect to 4A, M_{2C} = $(V_{2C}/V_{4A})M_{4A}$ = 16.3 ± .9 μV/μ bar, where V_{2C} is the magnitude of the response peak in the upper and middle charts and V_{4A} is the magnitude of the peak in the bottom chart.

The reciprocity calibrations used to determine microphone sensitivities were carried out in this way for transducers in both the older and newer top-plates. Two additional experimental runs were made exclusively for reciprocity calibration of microphones, one each with the older and newer top-plates, with the first sound plane wave driver (III-D-2) attached to the driver end of the waveguide. When

130
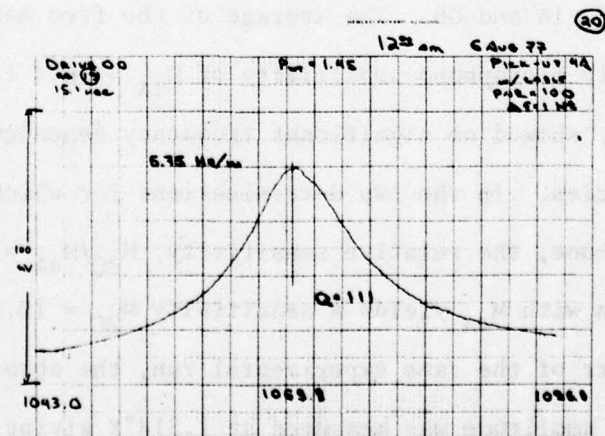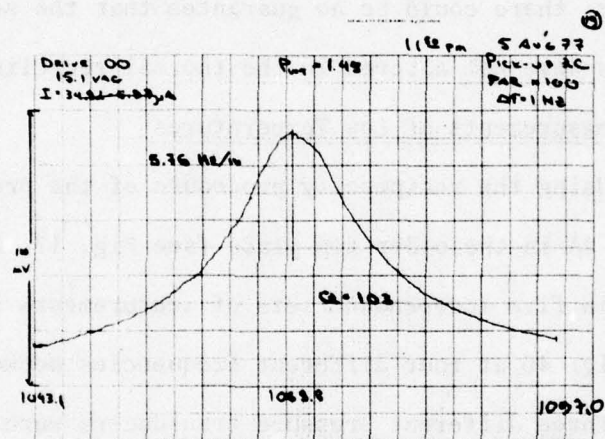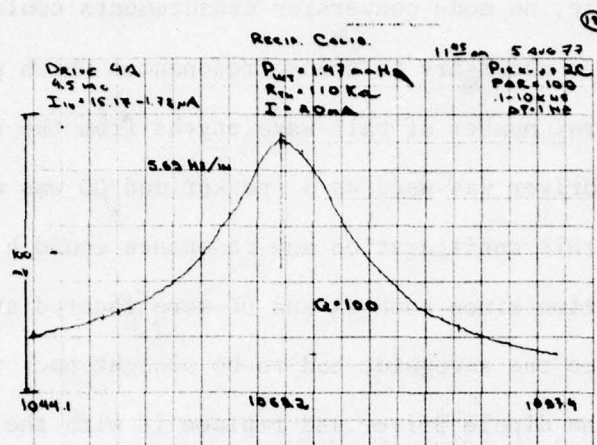
FIGURE 40. Raw data for reciprocity calibration of pressure transducer 4A at 1.308°K.

131

this was done, no mode conversion measurements could be made, but it was no longer necessary to choose resonances which put the microphone at an integral number of half-wavelengths from the reflector. The plane wave driver was used as a speaker and 00 was used as the microphone. In this configuration any resonance could be used for reciprocity calibration since both 4A and 00 were located at "rigid" terminations. Since the waveguide had to be brought back to room temperature to remove the dipole driver and replace it with the first sound plane wave dirver, there could be no guarantee that the sensitivities of the microphones were not altered in the thermal recycling process.

2. Measurements at Low Temperatures

Using the reciprocity procedure of the previous section, transducer 4A in the older top-plate (see Fig. 17, upper) was calibrated at 1.30°K in five independent sets of measurements similar to those shown in Fig. 40 at four different frequencies between 253 Hz and 1070 Hz. Three different pressure transducers were used as microphones: 2C, 1A and 0B. The average of the five measurements gives an open circuit microphone sensitivity of M_{4A} = 16.4 ± 4.9 μV/μ bar. The sensitivity showed no significant frequency dependence in that range of frequencies. In the two determinations for which 2C was used as the microphone, the relative sensitivity, M_{2C}/M_{4A} = .93 ± .31 which in combination with M_{4A} yields a sensitivity M_{2C} = 15.2 ± 6.8 μV/μ bar.

As part of the same experimental run, the absolute resonant mode conversion amplitude was measured at 1.314°K giving a value of p_2/w_1^2 = .061 ± .027 dyne cm^{-4} sec^{-2}. That point is plotted in Fig. 41 and is the lower of the two points at that temperature. After running

132
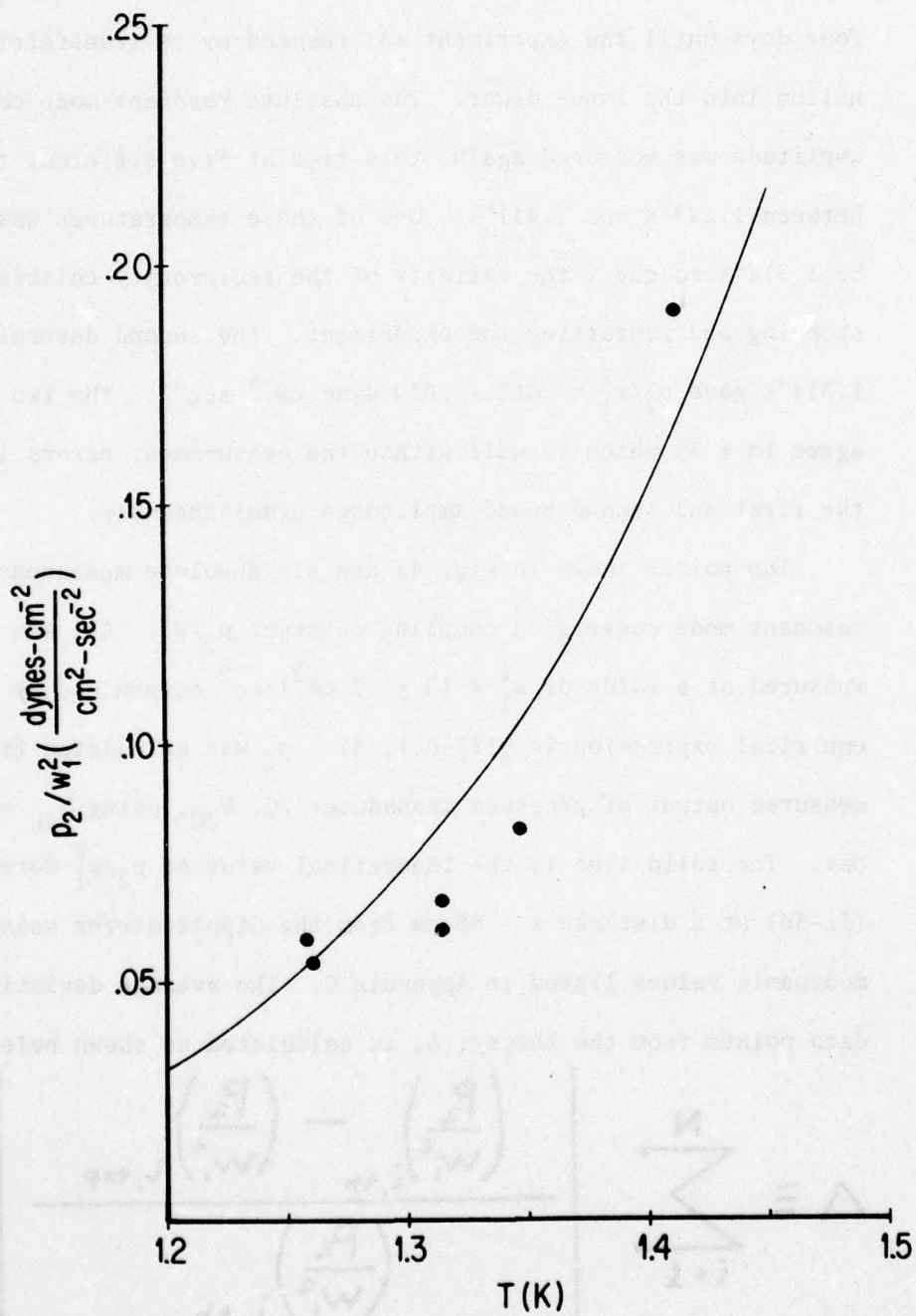
FIGURE 41. Absolute measurement of resonant mode conversion amplitude.

out of liquid helium, the entire experiment was kept evacuated for four days until the experiment was resumed by re-transferring liquid helium into the inner dewar. The absolute resonant mode conversion amplitude was measured again, this time at five different temperatures between $1.258°K$ and $1.411°K$. One of those temperatures was chosen to be $1.314°K$ to check the validity of the reciprocity calibration after stopping and restarting the experiment. The second determination at $1.314°K$ gave $p_2/w_1^2 = .067 \pm .030$ dyne cm^{-4} sec^{-2}. The two values agree to $\pm 5\%$ which is well within the measurement errors in determining the first and second sound amplitudes simultaneously.

The points shown in Fig. 41 are six absolute measurements of the resonant mode conversion coupling constant p_2/w_1^2. All six points were measured at a value of $w_1^2 = 15 \pm .5$ cm^2/sec^2 determined by the empirical expression in (III-D-1, 3). p_2 was calculated from the measured output of pressure transducer 2C, V_{2C}, using $M_{2C} = 15.2$ $\mu V/\mu$ bar. The solid line is the theoretical value of p_2/w_1^2 determined by (II-36) at a distance $x = 86$ cm from the dipole dirver using the thermodynamic values listed in Appendix C. The average deviation of the data points from the theory, Δ, is calculated as shown below.

$$\Delta \equiv \frac{\sum_{i=1}^{N} \left| \frac{\left(\frac{P_2}{W_1^2}\right)_{i,th} - \left(\frac{P_2}{W_1^2}\right)_{i,exp}}{\left(\frac{P_2}{W_1^2}\right)_{i,th}} \right|}{N}$$

In Fig. 41, N = 6 and Δ = 16%.

Resonant mode conversion was observed to occur at the theoretically
predicted frequency (see Fig. 32) and exhibited the quadratic amplitude
dependence characteristic of a second-order effect up to temperatures
of 2.04°K. Since absolute calibrations of the pressure transducers
were not available in the newer top-plate, that data could not be used
for an absolute experimental determination of p_2/w_1^2 at the higher
temperatures.

E.   SUMMARY OF RESULTS

At this point it is useful to review the experimental evidence
presented in this chapter which confirms the observation of the new
non-linear effect of resonant mode conversion of second sound to first
found in He II as observed in the waveguide geometry described in
Chapter II, Sections B and C.

(i)   In a waveguide the resonance condition is met at a specific
frequency (III-8) and Figs. 30 and 31 show unambiguous data generated
by the mode conversion process at four different temperatures. Figure
32 summarizes the results of 150 individual measurements of this effect
made over a six month time span at 55 different temperatures between
1.14°K and 2.0°K showing clearly that the resonance occurs precisely
(i.e. ± 0.1%) at the theoretically predicted frequency over the entire
temperature range.

(ii) Since the effect is due to a non-linear interaction, the mode
conversion amplitude is expected to have a linear dependence on the
square of the amplitude of the primary wave, in this case, second

135

sound. Figure 37 shows the dependence of the mode conversion amplitude on the square of the second sound amplitude, w_1^2, over a dynamic range of 1.3 decades at 1.41°K. The experimental points fall on a line of slope 1.06 within the small random experimental error. Figure 38 shows a similar plot of the experiment data at five different temperatures between 1.206°K and 2.04°K. The solid lines on the graph have a slope of 1.

(iii) The absolute value of the coupling between the mode converted wave and the primary waves, p_2/w_1^2, is given by the theory presented in Chapter II (II-36) and compared to the absolute experimental measurements in Fig. 41. The six data points shown for the temperature between 1.258°K and 1.411°K agree with the theory to within 16% on the average.

136

CHAPTER V.

CONCLUSION

Joy in looking and comprehending
is nature's most beautiful gift.
A. Einstein[119]

A. SUMMARY

In Chapter II the macroscopic description of superfluid helium known as the Two Fluid Theory was solved for perturbations from equilibrium in a consistent fashion which included all terms up to second order in the displacement from equilibrium. The theory revealed a new resonant non-linear coupling of second sound to first sound. Chapter III described an experimental geometry and transducers which allowed a quantitative test of the predicted resonant mode conversion. The results in Chapter IV show that such a process does take place when the resonance condition is met. Measurements of the mode conversion frequency and the quadratic dependence of the mode converted first sound amplitude on the primary second sound are in excellent quantitative agreement with the theory over the entire range of temperatures accessible to the apparatus (1.14°K to 2.04°K). The absolute magnitude of the coupling of second sound to first sound was measured between 1.258°K and 1.411°K and was found to be in quantitative agreement with values based on the measured thermodynamic properties of the superfluid.

It should be pointed out that $\partial \rho / \partial w^2$ is the dominant thermodynamic term in the non-linear coupling of second sound to first sound,

theoretically accounting for 80% of the total effect (see Fig. 6). The agreement of the measured and theoretical values of p_2/w_1^2 is a direct confirmation of the importance of the additional Galilean invariant internal variable, $w^2 = (\vec{v}_n - \vec{v}_s)^2$, in the thermohydrodynamics of superfluid helium, particularly for non-linear effects. It is also a confirmation of the validity of the expression for the differential of the chemical potential (I-7) which includes the intrinsically non-linear thermodynamic variable.

In conclusion it can be said that the results of this experiment confirm the validity of the Two Fluid Theory of He II up to terms of second order through the observation of a new acoustical effect that has not previously been observed in any fluid.

B. FURTHER EXPERIMENTS AND THEORETICAL INVESTIGATIONS

In the future, absolute measurement of the mode conversion coupling constant should be extended to cover at least the same range of temperature as the other measurements of mode conversion frequencies, Q's and drive dependence. An increase in the precision of the reciprocity calibrations and in signal-to-noise ratios, possibly by using both reversible transducers and low temperature FET pre-amplifiers, could lead to more precise measurements of the thermodynamics of the superfluid particularly with regard to $(\vec{v}_n - \vec{v}_s)^2$. Additional reciprocity calibrations leading to "calibration histories" of electret microphones at low temperatures, and subject to the severe thermal and humidity cycling effects between room environments and liquid temperatures, would be interesting and useful in and of itself.

There is another avenue of both experimental and theoretical investigation which is related to non-linear parametric mode coupling of pressure and temperature disturbances in He II that may also turn out to be both interesting and significant. It is possible for first or second sound to couple to the pressure or temperature fluctuations present in bulk He II through a non-linear interaction. The energy lost to the mode generated by this non-linear interaction might be detectable as an attenuation of the first or second sound which is linear in frequency. Careful measurements of the attenuation of second sound, for example, might reveal as "dip" in the attenuation coefficient at the point where the non-linear coupling coefficient vanishes. For attenuation of second sound due to the interaction with thermal fluctuations the coupling coefficient is γ (II-29) and it vanishes at 1.884°K at saturated vapor pressure as shown in Fig. 5.

It has been pointed out[120] that it will also be interesting to investigate whether the linear dissipation coefficients which arise from the non-linear mode coupling obey the Onsager symmetry relations.[121]

APPENDIX A.

PARAMETRIC AMPLIFICATION OF SECOND SOUND BY FIRST SOUND

The use of high intensity first sound to amplify second sound was first proposed by Pushkina and Khokhlov.[63] Their approach was to solve three coupled first order differential equations including damping and to express their results in terms of elliptic functions. Here the procedures will be identical to that used in Chapter II, Section D. From the second order wave equation for T_2 (II-22) only terms involving the product $p_1 T_1$ are selected.

$$\frac{\partial^2 T_2}{\partial t^2} - u_2^2 \nabla^2 T_2 = u_2^2 \left(\vec{N}_{m,1} \cdot \vec{A}_1 \right) \qquad (A-1)$$

$$- \frac{1}{\rho} \left(\frac{\partial s}{\partial T} \right)^{-1} \left\{ \rho \frac{\partial^2 s}{\partial \rho \partial T} \frac{\partial^2 T_1 p_1}{\partial t^2} + \frac{\partial}{\partial t} \rho \frac{\partial s_1}{\partial t} \right.$$

$$\left. \frac{\partial}{\partial t} \vec{J}_1 \cdot \vec{\nabla} s_1 + \frac{\partial}{\partial t} \nabla \cdot \left(\vec{A}_1 \left[\frac{\rho \rho s^2}{\rho_m} \right]_1 \right) \right\}$$

Consider the amplification of a second sound wave, T_1, by the <u>anti-colinear</u> interaction with a "pump" wave of first sound, p_1, to generate a second order second sound wave, T_2, whose frequency has been up-shifted from that of T_1 by an amount of 2δ. The physical situation is diagrammed below
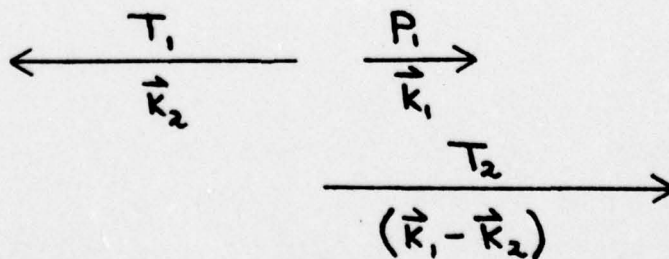
Function	Variable	Wavevector	Frequency
Pump	p_1	$\vec{k}_1$	$\omega_1 = \omega_o$
Seed	T_1	$\vec{k}_2$	$\omega_2 \quad \omega_o/2 - \delta$
Amplified	T_2	$\vec{k}_1 - \vec{k}_2$	$\omega_1 - \omega_2 = \omega_o/2 + \delta$

If the x-axis is taken along $\vec{k}_1$ then

$$p_1 = p' \exp\left[i\left(|\vec{k}_1|x - \omega_1 t\right)\right]$$

$$T_1 = T' \exp\left[i\left(|\vec{k}_2|x + \omega_2 t\right)\right]$$

$$p_1 T_1 = p'T' \exp\left[i\left(|\vec{k}_1| + |\vec{k}_2|\right)x - i\left(\omega_1 - \omega_2\right)t\right]$$

A resonance will occur when $p_1 T_1$ has the same phase velocity as the wave operator on the right hand side of (A-1). This condition can be expressed as

$$\frac{\omega_1 - \omega_2}{|\vec{k}_1 - \vec{k}_2|} \qquad \frac{\omega_1 - \omega_2}{|\vec{k}_1| + |\vec{k}_2|} = u_2 \qquad \text{(A-2)}$$

$$\delta = \frac{\omega_o}{2} \frac{u_2}{u_1}$$

Putting all first order quantities in (A-1) in terms of p_1 and $T_1^{(54)}$ and expanding the square bracketed term with respect to first order pressure excursions,

$$\left[\frac{p_1 \rho s^2}{\rho_m}\right]_1 = s^2 \left\{ \frac{\rho_1}{\rho_m} \frac{1}{u_1^2} - \rho\left(\frac{\rho}{\rho_m}\right) \frac{\partial \frac{s_1}{s}}{\partial p} - \frac{2\rho_1}{\rho_m} \frac{\beta_p}{s} \right\} p_1$$

the wave equation (A-1) can be written for the resonant case,

$$\frac{\partial^2 T_2}{\partial t^2} - u_1^2 \frac{\partial^2 T_2}{\partial x^2} = \frac{E p' T' \omega_o}{4} \left(1 + \frac{u_2}{u_1}\right) e^{i(\vec{k}_1 - \vec{k}_2) \cdot \vec{x} - i(\omega_1 - \omega_2)t} \qquad \text{(A-3)}$$

$$E \equiv \frac{1}{\rho u_1^2} + \frac{\partial^2 s}{\partial p \partial T} \left(\frac{\partial s}{\partial T}\right)^{-1} + \frac{\partial \ln(\rho_1 \rho/\rho_m)}{\partial p}$$

141
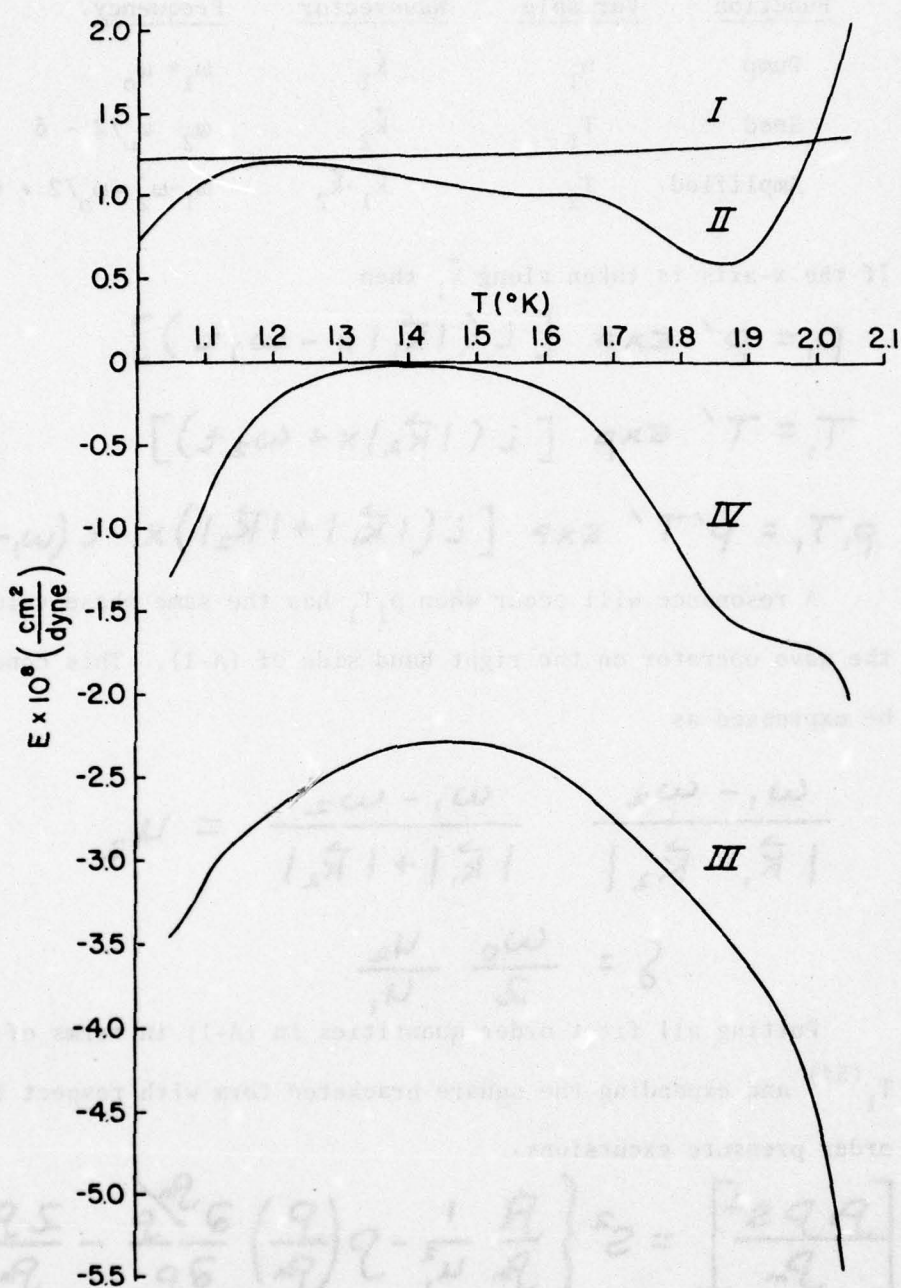
FIGURE 42. The temperature dependence at the vapor pressure of the thermodynamic quantities determining the parametric amplification of second sound by first sound. (I) $1/\rho u_1^2$; (II) $(\partial s/\partial T)^{-1} \partial^2 s/\partial p \partial T$; (III) $\partial[\log \rho_s \rho/\rho_n]\partial p$; (IV) = I + II + III.

142

Fig. 42 is a graph of the relevant thermodynamic terms in E as a function of temperature at the vapor pressure.

If it is assumed that the primary first and second sound waves have attenuation coefficients γ_1 and γ_2 respectively, techniques analogous to those in II-D yield the following solution for the asymptotic of T_2

$$\frac{E\,P'\,T'\,\omega_o}{8\,i\,u_2\,(\gamma_1+\gamma_2)}\left(1+\frac{u_2}{u_1}\right) \qquad (A-4)$$

for the case where $|\vec{k}_1-\vec{k}_2| \gg (\gamma_1+\gamma_2)$.

Pushkina and Khokhlov assert that there is a threshold for this process. This is not true although there is a "breakeven" point at which the process gives unity gain. They obtain a value for their threshold at 1.5°K for the following choice of parameters:

$$\omega_o = 2\pi \times 2 \times 10^5 \text{ sec}^{-1}$$
$$\alpha = 0.1 \text{ cm}^{-1} \text{ (64)}$$
$$c_1 = 2.3 \times 10^4 \text{ cm/sec}$$
$$c_2 = 2 \times 10^3 \text{ cm/sec}$$
$$\rho = .14 \text{ gm/cm}^3$$
$$\rho_s = 0.9\,\rho$$

Based on the above values they calculate a threshold intensity, $I_{th} = 3 \times 10^{-3} \text{ W/cm}^2$, corresponding to pressure swings of 1.4×10^4 dynes/cm^2 peak. This is nearly an order of magnitude larger than the measured cavitation threshold in He II at this temperature.[65] Furthermore in the calculation of their coupling coefficient they neglected a term proportional to the mixed partial derivative of entropy which cancels their leading term.

Proper evaluation of the breakeven pressure amplitude

$$p_1 (\text{BREAKEVEN}) = \left(\frac{T_2}{\rho' T'} \right)^{-1} \qquad (A-5)$$

from (A-4) using Pushkina's choice of parameters gives p_1 (breakeven) = 1.1×10^6 dynes/cm^2 (using the correct value of the attenuation coefficient[64] this would be 5.5×10^6 dynes/cm^2). This would correspond to an intensity of 18 W/cm^2. In air such a sound field would ignite cotton in a fraction of a second!

A later paper by the same authors[66] suggested that this process might be used to generate high frequency sound in superfluid ^{3}He-A. Their incorrect assumption that the attenuation of second sound in ^{3}He-A has the same value as in ^{4}He alone (they also assumed without justification that the coupling coefficient would be the same) leads to an estimation of I_{th} which is too small by at least 20 orders of magnitude.

144

APPENDIX B.

RECIPROCITY CALIBRATION OF MICROPHONES
IN A PLANE WAVE RESONATOR[102]

1. Introduction

The principle of reciprocity was first introduced into acoustics by
Rayleigh in 1873 when he derived the reciprocity relation for a system
of linear equations and gave "a few examples [to] promote the comprehen-
sion of a theorem which, on account of its extreme generality, may appear
vague".[103] He cited physical examples in acoustics, optics and elec-
tricity and credited Helmholtz with a derivation of the result in a
uniform, invisid fluid in which is immersed any number of rigid, fixed
solids, pointing out the principle "will not be interfered with" even
in the presence of damping. The first physical example of the reci-
procity theorem given by Rayleigh, and the most relevant for the dis-
cussion of the calibration of microphones in a plane wave resonator,
is the following:

> Let A and B be two parts of a uniform or variable
> stretched string. If a periodic transverse force
> acts at A, the same vibration will be produced at
> B as would have ensued at A had the force acted
> at B.

The consequences of the reciprocity theorem for the absolute cali-
bration of microphones without a primary standard were not exploited
until 1940 when Mac Lean,[104] and independently Cook,[105] showed it
was possible to find the absolute sensitivity of an electroacoustic

145

transducer by making purely electrical measurements. Since that time it has been generally recognized that reciprocity calibration is the method of choice for absolute determination of the sensitivity of microphones and in careful experiments the precision of this method is limited only by the quality of the electrical attenuators that are available.[106]

2. Reciprocity Relations

If we consider the following linear, passive, 4-pole network,

$$V_1 = ai_1 + bi_2 \qquad (B\text{-}2)$$
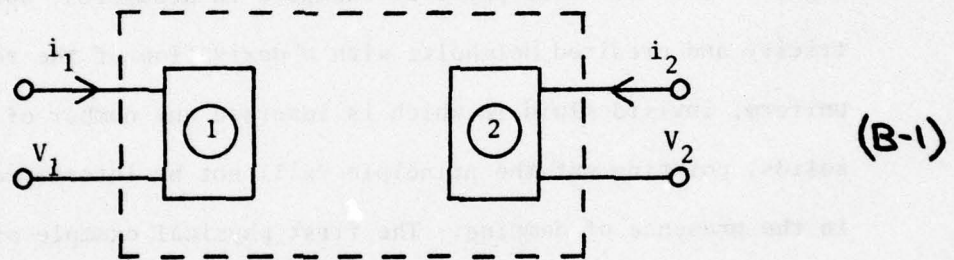
$$V_2 = bi_1 + ci_2 \qquad (B\text{-}3)$$

the response can be written as two linear equations

where the co-efficient b is the same in (B-2) and (B-3) because of reciprocity condition.[107]

If 1 and 2 are reversible electroacoustic transducers then, following Mac Lean, but not restricting ourselves as yet to a particular geometry, we can define their sensitivity when used as a microphone M and their strength as a sound source, S, as follows

146

$$M_o = \frac{\text{Open circuit voltage}}{\text{pressure at microphone}} \qquad \text{(B-4)}$$

$$M_s = \frac{\text{Short Circuit current}}{\text{pressure at microphone}} \qquad \text{(B-5)}$$

$$S_o = \frac{\text{Pressure at microphone location}}{\text{current into speaker terminals}} \qquad \text{(B-6)}$$

$$S_s = \frac{\text{Pressure at microphone location}}{\text{voltage across speaker terminals}} \qquad \text{(B-7)}$$

If transducer 1 is driven with a current i_1, and transducer 2 is short circuited, (B-2) and (B-3) become

$$V_1 = a i_1 + b i_2$$

$$0 = b i_1 + c i_2$$

or

$$\frac{V_1}{i_2} = b - \frac{ac}{b} \qquad \text{(B-8)}$$

Similarly if 2 is driven and 1 is shorted

$$0 = a i_1 + b i_2$$

$$V_2 = b i_1 + c i_2$$

or

$$\frac{V_2}{i_1} = b - \frac{ac}{b} \qquad \text{(B-9)}$$

so

$$\frac{V_2}{i_1} = \frac{V_1}{i_2} \qquad \text{(B-10)}$$

147

From the definitions (B-5, 7)

$$V_1 S_{s1} = \text{pressure at mike 2}$$

$$V_1 S_{s1} M_{s2} = i_2 \qquad \text{(B-11)}$$

where i_2 is the short circuit current produced in mike 2 due to the voltage applied to the terminals of speaker 1. (B-11) yields

$$\frac{V_1}{i_2} = 1 / M_{s2} S_{s1} \qquad \text{(B-12)}$$

similarly

$$V_2 S_{s2} M_{s1} = i_1 \qquad \text{(B-13)}$$

and

$$\frac{V_2}{i_1} = \frac{1}{M_{s1} S_{s2}} \qquad \text{(B-14)}$$

Combining (B-12, 14)

$$\frac{M_{s2}}{S_{s2}} = \frac{M_{s1}}{S_{s1}} \qquad \text{(B-15)}$$

Therefore the ratio of a transducer's sensitivity as a microphone to its strength as a source is independent of the particular construction of the transducer and depends only on the properties of the space through which the sound is radiated. Two more repetitions of arguments similar to (B-8) through (B-15) give the results of Mac Lean

$$\frac{M_{s1}}{S_{s1}} = \frac{M_{s2}}{S_{s2}} = \frac{M_{o1}}{S_{o1}} = \frac{M_{o2}}{S_{o2}} \qquad \text{(B-16)}$$

For the case where both transducers are identical, for example $M_{o1} = M_{o2}$, and define

148

$$\frac{M_0}{S_0} = \frac{1}{Z} \qquad (B-17)$$

where, for the moment, Z is a quantity which characterizes the acoustic geometry and has the units of an acoustical impedance (pressure/volume velocity = gm/cm^4-sec) we can put a current, i_1, into one transducer and measure V_2 out of the other

$$i_1 \, S_{o1} \, M_{o2} = V_2 \qquad (B-18)$$

and since 1 and 2 are identical

$$\frac{V_2}{i_1} = Z \, M_0^2 \qquad (B-19)$$

or

$$M_0 = \left(\frac{V_2}{i_1} \frac{1}{Z} \right)^{1/2} \qquad (B-20)$$

The above expression will give an absolute calibration of the transducer from purely electrical measurements if a means of calculating Z is known for the specific geometry.

3. Acoustical Transfer Impedance

Since Z is only a function of the acoustical geometry and not a property of the specific transducer, it is sensible to try to interpret Z for a pair of "ideal" transducers. For this section ideal will be taken to mean: (1) The transducer is so small compared to the wavelengths of interest that its presence in the sound field does not alter the pressure distribution that existed before it was introduced, that

149

is, diffraction effects of the transducer are negligible. (2) The
transducer is "stiff". That is, it does not "feel" the acoustic "load".
When used as a source its displacement (volume velocity) is the same
whether it is in a vacuum or in contact with the medium. As a micro-
phone, it means that any compliance it has does not effect the pressure
produced at its surface. The following is an equivalent circuit for
the associated linear equation for such an ideal transducer used as a
source.

$$(B-21)$$
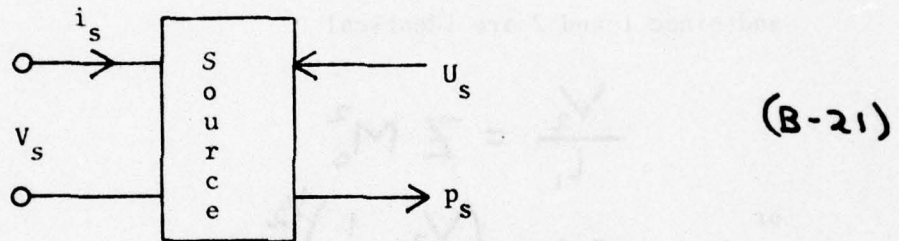
where U_s is the volume velocity generated at the source and p_s is the
pressure at the source.

$$V_s = a\, i_s + b\, U_s \qquad (B-22)$$

$$P_s = 0 = b\, i_s + c\, U_s \qquad (B-23)$$

where p_s is zero since U_s is independent of p for the ideal transducer.
Combining (B-22,23)

$$\frac{V_s}{U_s} = b - \frac{ac}{b} \qquad (B-24)$$

Considering now the microphone in a short circuited configuration

$$U_m \longrightarrow \boxed{\begin{array}{c} M \\ i \\ k \\ e \end{array}} \longleftarrow i_m$$

$$p_m \longleftarrow$$

(B-25)
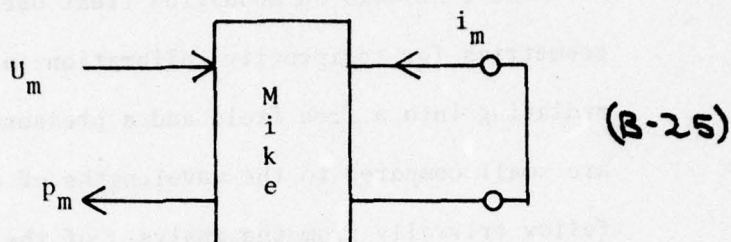
$$O = a\, i_m + b\, U_m \qquad \text{(B-26)}$$

$$P_m = b\, i_m + c\, U_m \qquad \text{(B-27)}$$

Combining (B-26, 27)

$$\frac{P_m}{i_m} = b - \frac{ac}{b} \qquad \text{(B-28)}$$

or from (B-24,28)

$$\frac{P_m}{i_m} = \frac{V_s}{U_s} \qquad \text{(B-29)}$$

Eliminating $i_m = p_m M_s$ and $V_s = p_m/S_s$ and using (B-16, 17)

$$\frac{P_m}{U_s} = \frac{S_s}{M_s} = \frac{1}{Z} \qquad \text{(B-30)}$$

where Z is now the acoustic transfer impedance defined by (B-30) as

$$Z = \frac{\text{pressure at the mike}}{\text{volume velocity at the source}}$$

With the above identification of Z it is now possible to calculate

a form for (B-20) that will give microphone sensitivities from purely

electrical measurements in many useful geometries.

151

4. Plane Wave Resonators

Most textbooks on acoustics treat one or both of two standard geometries for reciprocity calibration: a spherically symmetric source radiating into a free field and a pressure coupler whose dimensions are small compared to the wavelengths of interest. Those two cases follow trivially from the analysis of the previous sections (B-20, 30) as will be shown. For absolute determination of mode conversion amplitudes, it would be useful to have an expression of the form (B-20) for a reciprocity calibration in a plane wave resonator. This can be done using an expression for the acoustic transfer impedance calculated here for the case of two transducers at the ends of a plane wave resonator.

The expression for the sensitivity of a microphone in a free field follows from the usual expression for the pressure field of a sphere executing symmetric pulsations of volume velocity, $U_s = 4\pi a^2 u_o$ where a is the equilibrium radius of the sphere and u_o is the radial velocity of a point on its surface.[108]

$$P = \frac{i\rho c}{2d\lambda} U_s \exp i(k_n - \omega t) \qquad (B-31)$$

Neglecting the phase of the pressure with respect to the volume velocity, the transfer admittance becomes

$$\frac{1}{Z} = \frac{2d\lambda}{\rho c} \qquad (B-32)$$

and neglecting the dissipation within the medium between the spherical source and the microphone, (B-20) becomes

152

$$M_0 = 10^{-7/2} \left(\frac{V_m}{i_s} \frac{2 d \lambda}{\rho c} \right)^{1/2} \qquad \text{(B-33)}$$

The factor $10^{-7/2}$ occurs if V and i are in practical (MKS), rather than electrostatic units (abvolts and abamperes) and M is given in volts/dyne-cm^2.

In a rigid walled cavity of dimensions much less than a wavelength, the adiabatic gas law

$$pV^{\gamma} = const. \qquad \text{(B-34)}$$

can be differentiated to give the transfer impedance if $\partial p/\partial t = -i\omega \, p_m$ and $U_s = \partial V/\partial t$ and $\gamma p_o/\rho = c^2$ where c is the adiabatic sound speed

$$\frac{\partial p}{\partial t} V^{\gamma} + p_o \gamma V^{\gamma-1} \frac{\partial V}{\partial t} = 0 \qquad \text{(B-35)}$$

$$1/Z = i\omega V / \rho c^2 \qquad \text{(B-36)}$$

where V is the volume of the cavity. Putting (B-36) into (B-20) the standard result[109] is again obtained.

$$M_0 = 10^{-7/2} \left(\frac{V_m}{i_s} \frac{i\omega V}{\rho c^2} \right)^{1/2} \qquad \text{(B-37)}$$

The case of the plane wave resonator can be treated in the following way. Suppose there is an identical source and microphone in the geometry schematically indicated on the next page.

153

Plane Wave Resonator

$(B\text{-}38)$
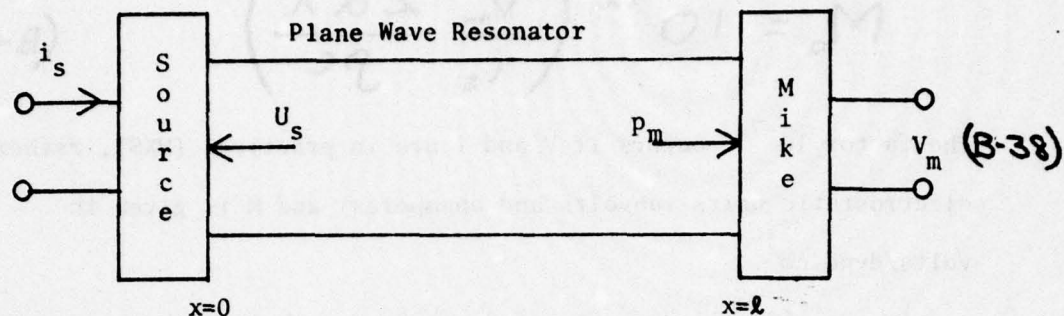
One way to model the losses in the resonator is to let the source be a perfect reflector and give the microphone an amplitude reflection coefficient of $R < 1$ and $1-R = \varepsilon \ll 1$. For our present purposes, the solution to the calibration problem would be unaffected if an attenuation coefficient were introduced instead of a reflection coefficient which gave a continuous degradation of the wave amplitude along its path instead of a transmission loss at one location since there is no way to distinguish between the two models based on an amplitude measurement made at a single point.

If we are only concerned with the reciprocity calibration of first sound ($v_n = v_s$) transducers and we let all of the loss occur at $x = \ell$, the medium within the resonator can be treated as a classical Euler fluid[110] and a single velocity potential, ϕ, can be defined for the particle velocity, u, in one dimension

$$u = \frac{\partial \phi}{\partial x} \qquad\qquad (B\text{-}39)$$

154

and the volume velocity, U_s = Su where S is cross-sectional area of the resonant cavity. The Euler Equation[110] gives to lowest order

$$P = -\rho \frac{\partial \phi}{\partial t} \qquad (B\text{-}40)$$

The standing wave field within the resonator can be written as the sum of a left-going and right-going wave and the velocity potential can be written

$$\phi = \phi_o \left\{ \exp\left[i\omega t - ik(x-\ell)\right] \right. \qquad (B\text{-}41)$$
$$\left. + R \exp\left[i\omega t + ik(x-\ell)\right] \right\}$$

This is consistant with the model we have chosen of a wave of unit amplitude being radiated to the right from the source, reflected with amplitude R, reflected from the source with amplitude R, and coming back from the microphone with amplitude R^2, etc. The coefficient of the right-going wave would be given by the infinite geometric series $1 + R + R^2 + R^3$ .... and the left-going wave would be R times that. Absorbing the sum of the series into ϕ_o, (B-41) has the proper form. From (B-39, 40)

$$P_m = P(x=\ell) = i\rho\omega \phi_o (1+R) e^{i\omega t} \qquad (B\text{-}42)$$

$$U_s = S\frac{\partial \phi}{\partial x}\bigg|_{x=0} = ikS\phi_o \left[e^{ik\ell} - Re^{ik\ell}\right] e^{i\omega t} \qquad (B\text{-}43)$$

giving an acoustic transfer impedance

155

$$Z = \frac{P_m}{U_s} = \frac{-\rho c}{S} \frac{(1+R)}{e^{ik\ell} - R e^{-ik\ell}} \qquad (B-44)$$

At resonance, $k_n \ell = n\lambda$ or $\omega_n = n\pi c/\ell$

$$Z = \frac{P_m}{U_s} = \frac{\rho c}{S} U_s \frac{(1+R)}{(1-R)} \qquad (B-45)$$

As expected the transfer impedance at resonance is dependent upon the amount of loss in the resonator, measured in (B-45) by the value of R. The quantity which is much easier to determine experimentally is the quality factor for the $n\underline{th}$ resonance, $Q_n = \omega_n/2\Delta\omega_n$ where $\omega_\pm = \omega_n \pm \Delta\omega_n$ are the -3 dB points for the resonance. For convenience let $\delta_n = \Delta\omega_n \ell/c$.

$$\left[\frac{P(\omega_n + \Delta\omega_n)}{P(\omega_n)} \right]^2 = \frac{1}{2} = \frac{(1-R)^2}{\left(e^{+i\delta_n} - R e^{-i\delta_n} \right)\left(e^{-i\delta_n} - R e^{+i\delta_n} \right)} \qquad (B-46)$$

which yields

$$\delta_m = \frac{1-R}{R^{1/2}} \qquad (B-47)$$

in the limit $\delta_m \ll 1$. From the definition of Q, (B-47) can be re-expressed

$$1-R = R^{1/2} \frac{m\pi}{Q_m} \qquad (B-48)$$

and substituting (B-48) into the transfer impedance at resonance (B-45)

156

$$Z = \frac{P_m(\omega_m)}{U_s} = \frac{\rho c}{S} \frac{1+R}{R^{1/2}} \frac{Q_m}{m\pi} \qquad \text{(B-49)}$$

or small values of ε (i.e. high Q)

$$\frac{1+R}{R^{1/2}} \simeq 2 - \frac{\varepsilon^2}{2} + \ldots \qquad \text{(B-50)}$$

so to first order in ε, the microphone sensitivity for identical transducers at the ends of a plane wave resonator in terms of Q_n is

$$M_0 = 10^{-7/2} \left(\frac{V_m}{i_s} \frac{S}{\rho c} \frac{m\pi}{2Q_m} \right)^{1/2} \qquad \text{(B-51)}$$

157

APPENDIX C

THERMODYNAMIC TABLES FOR HE II

The most consistent and precise values for the thermodynamic para-
meters of He II were produced at UCLA from simultaneous measurements of
first, second and fourth sound speeds between 1.2°K and 2.15°K, from
saturated vapor pressure to 25 atm. pressure. The results of the sound
speed measurements[117] and their subsequent analysis[116] giving the
thermodynamic parameters at saturated vapor pressure, are reproduced
here in Table IA with the addition of the normal fluid viscosity, η,
from Ref 37, Table A. Table IB gives the precision of the results in
Table IA. The second order derivatives of the thermodynamic functions,
also at saturated vapor pressure, were evaluated by calculating differ-
ences due to small changes in T or P (10^{-5}°K or 10^{-4} bar respectively).
Those values are listed in Table II.

There were three difficulties with the data in Table IA and II at
the lowest temperatures: (1) The data did not extend to low enough
temperatures. For several calculations, it was useful to have a con-
sistent set of values that extended down to 1.0°K (see Figs. 5, 12, 15,
32 and 42). (2) At low temperatures there were more precise determina-
tions of the isobaric expansion coefficient, β_p. (3) Some of the second
order derivatives in Table II were based on the poorer values of β_p
and/or showed unphysical behavior when extrapolated to lower tempera-
tures (see Figs, 43, 44). Tables III and IV were constructed to remove
these difficulties.

158

TABLE IA. Density, ρ, thermal expansion co-efficient, β_p, normal fluid fraction, ρ_n/ρ, specific entropy, S, specific heat at constant pressure, C_p, ratio of specific heats, γ, isothermal compressibility, κ_T, first, second and fourth sound velocities, C_1, C_2, C_4, and viscosity, η, at saturated vapor pressure. Ref. 116.

T (K)	ρ (g cm^{-3})	$-10^3\beta_p$ (K^{-1})	ρ_n/ρ	S (Jg^{-1}K^{-1})	C_P (Jg^{-1}K^{-1})	$10^2(\gamma-1)$	$10^2\kappa_T$ (bar^{-1})	C_1 (m sec^{-1})	C_2 (m sec^{-1})	C_4 (m sec^{-1})	η (μ poise)
						$P=0.0$					
1.20	0.1452	0.02	0.0283	0.0515	0.318	0.000	1.222	237.4	18.55	234.0	17.7
1.25	0.1452	0.42	0.0368	0.0663	0.408	0.003	1.225	237.1	18.78	232.8	16.8
1.30	0.1452	0.78	0.0472	0.0943	0.515	0.009	1.228	236.8	19.03	231.2	16.0
1.35	0.1452	1.11	0.0598	0.1060	0.641	0.015	1.231	236.5	19.30	229.4	15.6
1.40	0.1453	1.45	0.0748	0.1319	0.786	0.021	1.236	236.1	19.58	227.2	15.1
1.45	0.1453	1.84	0.0924	0.1623	0.953	0.029	1.240	235.6	19.84	224.7	14.6
1.50	0.1453	2.32	0.1131	0.1978	1.142	0.039	1.245	235.2	20.07	221.7	14.1
1.55	0.1453	2.91	0.1369	0.2387	1.357	0.053	1.251	234.6	20.25	218.3	13.6
1.60	0.1453	3.62	0.1643	0.2855	1.598	0.072	1.257	234.0	20.37	214.3	13.0
1.65	0.1453	4.44	0.1955	0.3387	1.869	0.095	1.264	233.4	20.41	209.8	12.5
1.70	0.1454	5.30	0.2310	0.3990	2.174	0.119	1.272	232.7	20.36	204.6	12.8
1.75	0.1454	6.17	0.2712	0.4668	2.514	0.142	1.281	231.9	20.19	198.6	12.8
1.80	0.1454	7.00	0.3166	0.5429	2.896	0.162	1.291	231.0	19.89	191.7	12.8
1.85	0.1455	7.79	0.3677	0.6279	3.323	0.178	1.302	230.0	19.43	183.7	13.3
1.90	0.1455	8.63	0.4253	0.7228	3.804	0.195	1.315	228.8	18.78	174.4	13.8
1.95	0.1456	9.79	0.4901	0.8285	4.351	0.222	1.331	227.4	17.89	163.5	14.2
2.00	0.1457	11.72	0.5632	0.9465	4.990	0.281	1.350	225.8	16.69	150.4	14.6
2.05	0.1458	15.09	0.6469	1.0791	5.791	0.405	1.373	224.0	15.00	134.4	15.6
2.10	0.1459	19.61	0.7484	1.2316	6.972	0.570	1.401	221.8	12.39	112.6	16.5
2.15	0.1460	22.85	0.8856	1.4162	8.723	0.619	1.434	219.2	7.99	75.1	21.5

159

TABLE IB. Precision of the results in Table IA.

	Saturated Vapor Pressure		
	1.2 K	Inter-mediate T	Highest T
ρ	0.1%	0.1%	0.1%
β_p	$0.2 \times 10^{-3} K^{-1}$	3%	8%
ρ_n/ρ	0.0005	0.3%	0.05%
s	0.0002 $J\text{-}gm^{-1}\text{-}K^{-1}$	0.3%	0.6%
c_p	0.002 $J\text{-}gm^{-1}\text{-}K^{-1}$	0.3%	0.6%
$\gamma-1$	50%	6%	10%
κ_T	0.2%	0.2%	0.8%
c_1	0.1%	0.1%	0.4%
c_2	0.2%	0.1%	0.4%
c_4	0.2%	0.1%	0.4%

TABLE II. Second order derivatives evaluated at saturated vapor pressure. From Ref. 116.

T (K)	$\dfrac{\rho}{C_1}\dfrac{\partial C_1}{\partial \rho}$	$10^2\dfrac{\partial(\rho_n/\rho)}{\partial P}$ (bar^{-1})	$\dfrac{\partial(\rho_n/\rho)}{\partial T}$ (K^{-1})	$-10^3\dfrac{\partial\beta_\rho}{\partial P}$ (bar^{-1}K^{-1})	$-10^3\dfrac{\partial\beta_\rho}{\partial T}$ (K^{-2})	$\dfrac{\partial C_\rho}{\partial T}$ (Jg^{-1}K^{-2})
1.20	2.724	0.064	0.152	0.47	8.45	1.64
1.25	2.749	0.111	0.188	0.51	7.57	1.97
1.30	2.779	0.158	0.229	0.66	6.79	2.33
1.35	2.808	0.204	0.275	0.90	6.56	2.71
1.40	2.831	0.250	0.326	1.18	7.16	3.12
1.45	2.849	0.300	0.382	1.57	8.50	3.55
1.50	2.862	0.356	0.444	1.84	10.64	4.03
1.55	2.869	0.422	0.511	2.06	13.10	4.55
1.60	2.872	0.502	0.585	2.23	15.37	5.12
1.65	2.871	0.597	0.666	2.37	16.95	5.74
1.70	2.867	0.706	0.755	2.52	17.50	6.44
1.75	2.860	0.826	0.854	2.74	17.02	7.21
1.80	2.851	0.951	0.963	3.09	16.04	8.07
1.85	2.839	1.075	1.085	3.61	15.87	9.05
1.90	2.825	1.192	1.221	4.30	18.87	10.22
1.95	2.809	1.304	1.374	5.14	28.88	11.74
2.00	2.789	1.423	1.557	6.09	50.91	14.04
2.05	2.763	1.563	1.813	7.27	84.61	18.64
2.10	2.731	1.592	2.315	10.69	81.25	30.43
2.15	2.687	1.273	3.126	25.16	190.35	24.08

Table III is an extension of Table IA. The values of β_p below 1.35°K were taken from Ref. 37, Table A. The values of ρ_n/ρ were taken from Ref. 37. Table E down to 1.1°K, and then extrapolated down to 1.0°K using the following quadratic "bootstrapping" method. A second order polynomial was fit to the last three tabulated values of ρ_n/ρ at 1.2, 1.15 and 1.1°K and used to generate a new point at 1.05°K. The process was repeated with the last two tabulated points and the new point to generate a point at 1.0°K. Specific entropy, S, and specific heat at constant pressure, C_p, first and second sound speed, C_1 and C_2, were generated from the temperature dependences in Ref. 94, Tables 6, 7, 10 and 12 normalized to their low temperature values in Table IA of this appendix.

Some of the low temperature values of second order thermodynamic derivatives listed in Table IV could not be extrapolated from the values in Table II as can be seen from the unrealistic behavior of $\partial\beta_p/\partial T$ and $\partial(\rho_n/\rho)/\partial P$ shown in Figs. 43 and 44 respectively. Since these second order derivatives are the dominant terms in the coupling coefficient, β, for resonant mode conversion of second sound to first sound (see II-32 and Fig. 6), their values were found by taking numerical derivatives of tabulated values and normalizing to data in Table II at temperatures where both the numerical derivatives and the values in Table II have the same temperature dependence. $\partial\beta_p/\partial T$ was obtained numerically from the values in Table II and is shown as the line in Fig. 43. The solid circles on the same graph are the values from Table II. No normalization constant was necessary. $\partial(\rho_n/\rho)/\partial P$ was determined numerically from the calculated values of ρ_n/ρ [118]

162

TABLE III

Low temperature values of thermodynamic quantities at saturated vapor pressure

T	$-10^3 \beta_p$	ρ_n/ρ	S	C_p	C_1	C_2	η
(0°K)	(°K^{-1})		(J/gm°K)		(m/s)	(cm/s)	(μ poise)
1.00	-0.48	.0077 [5%]	.0164	.10 [10%]	237.9 [.1%]	1920	37
1.05	-0.38	.0103	.0223	.14	237.8	1880	30
1.10	-0.28 [20%]	.0146 [3%]	.0298 [3%]	.188 [1.5%]	237.7	1855	23
1.15	-.09 [50%]	.0205	.0395	.247	237.6	1850	20.4
1.20	0.10 [20%]	.0281 [2%]	.0515 [3%]	.318 [1%]	237.4 [1%]	1855 [2%]	17.7
1.25	0.39	.0368	.0663	.408	237.1	1878	16.8
1.30	0.63 [10%]	.0472	.0843	.515	236.8	1903	16.0
1.35	1.11	.0598	.1060	.641	236.5	1930	15.6

TABLE IV

Low temperature values of second order thermodynamic derivatives

T	$+10^2 \dfrac{\partial(\rho_n/\rho)}{\partial P}$	$\dfrac{\partial(\rho_n/\rho)}{\partial T}$	$-10^3 \dfrac{\partial\beta_p}{\partial T}$	$\dfrac{\partial C_p}{\partial T}$
(°K)	(bar^{-1})	(°K^{-1})	(°K^{-2})	(Jg^{-1}°K^{-2})
1.00	.033 [3%]	.058	1.05 [10%]	0.62
1.05	.046	.074	1.85	0.83
1.10	.063	.095	2.70 [10%]	1.07
1.15	.082	.121	3.65	1.34
1.20	.106	.152	4.60	1.64
1.25	.134	.188	5.70	1.97
1.30	.166	.229	6.70	2.33
1.35	.202	.275	7.80	2.71
1.40	.245	.326	9.00 [5%]	3.12
1.45	.295	.382	10.2	3.55
1.50	.355	.444	11.4	4.03
1.55	.421	.511	12.8	4.55
1.60	.502 [3%]	.585	14.4	4.12
1.65	.597	.666	16.4	5.74

164
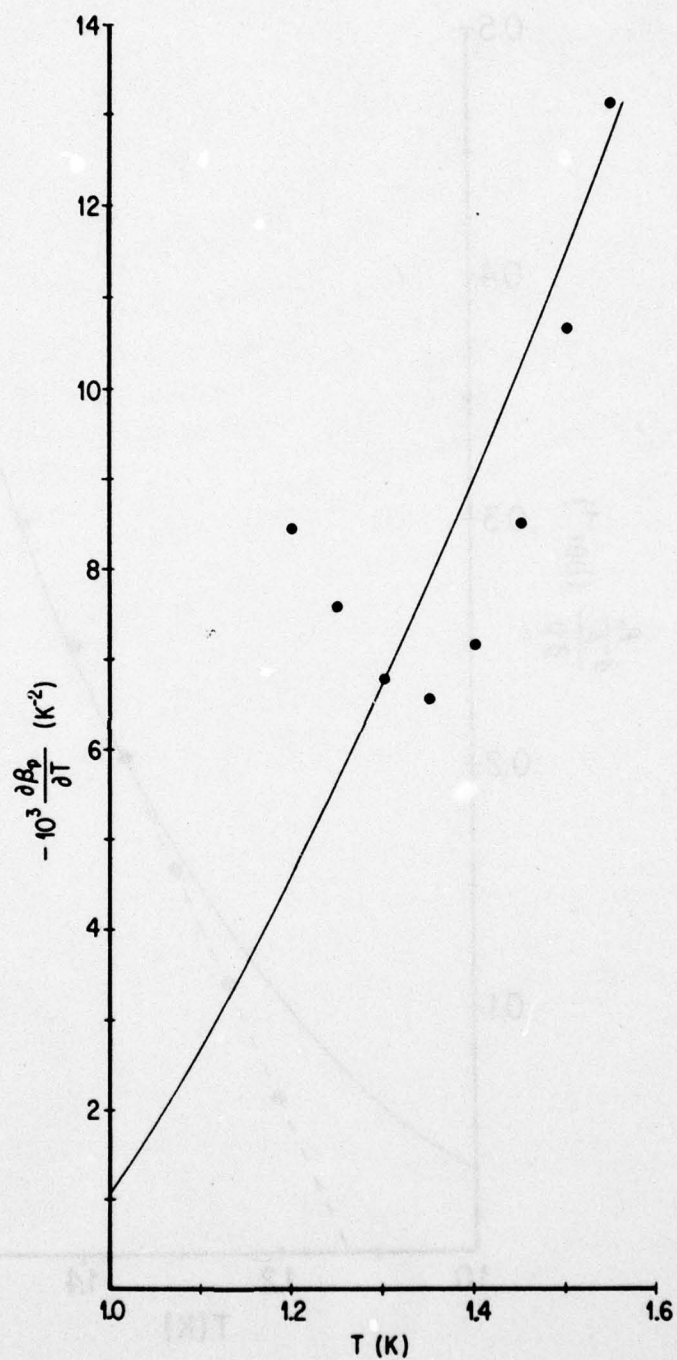
FIGURE 43. Low temperature values of $\partial\beta_p/\partial T$. The solid line represents the numerical derivative taken from Ref. 37, Table A and the circles are from Table II of this appendix.
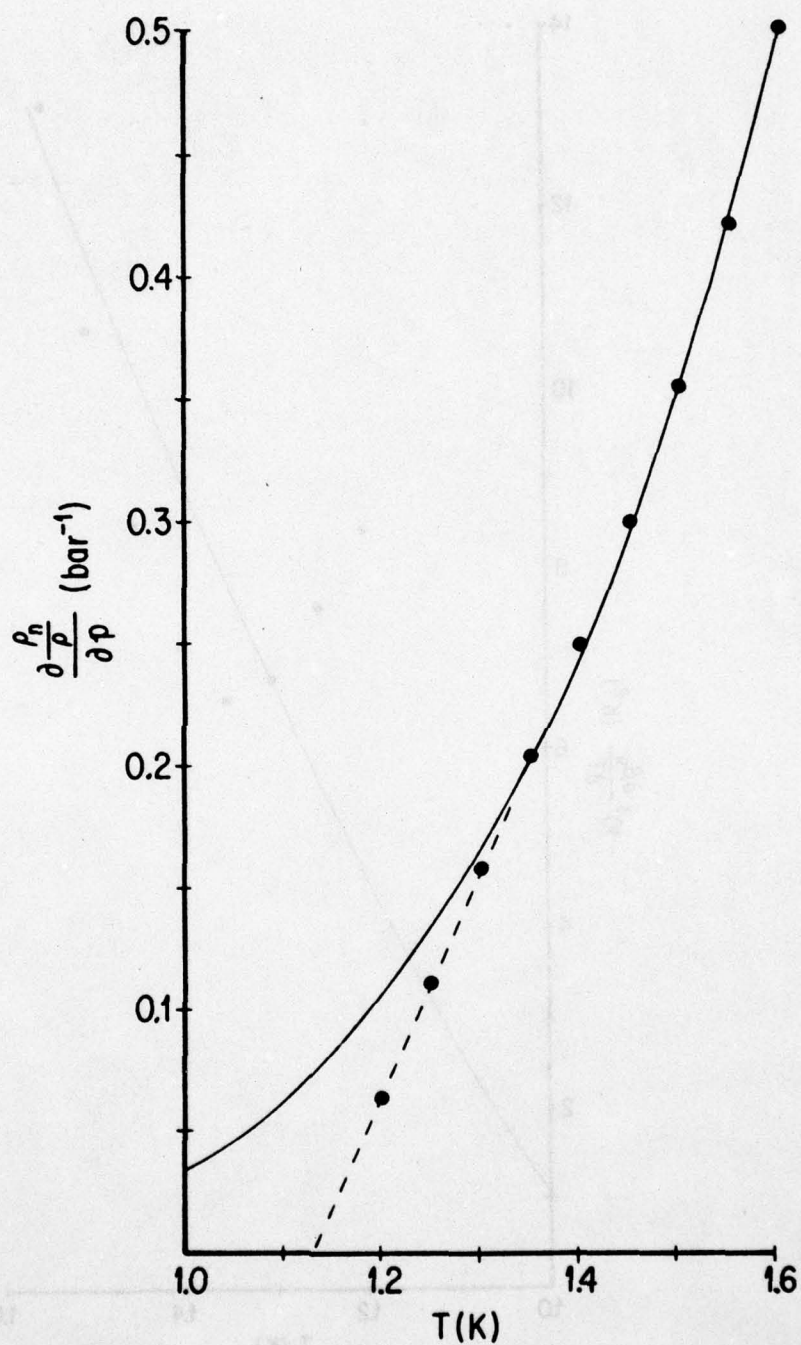
FIGURE 44. Low temperature values of $\partial(\rho_n/\rho)/\partial P$. The solid line represents the numerical derivative taken from Ref. 118, Table XIV and the circles are from Table II of this appendix.

166

and normalized to the value of $\partial(\rho_n/\rho)/\partial P$ in Table II at 1.6°K by multiplying the numerical derivative by .867. The normalized temperature dependence of $\partial(\rho_n/\rho)\partial P$ is shown in Fig. 44 and the values from Table II are shown as solid circles. It is clear that the extrapolation of the values in Table II (dashed line) leads to an unphysical result.

The values of $\partial(\rho_n/\rho)/\partial T$ and $\partial C_p/\partial T$ in Table IV were used to determine $E(T)$, (see A-3 and Fig. 42). Their values were extrapolated from values in Table II by the same "bootstrapping" method used to generate values of ρ_n/ρ below 1.1°K.

APPENDIX D.

RESONANT MODE CONVERSION AT ELEVATED PRESSURE

The thermodynamic coupling coefficient, β (II-32), which character-
izes the interaction of two second sound waves to create first sound
through the process of resonant mode conversion (II-D), is plotted in
Fig. 45. The second order thermodynamic derivatives used in the cal-
culation of β were evaluated numerically at P_o = 5, 10, 15 and 20 bars
from the thermodynamic tables of Maynard.[116]

$\partial(\rho_n/\rho)/\partial P$ is determined by taking the difference of the tabulated
values at $P_o \pm 1$ bar and dividing by 2×10^6 dynes/cm^2. This method of
determining the derivative is valid since the change in ρ_n/ρ with
pressure is smooth and monotomic. A plot of $\partial(\rho_n/\rho)/\partial P$ as a function
of P_o determined in this way shows smooth isotherms which extrapolate
to the values of $\partial(\rho_n/\rho)/\partial P$ listed in Tables II and IV saturated vapor
pressure. $\partial\beta_p/\partial T$ is also determined numerically from the same thermo-
dynamic tables by taking differences in β_p at 50 m°K intervals and
then making a quadratic interpolation which smoothed the data. Again,
the $\partial\beta_p/\partial T$ isotherms extrapolated to the vapor pressure values listed
in Tables II and IV.

Fig. 45 is a graph of the coupling coefficient, β, for resonant
mode conversion as a function of temperature. The lines are isobars
at SVP and 5, 10, 15 and 20 bars. The line at SVP can be compared to
line III in Fig. 6 by multiplying the values in Fig. 6 by $8u_2^2$. At
1.2°K the application of 20 bars of pressure increases β by a factor
of 3.3 whereas at 0.7°K the factor is only about 2.1.

168
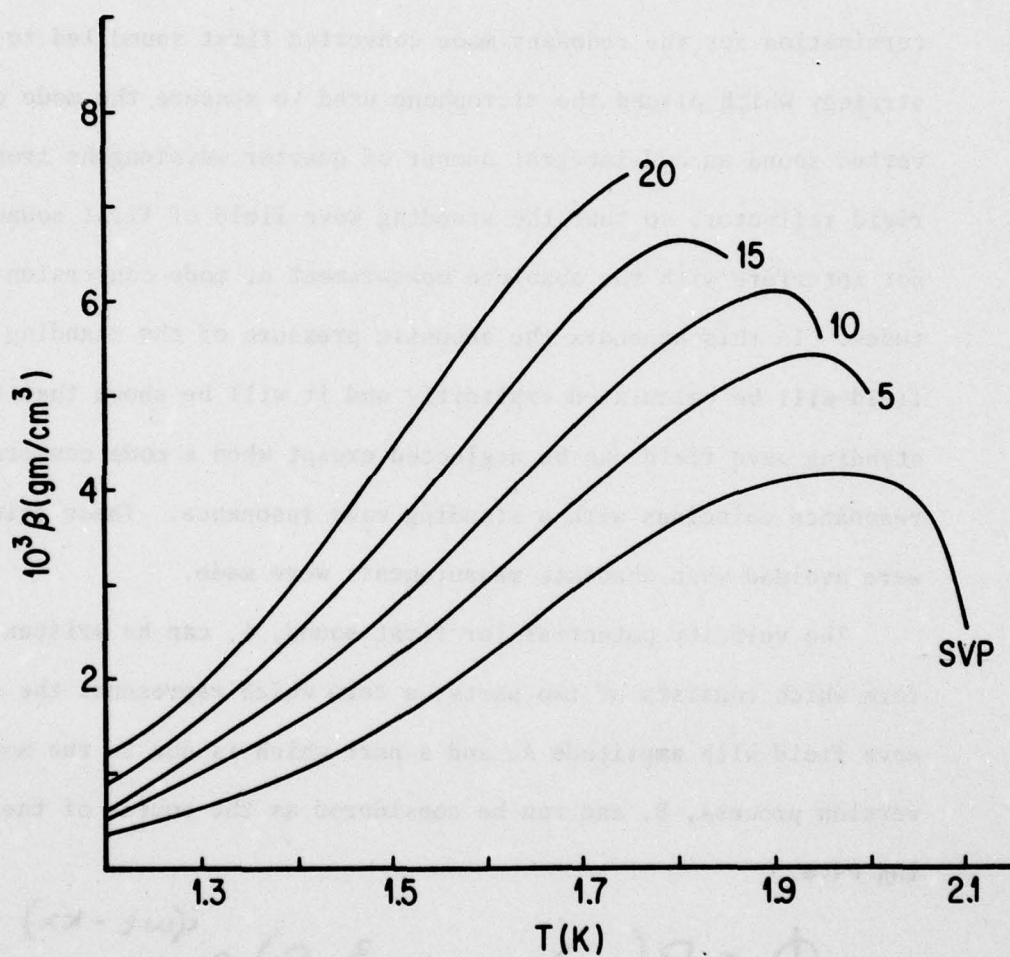
FIGURE 45. Isobars for the resonant mode conversion thermodynamic coupling coefficient, β.

APPENDIX E

CANCELLATION OF STANDING WAVE EFFECTS

In (III-C-5) the impracticability of making a non-reflecting
termination for the resonant mode converted first sound led to a
strategy which placed the microphone used to measure the mode con-
verted sound an odd-integral number of quarter wavelengths from a
rigid reflector, so that the standing wave field of first sound would
not interfere with the absolute measurement of mode conversion ampli-
tudes. In this appendix the acoustic pressure of the standing wave
field will be calculated explicitly and it will be shown that the
standing wave field can be neglected except when a mode conversion
resonance coincides with a standing wave resonance. These coincidences
were avoided when absolute measurements were made.

The velocity potential for first sound, ϕ, can be written in a
form which consists of two parts: a term which represents the standing
wave field with amplitude A, and a part which is due to the mode con-
version process, B, and can be considered as the source of the stand-
ing wave.

$$\phi = B\left(x, \lambda_s, \omega, \omega_i^2, \beta\right) e^{i(\omega t - kx)}$$
$$+ A\left[e^{i(\omega t + kx)} + R\, e^{i(\omega t - kx)}\right] \qquad (E-1)$$

170

This expression refers to the geometry diagrammed below and is similar to (B-38).
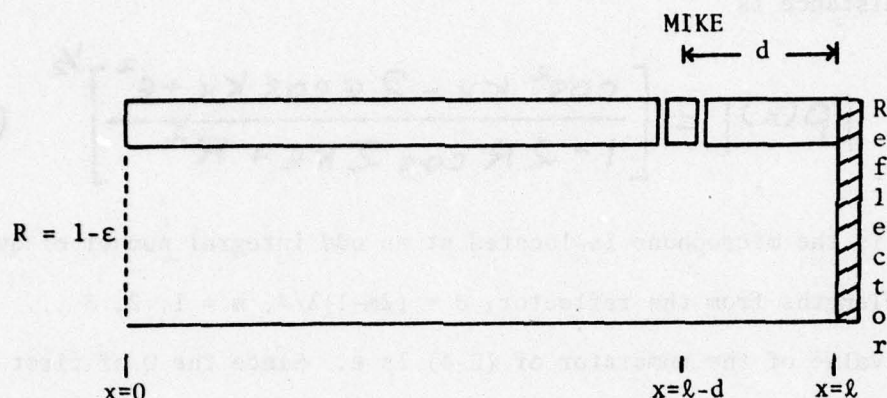
The rigid reflector is at $x = \ell$ and the arbitrary termination at the left has a reflection coefficient R, $1-R = \varepsilon \ll 1$. The absolute measurements discussed in (IV-D-2) were made at or below $1.41°K$, so if the microphone in (E-2) represents the microphone in the older top-plate designated 2C (see Fig. 17, upper), then the mode converted first sound amplitude has grown to its asymptotic value by the time it has reached the microphone location, $x = \ell - d$, in (E-2).

The pressure and particle velocity have been given in terms of the velocity potential in (B-39, 40). The amplitude of the standing wave field, A, can be expressed in terms of the incident mode converted wave, B, by applying the rigid boundary condition at the reflectior (i.e. $u(x=\ell) = 0$).

$$|A| = \frac{|B|}{(1 - 2R\cos 2k\ell + R^2)^{1/2}} \qquad (E-3)$$

171

$|A|$ has its maximum value at resonance equal to B/ε and its minimum value is $B/2$. The amplitude of the standing wave field as a function of distance is

$$|P(x)| = \left[\frac{\cos^2 kx - 2\varepsilon \cos kx + \varepsilon^2}{1 - 2R \cos 2k\ell + R^2}\right]^{1/2} \quad (E\text{-}4)$$

If the microphone is located at an odd integral number of quarter-wavelengths from the reflector, $d = (2m-1)\lambda/4$, $m = 1, 2, 3 \ldots$ then the value of the numerator of (E-4) is ε. Since the Q of first sound resonances in the waveguide is high at low temperatures, the effects of the standing wave field can be neglected if the mode conversion frequency is not close to a first sound resonance of the waveguide.

172

REFERENCES

1. S. Muktananda, Siddha Meditation, S.Y.D.A. Foundation, Oakland (1975).

2. U. Ingard and D. C. Pridmore-Brown, J. Acoust. Soc. Amer. 28, 367 (1956).

3. P. J. Westervelt, J. Acoust. Soc. Amer. 29, 199 (1957); 29, 934 (1957).

4. O. V. Rudenko and S. I. Soluyan, Soviet Physics-Acoustics 18, 352 (1973).

5. P. J. Westervelt, J. Acoust. Soc. Amer. 35, 535 (1963).

6. N. S. Shiren, Phys. Rev. Lett. 11, 3 (1963).

7. G. Jones and D. Kobett, J. Acoust. Soc. Amer. 35, 5 (1963). L. D. Landau and E. M. Lifshitz, Theory of Elasticity, Pergamon, London (1959) p. 120.

8. F. R. Rollins, Jr., Appl. Phys. Lett. 2, 147 (1963); F. R. Rollins, Jr., L. J. Taylor and P. H. Todd, Jr., Phys. Rev. 136, A597 (1964).

9. L. D. Landau, J. Phys. U.S.S.R., 5, 71 (1941). A more accessible version of this classic paper in English can be found in the Collected Papers of L. D. Landau, D. Ter Haar, ed., Pergamon, London (1965) p. 301.

10. L. D. Landau and E. M. Lifshitz, Fluid Mechanics, Pergamon, London (1959), Ch. 16.

11. G. A. Sorge, Anwesung zur Stimmung der Orgelwerke und des Claviers, Hamburg (1744) p. 40.

12. G. Tartini, Trattato di Musica, Padua (1754).

13. R. T. Beyer, Nonlinear Acoustics, written for the Naval Ship Systems Command, Dept. of the Navy (1974) p. 10.

14. H. Helmholtz, On the Sensation of Tone, Dover, New York (1954) Ch. VII.

15. E. G. Wever and M. Lawrence, Physiological Acoustics, Princeton University Press, New Jersey (1954) Ch. 8 and 9.

16. H. Lamb, The Dynamical Theory of Sound, 2nd ed., Dover, New York (1960) p. 182.

17. A. L. Thuras, R. T. Jenkins and H. T. O'Neil, J. Acoust. Soc. Amer. 6, 173 (1935).

18. O. N. Geertsen, Technical Report No. 3, UCLA-Physics, Los Angeles, Calif. (1951); J. Acoust. Soc. Emer. 25, 192(A), (1953).

19. P. J. Westervelt, J. Acoust. Soc. Amer. 32, 934(A), (1960).

20. J. L. S. Bellin, P. J. Westervelt, R. T. Beyer, J. Acoust. Soc. Amer. 32, 935(A), (1960).

21. H. O. Berktay, J. Sound. Vib. 2, 435 (1965).

22. H. O. Berktay, J. Sound Vib. 2, 462 (1965); J. Sound Vib. 5, 155 (1967).

23. H. K. Onnes, Proc. Roy. Aced. Amsterdam 13, 1903 (1911).

24. P. Kapitza, Nature 141, 74 (1938).

25. J. F. Allen and A. D. Misener, Nature 141, 75 (1938).

26. W. H. Keesom and G. MacWood, Physica 5, 737 (1938).

27. W. H. Keesom and A. P. Keesom, Physica 2, 557 (1935).

28. J. F. Allen, R. Peierls and M. Z. Uddin, Nature 141, 75 (1938)

29. J. C. McLannan, H. D. Smith and J. O. Wilhelm, Phil. Mag. 14, 161 (1932).

174

30. J. F. Allen and J. Jones, Nature 141, 243 (1939).

31. J. G. Daunt and K. Mendelsohn, Nature 143, 719 (1939).

32. P. Kapitza, J. Phys. U.S.S.R. 5, 59 (1941).

33. A. Einstein, Sitzber. Preuss. Akad. Wiss. 261, (1924); 3 (1938)

34. F. London, Nature 141, 643 (1938).

35. L. Tisza, Nature 141, 913 (1938).

36. Ref. 10, Sec. 130.

37. S. Putterman, Superfluid Hydrodynamics, North Holland/American Elsevier, New York (1974) Sec. 2.

38. S. Putterman and S. Garrett, J. Low Temp Phys. 27, 543 (1977).

39 L. Onsager, remark at the Low Temperature Physics Conference at Shelter Island, 1948. See also L. Onsager, Nuovo Cimento Suppl. No. 2, 249 (1949)

40. W. F. Vinen, Proc. Roy. Soc. (London) A260, 218 (1961).

41. G. W. Rayfield and F. Reif, Phys. Rev. Lett. 11, 305 (1963).

42. R. E. Packard and T. M. Sanders Jr., Phys. Rev. Lett. 22, 823 (1969).

43. G. A. Williams and R. E. Packard, Phys. Rev. Lett. 33, 280 (1974).

44. Some of the material in the first four sections of Chapter II appeared originally in Ref. 38.

45. A. Einstein, Ideas and Opinions, Dell, New York (1954) p. 228. This statement was made before the Prussian Academy of Sciences on January 27, 1921.

46. Such an assumption is reasonable since $(\partial\rho/\partial T)_p$ in the region of experimental interest is small and vanishes at $T = 1.17°K$. A derivation of the first and second sound speeds including terms

depending on the expansion coefficient is given by F. London, Superfluids, Vol. II, Dover, New York (1954) p. 84.

47. J. C. Findlay, A. Pitt, H. Grayson-Smith and J. O. Wilhelm, Phys. Rev. $\underline{54}$, 506 (1938).

48. V. P. Peshkov, J. Phys. U.S.S.R. $\underline{10}$, 389 (1946).

49. I. Rudnick and K. A. Shapiro, Phys. Rev. Lett. $\underline{9}$, 191 (1962).

50. I. Rudnick, Proceedings of the International School of Physics - "Enrico Fermi" - Course LXIII - New Directions in Physical Acoustics, D. Sette, ed., North Holland, New York (1976) p. 139ff.

51. For discussions of superfluid sound propagation under "clamped conditions" (i.e. v_n=0) see Ref. 50, Sec. 1.3, 1.4, 1.6, 2.3 and 2.4 or Ref. 37, Ch. V.

52. O. V. Rudenko and S. I. Soluyan, Theoretical Foundations of Nonlinear Acoustics, Consultants' Bureau, New York (1977) Ch. I.

53. R. S. Sorbello, J. Low Temp. Phys. $\underline{23}$, 411 (1976).

54. Expressions for the first order deviations of v_n, p and T in terms of v_s are given for plane wave first and second sound to lowest order in β_p in Ref. 10, p. 519.

55. J. Olsen, Physica $\underline{69}$, 136 (1973).

56. A. C. Mota, J. Olsen, R. Sorbello and V. Tomar, Phys. Lett. $\underline{46A}$, 343 (1974).

57. See Ref. 38, Appendix A.

58. J. R. Pellam and W. B. Dawson, Phys. Rev. $\underline{85}$, 216 (1952).

59. I. M. Khalatnikov, Introduction to the Theory of Superfluidity, Benjamin, New York (1965) Ch. 13

60. A. C. Scott, F.Y.E. Chu and D. W. MacLaughlin, Proc. I.E.E.E. <u>61</u>, 1443 (1973).

61. D. V. Osborne, Proc. Roy. Soc. <u>A64</u>, 114 (1951); A. J. Dressler and W. M. Fairbank, Phys. Rev. <u>104</u>, 6 (1956).

62. T. Wang and I. Rudnick, J. Low Temp. Phys. <u>9</u>, (1972).

63. N. I. Pushkina and R. V. Khokhlov, J.E.P.T. Lett. <u>19</u>, 348 (1974).

64. National Bureau of Standards data for the attenuation of second sound in bulk (see Ref. 70) gives $\alpha = .49$ cm^{-1} for $4\pi \times 10^{-5}$ sec^{-1} at 1.5°K. This would raise their threshold intensity by a factor of 24.

65. R. D. Finch, T. G. Wang, R. Kagiwada, M. Barmatz and I. Rudnick, J. Acoust. Soc. Amer. <u>40</u>, 211 (1966); R. D. Finch, R. Kagiwada, M. Barmatz and I. Rudnick, Phys. Rev. <u>134</u>, A1425 (1964).

66. R. V. Khokhlov and N. I. Pushkina in <u>Seventh International Symposium on Non-Linear Acoustics, Abstracts</u>, A. H. Nayfeh and J. E. Kaiser, eds., p. 141.

67. Ref. 37, p. 53.

68. Private communication.

69. J. W. S. Rayleigh, <u>The Theory of Sound</u>, Vol. II, Dover, New York (1945) Sec. 268.

70. W. B. Hanson and J. R. Pellam, Phys. Rev. <u>95</u>, 321 (1954).

71. Ref. 37, p. 136.

72. Ref. 10, Sec. 24.

73. J. Heiserman and I. Rudnick, J. Low Temp. Phys. <u>22</u>, 481 (1976). See Appendix, p. 494.

74. A Compendium of the Properties of Materials at Low Temperatures
    (Phase I), Part II - Properties of Solids, V. J. Johnson, ed.,
    National Bureau of Standards, Cryogenic Engineering Lab. (Oct. 1960)
    Wright Air Development Division Technical Reprt 60-56.

75. Ref. 10, p. 189.

76. G. L. Pollack, Rev. Mod. Phys. 41, 48 (1969).

77. P. L. Kapitza, J. Phys. U.S.S.R. 4, 181 (1941).

78. I. M. Khalatnikov, Usp. Fiz. Nauk. 60, 69 (1956). Available in
    English translation as University of California Radiation
    Laboratory Translation 675 L. Sec. 17.

79. Stycast 2850FT with catalust 24LV from Emerson and Cuming, Inc.,
    Gardena, California.

80. Malco, Chicago, Illinois.

81. Teflon F.E.P. 50R Fluoarcarbon release film, Saunder Corp.,
    Los Angeles, California.

82. G. M. Sessler, J. E. West and D. A. Bentley, Phys. Rev. Lett.
    38, 368 (1977).

83. See, for example, the experimental apparatus of Geertsen, Ref. 18.

84. See P. Morse and U. Ingard, Theoretical Acoustics, McGraw-Hill,
    New York (1968) p. 252. It should be pointed out that their
    expression for effective density (6.2.23) is in error due to
    their neglect of inertial terms (i.e. Kelvin drag - see Ref. 10,
    Sec. 11). A correct expression is given by I. Rudnick, J. Acoust.
    Soc. Amer. 19, 348 (1947), see equations (6) and (7).

85. R. W. Leonard, J. Acoust. Soc. Amer. 17, 240 (1946).

86. This result was first derived by I. Rudnick in an unpublished
    letter to the editors of the Physical Review (Aug. 18, 1964).

87. Ref. 37, Ch. VI.

88. Cinema Engineering Co., Burbank, CA.

89. Epibond 100 A, Furane Plastics, Los Angeles, CA.

90. P. R. Bevington, Data Reduction and Error Analysis for the Physical Sciences, McGraw-Hill, New York (1967) p. 119.

91. H. J. Wentle, J. Acoust. Soc. Amer. 53, 1578 (1973).

92. Results of an unpublished experiment by K. L. Telschow on a similarly prepared sample of alumnized teflon.

93. Dry graphite lubricant no. 204, Sprayon Products, Inc. Anaheim, Ca.

94. R. J. Donnelly. Experimental Superfluidity, University of Chicago Press, Chicago (1967), Appendix C.

95. G. F. Brickwedde, H. van Dijk, M. Durieux, J. R. Clement and J. K. Logan, National Bureau of Standards Monograph No. 10.

96. G. M. Sessler and J. E. West, J. Acoust. Soc. Amer. 53, 1589 (1973).

97. A theoretical model of solid dielectric capacitative microphones in contact with a microscopically rough backplate surface is given by E. P. Cornet, Ph.D. thesis, University of Texas at Austin (1972) unpublished, Appendix.

98. G. M. Sessler and J. E. West, J. Applied Phys. 43, 922 (1972).

99. S. Ballantine, J. Acoust. Soc. Amer. 3, 319 (1932).

100. J. Heiserman, Ph.D. Thesis, UCLA (1975) unpublished, Appendix I.

101. UT-85-SS standard 50-ohm stainless steel jacketed coax, Uniform Tubes, Inc., Collegeville, PA.

102. The material in this appendix is condensed from lectures given by I. Rudnick at UCLA (Elementary Acoustics for Advanced Students) on the subject of reciprocity calibrations (May 1977).

103. J. W. S. Rayleigh, Proc. London Math. Soc. 4, 357 (1873); Scientific Papers, Vol. I, Dover, New York (1964) p. 171.

104. W. R. MacLean, J. Acoust. Soc. Amer. 12, 140 (1940).

105. R. K. Cook, J. Res. Natl. Bur. Stand. 25, 489 (1940).

106. M. Greenspan, National Bureau of Standards, private communication.

107. The sign of b can be changed in either (B-2) or (B-3) if, for one of the transducers, the force is in phase with the current, as in the case of electrodynamic (or magnetic) transducers. Such transducers are referred to as "anti-reciprocal". In this experiment the transducers are electrostatic and the force is in phase with the charge (90° out-of-phase with the current) so the sign of b is the same in equations. See E. M. McMillan, J. Acoust. Soc. Amer. 18, 344 (1946).

108. See, for example, P. M. Morse, Vibration and Sound, 2nd ed., McGraw-Hill, New York (1948) p. 313; or L. E. Kinsler and A. R. Frey, Fundamentals of Acoustics, 2nd ed., Wiley, New York (1962) p. 164.

109. See, for example, L. L. Beranek, Acoustic Measurements, Wiley, New York (1949) Sec. 4-2; Acoustics, McGraw-Hill, New York (1954) Part XXIX.

110. Ref. 10, Sec. 2.

111. A. Sommerfeld, Thermodynamics and Statistical Mechanics, Academic Press, New York (1956) p. 136.

112. H. J. Seguin and R. W. Leonard, Rev. Sci. Instrum. 37, 1743 (1966).

113. A. C. Anderson, Rev. Sci. Instrum. 44, 1475 (1973).

114. MKS Instruments, Inc. Burlington, Mass.

115. Quoted in T.R.V. Murti, The Central Philosophy of Buddhism, Allen and Unwin, London (1955) p. 138.

116. J. Maynard, Phys. Rev. B 14, 3868 (1976).

117. J. Heiserman, J. P. Hulin, J. Maynard and I. Rudnick, Phys. Rev. B 14, 3862 (1976).

118. J. S. Brooks and R. J. Donnelly, The Calculated Properties of He II, Tech. Report from the Institute of Theoretical Science and Dept. of Physics, University of Oregon, Eugene (1973). Table XIV.

119. Ref. 45, p. 37.

120. S. Putterman, private communication.

121. L. D. Landau and E. M. Lifshitz, Statistical Physics, Pergamon, London (1958). Sec. 122. See Ref. 37, Sec. 21, 26 and 36 for the application of Onsager symmetry relations to He II dissipative coefficients.

DISTRIBUTION LIST FOR ONR PHYSICS PROGRAM OFFICE
UNCLASSIFIED CONTRACTS

Director   3 copies
Defense Advanced Research Projects Agency
Attn: Technical Library
1400 Wilson Blvd.
Arlington, Virginia 22209

Office of Naval Research   3 copies
Physics Program Office (Code 421)
800 North Quincy Street
Arlington, Virginia 22217

Office of Naval Research   1 copy
Assistant Chief for Technology (Code 200)
800 North Quincy Street
Arlington, Virginia 22217

Naval Research Laboratory   3 copies
Department of the Navy
Attn: Technical Library
Washington, D. C. 20375

Office of the Director of Defense   3 copies
    Research and Engineering
Information Office Library Branch
The Pentagon
Washington, D. C. 20301

U. S. Army Research Office   2 copies
Box CM, Duke Station
Durham, North Carolina 27706

Defense Documentation Center   12 copies
Cameron Station (TC)
Alexandria, Virginia 22314

Director, National Bureau of Standards   1 copy
Attn: Technical Library
Washington, D. C. 20234

Commanding Officer   3 copies
Office of Naval Research Branch Office
536 South Clark Street
Chicago, Illinois 60605

San Francisco Area Office   3 copies
Office of Naval Research
760 Market Street, Room 447
San Francisco, California 94102

Office of Naval Research   6 copies
Code 102 1P (ONR/L)
800 North Quincy Street
Arlington, Virginia 22217

Air Force Office of Scientific Research   1 copy
Department of the Air Force
Washington, D. C. 22209

Commanding Officer   3 copies
Office of Naval Research Branch Office
1030 East Green Street
Pasadena, California 91101

Commanding Officer   3 copies
Office of Naval Research Branch Office
495 Summer Street
Boston, Massachusetts 02210

Director   1 copy
U. S. Army Engineering Research
  and Development Laboratories
Attn: Technical Documents Center
Fort Belvoir, Virginia 22060

ODDR&E Advisory Group on Electron Devices   3 copies
201 Varick Street
New York, New York 10014

New York Area Office   1 copy
Office of Naval Research
715 Broadway, 5th Floor
New York, New York 10003

Air Force Weapons Laboratory   1 copy
Technical Library
Kirtland Air Force Base
Albuquerque, New Mexico 87117

Air Force Avionics Laboratory   1 copy
Air Force Systems Command
Technical Library
Wright-Patterson Air Force Base
Dayton, Ohio 45433

183

Lawrence Livermore Laboratory   1 copy
Attn: Dr. W. F. Krupke
University of California
P. O. Box 808
Livermore, California 94550

Harry Diamond Laboratories   1 copy
Technical Library
Connecticut Ave. at Van Ness, N. W.
Washington, D. C. 20008

Naval Air Development Center   1 copy
Attn: Technical Library
Johnsville
Warminster, Pennsylvania 18974

Naval Weapons Center   1 copy
Technical Library (Code 753)
China Lake, California 93555

Naval Training Equipment Center   1 copy
Technical Library
Orlando, Florida 32813

Naval Underwater Systems Center   1 copy
Technical Library
New London, Connecticut 06320

Commandant of the Marine Corps   1 copy
Scientific Advisor (Code RD-1)
Washington, D. C. 20380

Naval Ordnance Station   1 copy
Technical Library
Indian Head, Maryland 20640

Naval Postgraduate School   1 copy
Technical Library (Code 0212)
Monterey, California 93940

Naval Missile Center   1 copy
Technical Library (Code 5632.2)
Point Mugu, California 93010

Naval Ordnance Station   1 copy
Technical Library
Louisville, Kentucky 40214

Commanding Officer   1 copy
Ocean Research & Development Activity
National Space Technology Laboratories
Bay St. Louis, Mississippi 39520

Naval Explosive Ordnance Disposal Facility   1 copy
Technical Library
Indian Head, Maryland 20640

Naval Electronics Laboratory Center   1 copy
Technical Library
San Diego, California 92152

Naval Undersea Center   1 copy
Technical Library
San Diego, California 92132

Naval Surface Weapons Center   1 copy
Technical Library
Dahlgren, Virginia 22448

Naval Ship Research and Development Center   1 copy
Central Library (Code L42 and L43)
Bethesda, Maryland 20084

Naval Surface Weapons Center   1 copy
Technical Library
Silver Spring, Maryland 20910

Naval Avionics Facility   1 copy
Technical Library
Indianapolis, Indiana 46218